

Incorporating Quantified Mental Workload in Modeling of Driver's Handling Behavior

Hua Cai

A Thesis

in

The Department

of

Mechanical & Industrial Engineering

Presented in Partial Fulfillment of the Requirements

for the Degree of Master of Applied Science (Mechanical & Industrial Engineering) at

Concordia University

Montreal, Quebec, Canada

December 2005

© Hua Cai, 2005



Library and
Archives Canada

Bibliothèque et
Archives Canada

Published Heritage
Branch

Direction du
Patrimoine de l'édition

395 Wellington Street
Ottawa ON K1A 0N4
Canada

395, rue Wellington
Ottawa ON K1A 0N4
Canada

Your file Votre référence

ISBN: 0-494-14299-5

Our file Notre référence

ISBN: 0-494-14299-5

NOTICE:

The author has granted a non-exclusive license allowing Library and Archives Canada to reproduce, publish, archive, preserve, conserve, communicate to the public by telecommunication or on the Internet, loan, distribute and sell theses worldwide, for commercial or non-commercial purposes, in microform, paper, electronic and/or any other formats.

The author retains copyright ownership and moral rights in this thesis. Neither the thesis nor substantial extracts from it may be printed or otherwise reproduced without the author's permission.

AVIS:

L'auteur a accordé une licence non exclusive permettant à la Bibliothèque et Archives Canada de reproduire, publier, archiver, sauvegarder, conserver, transmettre au public par télécommunication ou par l'Internet, prêter, distribuer et vendre des thèses partout dans le monde, à des fins commerciales ou autres, sur support microforme, papier, électronique et/ou autres formats.

L'auteur conserve la propriété du droit d'auteur et des droits moraux qui protègent cette thèse. Ni la thèse ni des extraits substantiels de celle-ci ne doivent être imprimés ou autrement reproduits sans son autorisation.

In compliance with the Canadian Privacy Act some supporting forms may have been removed from this thesis.

Conformément à la loi canadienne sur la protection de la vie privée, quelques formulaires secondaires ont été enlevés de cette thèse.

While these forms may be included in the document page count, their removal does not represent any loss of content from the thesis.

Bien que ces formulaires aient inclus dans la pagination, il n'y aura aucun contenu manquant.


Canada

ABSTRACT

Incorporating Quantified Mental Workload in Modeling of Driver's Handling Behavior

Hua Cai

Driver's mental workload (MWL) influences the driver's performance. A mental workload that is either too high or too low may endanger driving safety. Few previous studies have discussed how to quantify the mental workload in an objective way and whether or not it is possible to discover the driver's mental workload over-reduction. Furthermore, the influence of driver mental workload has not yet been considered in driver models.

In this study, an ECG features-based driver mental workload estimation method was proposed. This measure is based on clustering analysis and Learning Vector Quantization neural networks. Furthermore, a fuzzy space model of the dangerous zone for a moving vehicle and the estimation method of driving risk level were proposed. Finally, two neural network based driver models with the input of driver mental workload were built up. The experiments and simulations show that the MWL estimation results are consistent with the evaluation of the Rating Scale of Mental Effort (RSME). The Driving risk level has potential to indicate the driver MWL over-reduction. In the driver steering performance simulation, Elman recurrent network based driver models show superiority than those based on multilayer perceptrons (MLP), and the MWL variance does have positive impacts on the performance of neural network based driver models.

This study is limited to the available data source. Future work could be done on following aspects: more psychological signals indicating MWL variance should be included to make the quantification results more reliable. Besides, the influence of instant driving risk level to the driver's performance in the scenario of MWL over-reduction could also be studied.

ACKNOWLEDGMENT

The author wishes to express his sincere appreciation to his supervisor, Dr. Y. Lin for providing the guidance and great support throughout this research.

Thanks are extended to the faculty members and staff of the Faculty of Engineering and Computer Science for their help during the study. Special thanks are given to the Dr. G. Yang, the visiting scholar in our Intelligent Human-Machine Systems Group.

Finally, the author would like to express his special thanks to his wife Dongxing and daughter Sijia, as well as many other good friends for their love, encouragement and support.

TABLE OF CONTENT

LIST OF TABLES	xiii
CHAPTER 1 INTRODUCTION	1
1.1 Background	1
1.2 Literature review	2
1.2.1 Mental workload measurement.....	2
1.2.2 Driving risk level	10
1.2.3 Neural network based driver behavior models	12
1.3 Scope and objectives of this research	14
1.4 Organization of the thesis	16
CHAPTER 2 GENERAL FRAMEWORK OF RESEARCH.....	18
2.1 Driver model in close-loop DVE systems	18
2.2 Framework of driver mental workload estimation.....	19
2.3 Framework of driving risk level esitmatation.....	21
2.4 Framework of driver model building.....	21
2.5 Data source.....	22
CHAPTER 3 DRIVER MENTAL WORKLOAD ESTIMATION	25
3.1 Introduction.....	25
3.2 ECG features extraction.....	26
3.2.1 Features of ECG signals in time domain	26
3.2.2 FFT analysis of ECG signals	27
3.2.3 Wavelet analysis of ECG signals.....	33

3.3 Methodology of mental workload estimation	37
3.3.1 Clustering analysis of ECG features	38
3.3.2 Determining the number of mental workload level	39
3.3.3 Sorting the mental workload levels.....	39
3.3.4 Mental workload estimated by competitive networks	41
3.4 Experiment and simulation	44
3.4.1 ECG features in the typical vehicle manoeuvre.....	44
3.4.2 Clustering results of ECG feature samples	49
3.4.3 Grading the mental workload levels	55
3.4.4 Estimation of mental workload level and variance.....	58
3.4.5 Results and discussion	61
3.5 Summary	65
CHAPTER 4 DANGER ZONE BASED RISK LEVEL ESTIMATION.....	67
4.1 Introduction.....	67
4.2 Danger zone of moving vehicle	68
4.2.1 Definition of danger zone	68
4.2.2 Fuzzy space denotation of danger zone	69
4.3 Methodology of driving risk level estimation.....	76
4.3.1 Background risk level estimation.....	76
4.3.2 Overall risk level estimation	77
4.4 Experiment and simulation	78
4.4.1 Calculation of the minimum safe headway.....	79
4.4.2 Estimation of DRL in the single-lane change.....	80

4.4.3 Relationship between MWL and DRL	83
4.5 Summary	84
CHAPTER 5 NEURAL NETWORK BASED DRIVER MODELS	85
5.1 Introduction.....	85
5.2 Background of Muti-Layer Perceptron (MLP) and Recurrent neural networks.....	86
5.2.1 Architecture of MLP networks and learning algorithms	86
5.2.2 Architecture of Elman recurrent networks.....	88
5.3 Neural networks based driver steering behavior models	91
5.3.1 Interaction between driver model and vehicle model	91
5.3.2 Back-propagation network based driver model	92
5.3.3 Elman network based driver model	93
5.4 Two-DOF linear vehicle model	94
5.4.1 State equations of 2-DOF vehicle model	94
5.4.2 Validation of the 2-DOF vehicle model.....	96
5.5 Experiment and simulation	99
5.5.1 Simulation results of MLP networks	99
5.5.2 Simulation results of Elman networks	103
5.5.3 2-DOF model based vehicle state simulation	106
5.6 Summary	109
CHAPTER 6 CONCLUSIONS AND FUTURE WORK	111
6.1 General conclusions	111
6.2 Recommendations for future work	112
REFERENCE.....	113

APPENDIX A.....	126
-----------------	-----

LIST OF FIGURES

Figure 2-1 A typical close-loop VME system	18
Figure 2-2 A new driver model in VME system.....	19
Figure 2-3 Driver mental workload estimation process.....	20
Figure 2-4 Process of driving risk level estimation	21
Figure 2-5 New driver model based on neural networks.....	22
Figure 2-6 Three typical vehicle manoeuvre	23
Figure 3-1 A typical cycle of ECG signal.....	26
Figure 3-2 A continuous ECG signal.....	27
Figure 3-3 Moving averaged heart rate.....	27
Figure 3-4 Instant heart rate variability	27
Figure 3-5 Segmented ECG signal	28
Figure 3-6 Interpolated ECG cycle	29
Figure 3-7 Frequency spectrum of a segmented ECG signal	29
Figure 3-8 Amplitude spectrum of a continuous ECG signal.....	30
Figure 3-9 ECG amplitude spectrum vs steering angle	31
Figure 3-10 Sliding windows of STFT on an ECG cycle.....	32
Figure 3-11 One ECG cycle and its corresponding STFT.....	33
Figure 3-12 ECG signal and its continuous wavelet transform	35
Figure 3-13 Overall structure of the LVQ competitive network	43
Figure 3-14 ECG signal of driver ‘Y’ (#1 single-lane, 60km/h)	44
Figure 3-15 Peaks of R waves (driver ‘Y’, #1 single-lane, 60Km/h).....	45

Figure 3-16 ECG QRS complex and its power spectrum.....	46
Figure 3-17 Power distribution of QRS complexes.....	47
Figure 3-18 Heart rate variability of driver 'Y' (#1 single-lane, 60Km/h).....	48
Figure 3-19 Wavelet coefficients of HRV (Driver 'Y', #1 single-lane, 60km/h).....	48
Figure 3-20 LF, HF, and HF/LF of the heart rate variability.....	49
Figure 3-21 ECG features of the #1 single-lane change manoeuvre (60Km/h)	50
Figure 3-22 ECG features of the #1 double-lane change manoeuvre (80Km/h)	51
Figure 3-23 ECG features of the #1 sine-lane motion manoeuvre (60Km/h).....	51
Figure 3-24 MWL Level of the #1 single-lane change manoeuvre (60Km/h)	53
Figure 3-25 MWL Level of the #2 double-lane change manoeuvre (80Km/h).....	53
Figure 3-26 MWL Level of the #1 sine-lane motion manoeuvre (60Km/h)	54
Figure 3-27 MWL Level in the #2 single-lane change manoeuvre (60 Km/h)	58
Figure 3-28 MWL level in the #1 single-lane change manoeuvre (80 Km/h).....	58
Figure 3-29 MWL level in the #1 double-lane change manoeuvre (60 Km/h)	59
Figure 3-30 MWL level in the #1 sine-lane motion manoeuvre (50 Km/h).....	59
Figure 4-1 Longitudinal danger zone.....	70
Figure 4-2 Lateral danger zone	70
Figure 4-3 Danger zone of a moving automobile at 60 km per hour.....	80
Figure 4-4 Track of the single-lane change manoeuvre.....	81
Figure 4-5 Driving risk level distribution in single-lane change manoeuvre (60km/h) ..	82
Figure 4-6 Driving risk level distribution in single-lane change manoeuvre (80km/h) ..	82
Figure 4-7 Driving risk level distribution in single-lane change manoeuvre (100km/h)	82
Figure 4-8 Comparison of MWL and DRL in the same single-lane change manoeuvre	83

Figure 5-1 One layer MLP with R input elements and S^1 neurons	86
Figure 5-2 A two-layer Elman network.	89
Figure 5-3 Interaction between vehicle model and driver model	91
Figure 5-4 MLP network based driver model.....	93
Figure 5-5 Elman network based driver model.....	93
Figure 5-6 Two-degree-of-freedom vehicle model [Wong , 1978]	95
Figure 5-7 2-DOF model based simulation of the #2 single-lane change	98
Figure 5-8 2-DOF model based simulation of the #1 sine-lane change	98
Figure 5-9 Training procedure of the MLP network	101
Figure 5-10 Simulation results of steering angle based on two MLP driver models.....	102
Figure 5-11 Training procedure of the Elman network	104
Figure 5-12 Simulation results of steering angle based on two Elman driver models ..	105
Figure 5-13 Yaw rate simulation on results of Elman network based driver models....	108

LIST OF TABLES

Table 2-1 Driving manoeuvre done by driver ‘Y’ [Lin 2005, 1997].....	24
Table 3-1 Relations between wavelet coefficients and frequency domain.....	36
Table 3-2 Define the variance scope of each MWL level	40
Table 3-3 Representative frequencies and the corresponding power value.....	46
Table 3-4 Set Q of ECG features	50
Table 3-5 Average distance $d(c)$ for different cluster numbers	52
Table 3-6 Cluster centroids of four MWL levels.....	54
Table 3-7 Typical durations of each MWL level in different manoeuvre	55
Table 3-8 Mean value of the power and frequency for ECG strips.....	56
Table 3-9 Sorting the mental workload levels	57
Table 3-10 The value scope of each mental workload level.....	57
Table 3-11 Summary of percentile distribution for each mental workload level	60
Table 3-12 Mental workload variance in typical vehicle manoeuvre.....	61
Table 4-1 Membership functions of the fuzzy space	75
Table 4-2 Sensitivity of the risk detection over the location variance.....	76
Table 4-3 Minimum safe headway in different speeds.....	79
Table 5-1 Vehicle parameters used for 2-DOF simulation [Lin, 1997].....	97
Table 5-2 Average mental workload in each trial.....	100
Table 5-3 MSE of the steering angle between the simulation and the experiments	103
Table 5-4 MSE of the steering angle between the simulation and the experiments	106
Table 5-5 MSE of the yaw rate between the simulation and the experiments.....	109

Table 5-6 C.C. of the yaw rate between the simulation and the experiments.....	109
--------------------------------------------------------------------------------	-----

CHAPTER 1 INTRODUCTION

1.1 Background

Driver, vehicle, and road environment are three key elements to safe driving. Especially, drivers' psychological status, usually mentioned as the driver mental workload, influences the performance of steering, even the safety of driving.

The driver's mental workload has been widely studied in the research on driving safety. For example, it has been reported that drivers are often distracted during daily driving, such as grooming, using mobile phones, eating and drinking [Stutts et al., 2003]. Almost half of all accidents are caused by too late recognition [ITS Japan, 2002]. Therefore, some technologies such as Driver Assistant Systems (DAS) have been developed to change this situation. However, human drivers may not be able to act as effective obstacle detectors because of their reduced mental workload when automobiles are equipped with DAS [Hogan, 1997]. Previous literature has also indicated that both too high and too low mental workloads can degrade the task performance [Cnossen, 1994]; hence it is beneficial to maintain the driver's mental workload at a proper level in driving.

Many studies have proposed various driver models to simulate drivers' steering behaviors; For example, neural network-based driver models take position, velocity, acceleration, and other parameters of the vehicle as input to simulate the driver's steering behavior, but the impact of the driver's mental workload on driver models has not been extensively explored.

In order to analyze the impacts of a driver's mental workload on driver models, the driver's mental workload variance has to be quantified firstly, and then the steering performance of the driver models under the influence of a mental workload can be simulated and discussed. Besides, the relationship between the driving risk level and the driver mental workload should also be explored. Literature related to the three parts of research above is reviewed in the next section.

1.2 Literature review

1.2.1 Mental workload measurement

1.2.1.1 Mental workload definition and mental workload control

In human-machine systems, a comfortable, effective, and safe operation environment is always anticipated by any operator. There is no exception to drivers and the task of driving. Growing demands of high transport safety require people to pay more attention to human factors, especially the mental workload change in a complex traffic environment.

There are several definitions of mental workload. The popular definition of mental workload is given by O'Donnell et al. (1986). It is defined as the portion of the operator's limited capacity actually required to perform a specific task. Rouse et al. (1993) proposed a concept of experienced workload. In this definition, the mental workload is both task dependent and individual dependent. Many factors including the operator's capability, the motivation to perform a task influence the experienced workload. De Warrd (1996) did extensive research on driver's mental workload measurement solution and called it a

demand placed upon human, but the quantification of mental workload was not discussed.

Although there are multiple versions of mental workload definition, none of them is widely accepted [Xie et al., 2001]. It is partly because of difficulty to quantify the mental workload according to the present definition. Currently, the research interest gradually shifts to the mental workload estimation and control. The purpose of mental workload control is to keep operators' mental stress staying within an optimized scope because both too high and too low mental workloads can lead to degraded performance [Cnossen, 1994]. Based on the effort of mental workload control, the reduction of operation errors and the improvement of productivity can be achieved [Moray, 1988]. However, in order to limit the mental workload, the mental workload estimation should be done firstly.

1.2.1.2 Methods of mental workload estimation

Due to the definition of mental workload, mental workload cannot be measured directly. It can only be estimated indirectly through measuring other variables having close relations with the mental workload alteration. These methods can be roughly classified to the following categories: primary-task performance measurement and secondary-task performance measurement [O'Donnell et al., 1986], subjective estimation (including self-report) [Wickens, 1984], and physiological parameters measurement [Kramer, 1991].

Performance based estimation evaluates the possible mental workload from operators' action speed, action effects, and interaction time between human and machine. As for the task of driving, De Waard (1996) used the standard deviation of the lateral position (SDLP), the standard deviation of the steering-wheel movement (SDSTW), and

the Time-to-Line Crossing (TLC) to estimate the driver's mental workload. De Waard also used the following secondary task performance to estimate the mental workload: the frequency of mirror checking, the time delay in speed adaption to the next vehicle, and the frequency of eye movement. Lin et al. (2005) studied the hand movement in the steering wheel operation and used it as an indication of mental workload change.

Subjective estimation is usually adopted as an offline measure to do post-event evaluation. Operators are required to state their feelings and attitudes. Popular assessment techniques include the Subjective Workload Assessment Technique (SWAT) [Reid et al., 1988], the Task Load Index (TLX) [Hart et al., 1988] and the Rating Scale Mental Effort (RSME) [De Waard, 1996]. Although subjective workload estimation has been paid much attention due to the fact that no one can make more accurate comments to the mental workload than the person who experienced it personally, two limitations are obvious. One is that the subjective workload estimation usually provides overall estimation only and cannot provide real time estimation results; another is personal dependant. Hence, these limitations restrict the applications of the subjective estimation method. In practical, subjective estimation is usually used to verify the estimation results coming from other measures.

The physiological measurement looks at the operator's physiological response to the given task. The detectable physiological parameters mainly include EEG (Electroencephalogram) [Mazaeva et al., 2001], ECG (Electrocardiograph) [Kuriyagawa et al., 1999; Rouse et al., 1993; Murai, et al., 2004, 2003, 2001; Seong et al., 2004], EOG (Electro-Culogram), EMG (Electro-Myogram), blood pressure, respiration wave, eye fixation [Simon et al., 1993], eye blink, pupil diameter, head movement, and facial

expression [Ji et al., 2004]. The benefit of physiology measurement is the capability of real time process and the objectivity of assessment. Physiology measurement can even indicate the change process of mental workload.

Among all mental workload estimation methods, which measure is more sensitive and suitable for the driving task than the others? Whether one measure is sufficient to scale the driver's mental workload? Some literature has discussed the criteria of selecting a workload-measure for a general task from multiple aspects such as sensitivity, interference to the primary-task, equipment requirement, and operator acceptance [O'Donnell & Eggemeier, 1986; Eggemeier et al., 1991; Unema, 1995]. However, few studies have addressed the comparisons between the different measures for driver's mental workload estimation.

For the driving task, the physiological measurement of mental workload has some obvious advantages. There are many physiological parameters having close relationship with the driver's mental workload alteration. The most commonly used parameters contain eye activity, EEG, and ECG [Hanskins et al.1998; Wilson et al.1995b]. Among them, ECG signal has been recognized as a popular parameter used to estimate the mental workload for a long time [De Warrd, 1996; Jorna et al.1992; Roscoe et al.1992]. Hence, ECG features-based driver mental workload estimation is the focus of this study.

1.2.1.3 ECG features based mental workload estimation

The mental workload estimation based on ECG features involves two steps: ECG features extraction and pattern classification. Typical ECG features will be discussed in the following sections.

(1) Heart rate

In physiology, the heart contraction of human body is controlled by the parasympathetic nervous system (PNS) and sympathetic nervous system (SNS) [Roscoe et al. 1992]. Heart rate (HR) is possible for the mental workload estimation. De Warrd (1996) found that drivers' heart rate may increase or decrease in the weaving section. Murai et al. (2004, 2003, 2001) analyzed the mean value and the standard deviation of heart beat intervals to assess a ship navigator's mental workload during the procedure of the ship leaving and entering the port. Laine et al. (2002) pointed out that the time period of beat to beat decreases with the increased workload demands. Seong (et al., 2004) found that the width of the QRS complex (WQ) increases with the decreased workload demands.

(2) Heart rate variability

Heart rate variability (HRV) has been used for analyzing mental workload alteration in field workplaces. Kuriyagawa and Kageyama (1999) described a model of estimating mental workload by using the heart rate variability. However its indication function of mental strain, especially sensitivity and diagnosticity, is doubted in some studies [Wilson, 1992; Nickel et al.2003].

(3) FFT analysis of HRV

The frequency spectrum of HRV can be acquired by performing the Fast Fourier Transform analysis (FFT). Its spectrum contains three major regions. VLF (very low frequency): 0.004~0.04Hz; LF (low frequency): 0.04~0.15Hz; HF (high frequency): 0.15~0.4Hz. LF mainly indicates the activities of the sympathetic division of the autonomic nervous system (ANS). HF reflects the activities of the parasympathetic division of the ANS. LF/HF ratio reflects the balance of the sympathetic division and the parasympathetic division of the ANS [McCraty et al., 1995] and can indicate the change of the mental stress. Backs et al. (1994) found that the change of high frequency power shows relations to the variance of the task demands. Murai et al. (2004) studied the mental workload of a bridge team (crews on a ship) by calculating the LF/HF ratio and found that the bridge teammate's mental workload increases while judging for ship handling and paying attention to targets.

The study of cardiac variability based on the FFT spectral analysis looks at the whole ECG signals. There are limitations for the classical FFT analysis. For example, it is difficult to know the particular happening time of certain components of frequencies. In addition, the ECG analysis usually involves the task of QRS recognition. In time-domain, R-waves (containing ECG peaks) are relatively easy to detect while Q-wave and S-wave are hard to be recognized. Previous literature has suggested some ways of QRS-complex detection such as Short Time Fourier Transforms (STFT) and Wavelet Transforms (WT) [Okada, 1979; Schilling, 1998].

(4) Wavelet transforms of HRV

The wavelet transform (WT) is a very promising technique because it can provide a description of the signal in both time and frequency domains. WT can also characterize

the local regularity of the signal, which can be used to distinguish the real signal from noise, and the baseline drift. Therefore, WT is a suitable tool to analyze the ECG signal [Sahambi et al., 2003; Newandee et al., 2003, 2002]. Taking the quadratic spline originally proposed by Mallat et al. (1992) as the prototype wavelet functions, Li et al. (1995), Gamo et al. (2000) and Martínez et al. (2004) proposed a multiscale QRS detector including a method for detecting the monophasic P and T waves. Bahoura et al. (1997) implemented wavelet transforms for the real time detection of ECG R wave and the heart rate analysis based on the digital signal processing (DSP). Murai et al. (2001) analyzed a navigator's HRV at departure or arrival by the Haar wavelet functions, and pointed out that the wavelet decomposition coefficients at $n=3, 4$ levels and $n=1, 2$ levels correspond to the LF and HF components, respectively.

1.2.1.4 Workload estimation based on pattern recognition

Mental workload can also be estimated by using pattern recognition. Methods of mental workload classification using non-intrusive physiological features mainly include analyses of variance (ANOVA) models, principal components analyses, as well as artificial neural networks [Greene et al. 2000; Laine, et al. 2002; Sirevaag et al. 1993; Wilson et al. 1995a]. Among these methods, the artificial neural network is widely used because neural networks bring the low-level learning and the computational power to a decision system for capturing the non-linearity of system behaviors [Juang et al., 1998].

Among neural networks, two common architectures are the Multilayer perceptrons (MLP) and the Learning Vector Quantization (LVQ) [Antognetti & Milutinovic, 1991]. Some literature [Antognetti & Milutinovic, 1991] suggested that LVQ shows advantages over MLP in many pattern classification tasks. For example, the MLP networks trained

by using the Back-Propagation (BP) algorithm usually adopt the squared error for the output control; however, LVQ networks have many other suitable distortion measures, such as the Euclidean distance, correlation coefficient. Also, the MLP networks with the BP algorithm need complete training for each classification task, while the LVQ networks permit a common training and can automatic learn under unsupervised.

Al-Fahoum et al. (1999) developed a classifier based on using WT for extracting features and then using a radial basis function neural network (RBFNN) to classify the arrhythmia. This classifier appears to be well suited to classify the arrhythmia, owing to the feature vectors' linear inseparability and the tendency to cluster. Michael et al. (2004) used a self-organizing map (SOM) to separate the time-series of 84 subjects into groups based on characteristics of the cardiac data recorded around the interval. In order to estimate the mental stress based on the physiological index, Fukuda et al. (2001) proposed a new evaluation method of HRV by combining WT with recurrent neural networks. In the study proceeded by Wilson et al. (2003), physiological signals including the brain electrical activity, the eye movement, the heart rate, and the respiration waves were fed into an artificial neural network which was used to monitor the functional states of the participants in real time while they were performing a Multi-Attribute Task Battery with two levels of task difficulty.

In brief, the mental workload estimation is a hot topic in the field of human factors research. Many measures have been proposed but challenges still exist. There are two obvious limitations in previous research. (1) Most studies still stay on the level of qualitative analysis by associating certain physiological features with the mental workload change, such as 'high', 'low', or 'baseline'. (2) Some estimation methods have

much subjectivity; Furthermore, some results of different physiological signals based mental workload estimation may show inconsistency and be difficult to explain the difference.

1.2.2 Driving risk level

Due to the increasing complex of the traffic environment, the traffic safety has been paid higher demands than ever before and some new equipment for better safety has been developed, such as driver assistance systems (DAS). DAS can reduce a driver's physical workload and mental workload [Tanaka et al. 2000]; however, too much mental workload reduction may cause the driver's distraction because of the increasing disengagement. Hogan (1997) pointed out that drivers may not be able to act as effective obstacle detectors when DAS are provided. Hence, even though the automobile is equipped with DAS for the purpose of better safety, there are still needs for the early danger warning and the driver's mental state monitoring. Therefore, there should be approaches to possibly recognize the driver's mental workload over-deduction in the field. One of the ways is to make a comparison between the driver's mental workload and the risk of collision in driving.

Risk assessment of road users is an important area for investigation. Based on the NASS General Estimates System (GES), the Fatality Analysis Reporting System (FARS), and the Nationwide Personal Transportation Survey (NPTS), Kweon (2002) did a comprehensive assessment of overall risk to different drivers across different vehicle classes. Data are distinguished by driver age, gender, vehicle type, crash type (rollover versus non-rollover), and injury severity. Similarly, Mills et al. (2001) investigated the

influences of the following risk factors in driving: stimulants, sedatives, and fatigue. Stutts et al (2003) studied the risk factors in sleep-related crashes.

As for the possibility of accidents, Lanzilotta, E. J. (1995) proposed a probabilistic safety state model, which can be used to estimate the risk probability of an accident as a function of a human-machine system state. By using a discrete Markov network, the safety state model forms a framework to capture the human-machine and human-human interactions in the driving situation. Heino et al. (1996) used the time headway as an index for the risk scaling to analyze the difference of accident possibility between the sensation seekers and the sensation avoiders. Thakur (1997) proposed a driver-vehicle model to identify the safe value of Driver Daydream Factor and Driver Error for various driving situations. It was found that the perception process and the response process become large when the driver is relaxed. The author also used Risk Time, the time after which, the driver thinks the vehicle could reach “disaster” on the road, to estimate the coming risk. It indicated that a capable driver having a low Driver Daydream Factor can cope with a demanding situation easily even if the error he/she makes is large. Ward et al. (1998) studied the risk probability in terms of the time headway and the risk severity in terms of kinetic energy. Gorjestani et al. [1999] developed a radar based longitudinal virtual bumper collision avoidance system implemented on a truck. In this system, the virtual bumper is a programmable boundary defining a rectangle personal space around the host vehicle. Incursions into the personal space by neighbor vehicles impose a virtual force on the host vehicle to avoid the possible collisions.

Previous research has implied that there is possible association existing between the driver’s mental workload and the accident risk of driving. For example, De Warrd (1996)

discovered that a driver's mental workload in the car-phone use situation increases significantly compared with the baseline value. Laberge-Nadeau et al. (2003) investigated the association exists between the cell phone use and the road crashes. It was found that the relative risk of accidents and of accidents with injuries is higher (10% ~ 38%) for the users of cell phones than for the non-users. It implies that, when the collision risk in driving increases, the driver mental workload will usually grows up in order to maintain the similar task performance.

In brief, the driving safety and the driving risk are discussed yet the concept of driving risk level has not been intensively elaborated. Many factors, especially the time headway, can influence the risk feeling of drivers but few models have been built to quantify the risk. Furthermore, the relationship between the driver mental workload and the driving risk level has not been clearly disclosed.

1.2.3 Neural network based driver behavior models

Some studies have utilized neural networks to simulate drivers' handling behavior. Neural networks seem efficient to emulate the decision making process.

Neusser (1993) simulated the driver's handling patterns through a record of a 'perfect' driver's 50,000 steering behavior. A three-layer back-propagation (BP) network with the inputs of vehicle velocity, heading angle, road curvature, road width, and lateral deviation was built and good control accuracy was obtained.

An et al. (1996) suggested a basic architecture of an intelligent driver warning system, which embodies an adaptive neural network driver model for the indirect

collision avoidance. The input of this system contains the past history of throttle angle, vehicle speed, range and range rate to the front vehicle. The output is throttle angle.

Yang et al. (1998) applied a two-layer (sigmoid and linear) neural network for the directional control of a seven-axle vehicle. The inputs contain position, velocity and acceleration. The front wheel steering angle is the desired output. It was found that the lateral position error, preview error, and the lateral acceleration are the most important input variables for the neural network training.

Koike et al. (1999) proposed a multiple state estimation method for reinforcement learning model. The steering strategy of a vehicle is learned from a reward, which is evaluated by whether or not the vehicle is on the road. Simulation results show that this model can drive on an unknown road configuration or an unknown velocity condition. This research shows the benefits of considering the output feedback in driver models, too.

Ohno (2000) studied a MLP neural network based driver model with adaptive cruise control (ACC). This research shows that the control performance with ACC use is better than that of manual driving, but human errors occur during the ACC use. This paper suggested that proper warning systems should be deployed in ACC systems.

Ni (2003) reviewed and compared the car-following and the lane-changing strategies in some microscopic driver-vehicle-environment simulation systems, which evolved three aspects: vehicle modeling, driver modeling, and vehicle movement modeling. The possible input variables and the output variables of a BP neural network based driver models were suggested in this paper.

Lin et al. (2005) utilized three types of neural network to model a driver's handling behavior: Counter Propagation Networks (CPN), Radial Basis Function Networks (RBFN), and Back Propagation Networks (BPN). Besides the present vehicle states, the states of former ten instants are also contained in the inputs. Lin et al. concluded that RBFN shows better accuracy than BPN and CPN but RBFN shows only medium level of error tolerance.

In summary, artificial neural networks have been applied in driver models to study driver's handling behavior. Most neural networks in these models are based on Multilayer Perceptrons (BP networks). The feedback of errors such as the lateral offset has been contained in the inputs to achieve the goal of close-loop control.

However, there are still two points worthy to do the further study. (1) Few models have utilized recurrent networks directly to simulate the driver's steering behaviors. In fact, the architecture of recurrent network is especially suitable to simulate the time-series system. (2) Few driver models have concerned the influences of driver mental workload on driver's performance although previous studies have pointed out that driver mental workload definitely affects the driver's performance in the field.

1.3 Scope and objectives of this research

As discussed in the previous literature review, this study looks at the quantification of driver mental workload, the estimation of driving risk level, and the impacts of driver mental workload on driver's steering performance simulation.

Regarding the three topics above, the limitations exposed in previous literature are the following:

(1) Few studies have discussed the quantification of driver mental workload and compared the quantification value with the subjective MWL estimation results. Without the quantification of the mental workload, its influence on driver model's performance cannot be analyzed extensively.

(2) There is much subjectivity in the previous driver mental workload estimation methods. This subjectivity may cause obvious inconsistency between the results of different estimation methods.

(3) The concept and modeling of the driving risk level has not been intensively discussed. Moreover, the possible relationship between the driving risk level and the driver mental workload has not been discussed.

(4) Neural networks such as Multilayer Perceptrons, and other similar feed-forward structures have been used to simulate drivers' steering behaviors with the feedback of control error. However, recurrent networks specializing in time-series system simulation have not been adopted in driver models.

(5) Many field experiments have indicated that driver mental workload definitely influences driver's steering performance, but the influence of driver mental workload has not been considered in the simulation of driver behavior models.

Regarding the limitations above, this study pursues the following three objectives:

(1) To propose a relatively objective method for driver mental workload quantification.

The driver mental workload quantification method in the present thesis is based on cluster analysis and competitive neural network quantification of ECG features, which

are analyzed by multiple time-frequency analysis tools, including short time Fourier Transforms and wavelet transforms.

(2) To do a preliminary study on driving risk level modeling for indicating driver mental workload over-reduction.

In this thesis, the driving risk level model is based on the fuzzy space model of the danger zone for a moving vehicle. The danger zone is a two-dimension fuzzy space with adjustable membership functions of risk degree.

(3) To build up two types of neural network-based driver models with the input of the driver mental workload.

The two types of neural network are the classical Multilayer Perceptrons and the Elman recurrent networks. The input of neural network-based driver models contains the continuous variance of the driver mental workload or the average mental workload level.

1.4 Organization of the thesis

Chapter 1 gives an introduction of this research. In Chapter 2, the general framework is introduced. Sec.2.1 introduces the overall structure of driver-vehicle-environment (DVE). Secs. 2.1 to 2.4 present the overall architecture of driver mental workload estimation, the driving risk level estimation, and the driver model simulation. Sec. 2.5 introduces the data source of this research.

In Chapter 3, the method of driver mental workload estimation is discussed. Sec 3.2 introduces the ways of extraction of ECG features in time, frequency, and time-frequency domains. Sec 3.3 discusses mental workload classification and sorting. The driver mental

workload variance is estimated by Learning Vector Quantization neural networks. Sec 3.4 introduces the simulation based on experiment data. Simulation results are discussed and conclusions are drawn.

In Chapter 4, the danger zone based driving risk level estimation method is introduced. Sec 4.2 gives the definitions of driving risk level and the danger zone of a moving vehicle. The fuzzy space model of the danger zone is also discussed in this section. Sec 4.3 proposes a preliminary estimation method of the background driving risk level and the overall driving risk level. Sec 4.4 introduces the simulation based on the experiment data. The relationship between the driving risk level and the driver mental workload is discussed finally.

In Chapter 5, two neural network-based driver models with the input of the driver mental workload are presented. Sec 5.1 briefly reviews the architecture and the training algorithms of Multilayer Perceptrons and recurrent networks. Sec 5.3 proposes two driver models based on the two types of neural networks. Sec 5.4 introduces two-degree-of-freedom vehicle models for vehicle status and driver's performance simulation. Sec 5.5 gives the simulation impacts of the driver mental workload on the driver's performance, and comparisons between the two driver models are made.

Chapter 6 concludes this research. Some recommendations for further research are also included in Chapter 6.

CHAPTER 2 GENERAL FRAMEWORK OF RESEARCH

2.1 Driver model in close-loop DVE systems

In driver – vehicle - environment (DVE) systems, the driver performs steering, throttle controlling, and other actions. The vehicle changes its direction, velocity, and other status accordingly. Then, the driver senses the displacement error (or target track), velocity error, and some other feedbacks (for example, change of road environment) to issue new actions. The whole process is a close-loop control.

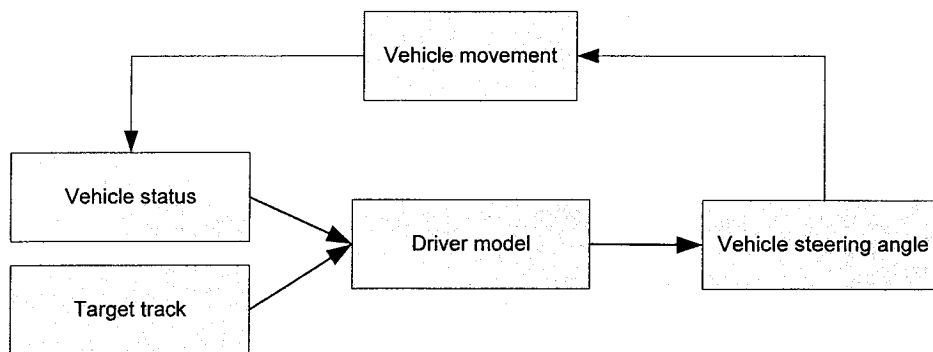


Figure 2-1 A typical close-loop VME system

In the close-loop system mentioned above (Figure 2-1), the driver model ignores the impact of driver's psychological status. As discussed in the literature review in Chapter 1, the driver mental workload and the driving risk level have strong relations with the driver model; therefore they should not be ignored in the driver model study. A new driver model, with reference to existing ones, is proposed in Fig. 2-2.

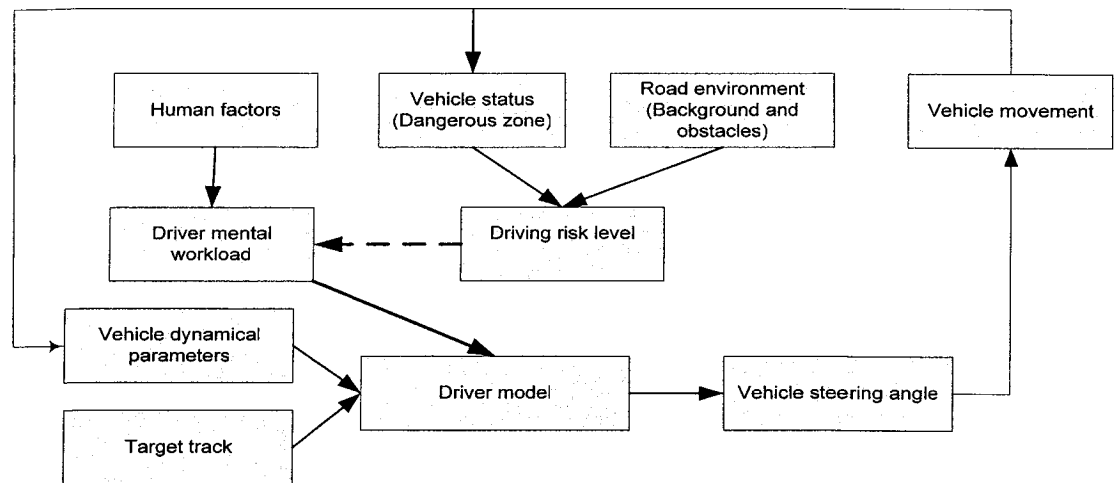


Figure 2-2 A new driver model in VME system

In Figure 2-2, the driver mental workload and the driving risk level are two important components in the new driver model. They will be explained in detail in the following sections.

2.2 Framework of driver mental workload estimation

To estimate the driver mental workload by using competitive neural networks, the first step is to specify the input of the network, but what features are suitable as the inputs of the neural network?

ECG signals contain many features (such as R-wave, T-wave, P-wave, QRS complex, HR, HRV, LF, HF, and LF/HF ratio). Some of these features have strong relations with the operator's MWL alteration, while others have less relation with the operator's MWL change.

In this present study, several typical ECG features being reported as having the capability of indicating the mental workload change are chosen as the neural network input, such as the power spectrum of WQ, LF and HF corresponding to HRV, as well as the LF/HF.

The LVQ (learning vector quantization) algorithm-based competitive network architecture is chosen to estimate the driver's mental workload in this study. The initial weight matrix of LVQ networks is derived by cluster analysis. The feature data representing the driver's mental workload status are classified into N levels. In each level the driver's mental workload is a function of the distance between the feature data and the centroid of the corresponding cluster.

The overall flowchart of the proposed quantification method is shown in Figure 2-3.

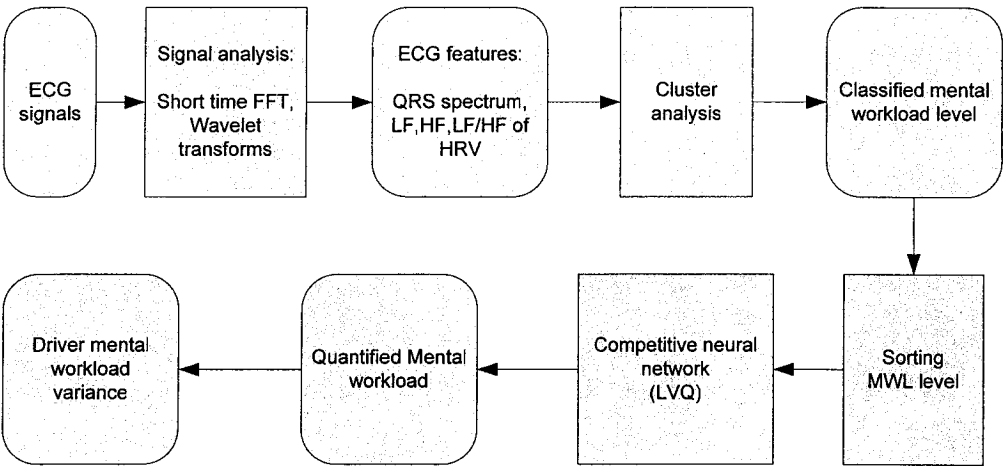


Figure 2-3 Driver mental workload estimation process

2.3 Framework of driving risk level estimation

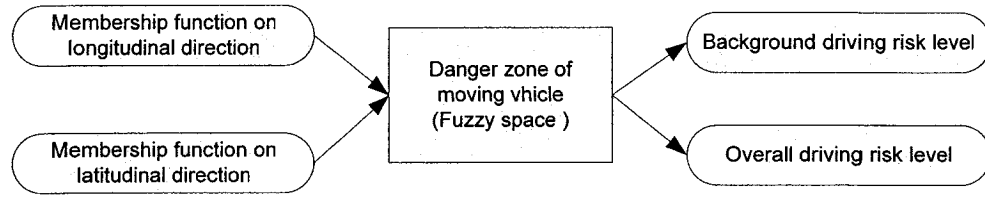


Figure 2-4 Process of driving risk level estimation

Figure 2-4 shows the process of the driving risk level estimation. Firstly, the fuzzy space model of the danger zone for a moving vehicle is constructed by combining two one-dimension membership functions: the membership functions of the driving risk level on the longitudinal direction and on the lateral direction. The time headway and the road shape are two key factors influencing the membership functions of the driving risk. The driving risk level caused by an obstacle is determined by its position in the moving danger zone.

2.4 Framework of driver model building

After estimating the driver mental workload and the driving risk level, the driver model can be implemented in different ways. In this thesis, neural networks are employed to fulfill the new driver model, shown in Figure 2-5.

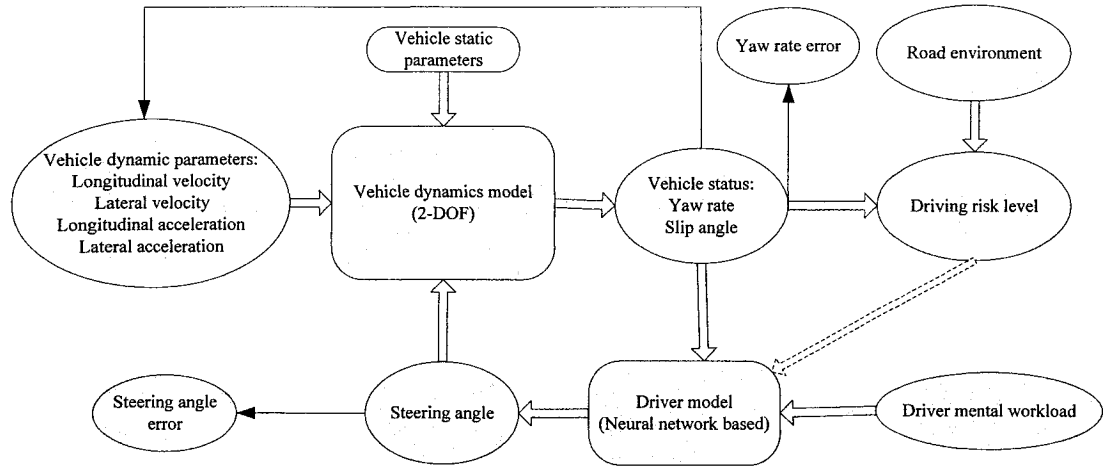


Figure 2-5 New driver model based on neural networks

In Figure 2-5, the dashed line represents the functional part un-implemented in this stage. Two types of neural network-based driver models simulate the steering angle under the influences of a constant driver mental workload and a varied driver mental workload, respectively. The errors of the steering angle between the experiment data and the simulation results indicate which driver model is better for the driver steering performance simulation. According to the further 2-DOF vehicle status simulation, the errors of yaw rate between the experiment data and the simulation value also indicate which driver model is better.

2.5 Data source

The expediency of the proposed models can be investigated in three typical vehicle manoeuvre: single-lane, double-lane, and sine-lane. The single-lane change is the most common vehicle manoeuvre for a driver. It performs the task of lane change. ISO 3888-1

[1999] defines the double-lane change manoeuvre. It performs a surpass action. ISO 3888-2 [2002] defines the sine-lane change manoeuvre. It performs an obstacle avoidance manoeuvre.

The tracks of the three motions are shown in Fig. 2-6.

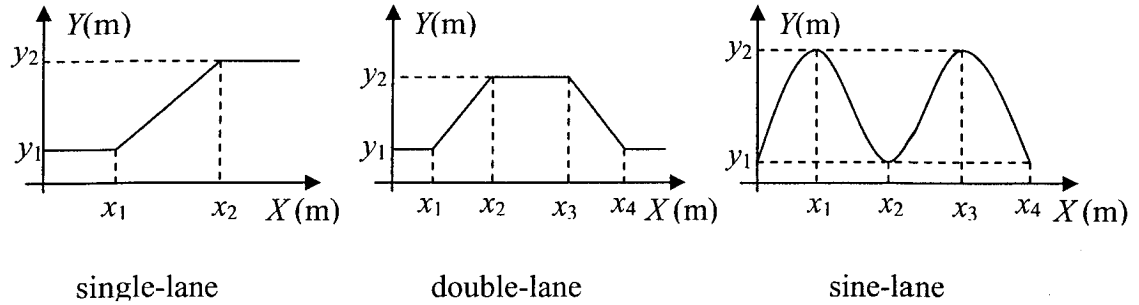


Figure 2-6 Three typical vehicle manoeuvre

The source of the experimental data comes from [Lin, 2005, 1997]. In those experiments, the drivers were required to proceed along the designated route at the required velocity. The following signals were sampled at the rate of 50 points per second: (1) longitudinal velocity, (2) lateral velocity, (3) longitudinal acceleration, (4) lateral acceleration, (5) yaw velocity, (6) roll angle, (7) steering angle, (8) ECG signal.

Table 2-1 shows the manoeuvre performed by a driver named “Y”, who was about 50 years old. In Table 2-1, the first character stands for the manoeuvre type. For example, “P” means single-lane change, “Q” means double-lane change, and “S” means sine-lane motion. The second character, such as “Y”, indicates the driver’s name. The third character stands for the vehicle speed. For instance, “5” means 50 Km/h, “6” means 60 Km/h, “8” means 80 Km/h, and “A” means 100 Km/h. In special, “5h” means 55 Km/h.

The last digit indicates the manoeuvre No. For example, #1 is the first trial and #2 is the second trial of the same type manoeuvre.

Table 2-1 Driving manoeuvre done by driver ‘Y’ [Lin 2005, 1997]

Vehicle Speed (Km/h)	Single-lane change	Double-lane change	Sine-lane motion
50	-	-	SY51
55	-	-	SY5h1
60	PY61, PY62	QY61	SY61
80	PY81, PY82	QY81, QY82	-
100	PYA1, PYA2	-	-

So, PY61 is the #1 single-lane change manoeuvre at 60 Km per hour by the driver “Y” while PY62 is his #2 single-lane change manoeuvre at the same speed. Similarly, QY81 is the #1 double-lane change manoeuvre of the driver “Y” at 80 Km per hour while QY82 is his #2 double-lane change manoeuvre at the same speed.

Based on the experimental data, the simulation of the driver mental workload quantification, the estimation of driving risk level, and the analysis of mental workload influences on drivers’ steering performance can be discussed in this research paper.

Due to the unavailability of the actual precise position of the vehicle, some validation work is limited in this research (discussed in Chapter 5).

CHAPTER 3 DRIVER MENTAL WORKLOAD ESTIMATION

3.1 Introduction

Among the three major mental workload measures: the task performance estimation, the subjective estimation, and the physiological parameters measurement. The ECG signal-based physiological parameters measurement is a very promising estimation method. Although previous research has suggested that heart rate variability and some other ECG features have the potential to indicate the change of the mental workload, few objective methods have been presented to classify the mental workload level and to quantify the variance of mental workload. This chapter presents a method of driver mental workload estimation based on cluster analysis and Learning Vector Quantization (LVQ) neural networks.

In this chapter, the tools of ECG signal analysis including short time FFT transforms and wavelet transforms are introduced firstly. Then, ECG feature data are applied by cluster analysis to determine the number of the mental workload category. LVQ neural networks are used to classify the mental workload level and to estimate the mental workload variance. Finally, the simulation based on the experiment data is done to demonstrate the estimation method.

3.2 ECG features extraction

3.2.1 Features of ECG signals in time domain

ECG signals indicate the working status of the human heart. Figure 3-1 shows a typical ECG signal including the P, Q, R, S, and T waves and some standard durations and segments. QRS complex is the most interesting part in the whole ECG period.

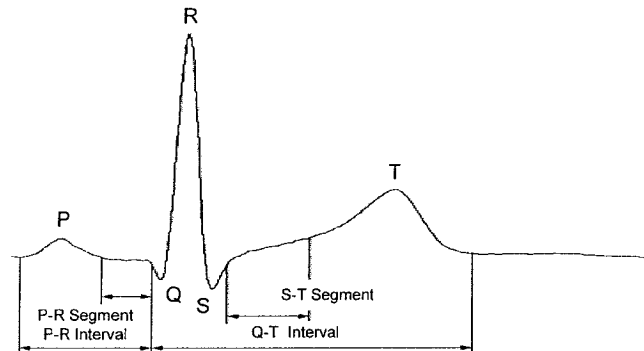


Figure 3-1 A typical cycle of ECG signal

A continuous ECG signal is comprised of many ECG cycles (Figure 3-2). In the time domain, the width of QRS complex, the heart rate (Figure 3-3) and the heart rate variability (Figure 3-4) are three key features and have potential to be used to assess the mental workload variance; however, human's ECG signals do not definitely show all P,Q,R,S,T waves in high-demanding working environment compared with the regular ECG signal pattern in the rest situation. Therefore, it may be difficult to recognize the start point and the end point of QRS complex due to the irregular ECG signal pattern. Furthermore, ECG signals may expose some abnormal characteristics related to medical problems. Recent development has enabled the analysis of frequency components based

on the mathematical manipulations performed on the same ECG-derived data, such as the Fourier transform and wavelet transform (WT).

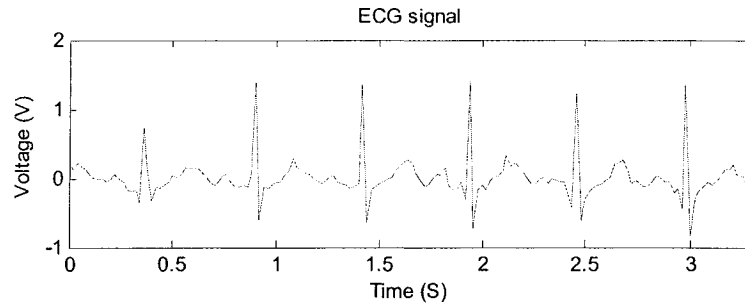


Figure 3-2 A continuous ECG signal

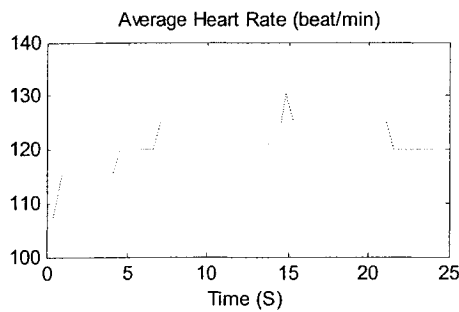


Figure 3-3 Moving averaged heart rate

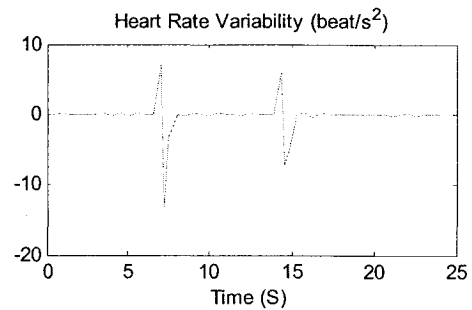


Figure 3-4 Instant heart rate variability

3.2.2 FFT analysis of ECG signals

(1) Classical FFT analysis

In general, for a continuous signal $x(t)$, its frequency spectrum $X(\omega)$ can be derived by the Fast Fourier Transform (FFT) (Young, 1985).

ECG signals are not strict periodic signals, but there are similarities between the heart beat cycles (P-P cycles). When the FFT transformation is applied to a long duration ECG

signal, its corresponding frequency spectrum in the whole time period can be obtained, but the frequency variance between adjacent P-P cycles cannot be observed.

(2) Segmented FFT analysis

In order to view the frequency change between the adjacent heart beat cycles, the long duration ECG signal can be cut into many segments (Figure 3-5). In each segment, there is only one P-P cycle and one R wave. Then the FFT transform can be applied to each P-P segment. Because the FFT transformation is applied to a segmented ECG signal, this process is also called segmented ECG FFT analysis. The segmented ECG FFT analysis can provide detail information of each ECG cycle along the time axis.

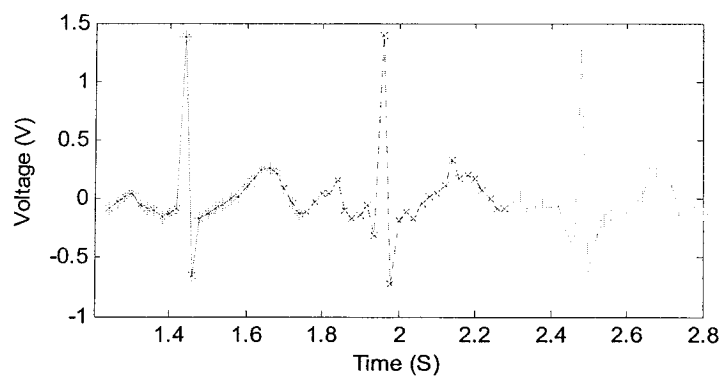


Figure 3-5 Segmented ECG signal

In practical, due to the limited sample frequency (must higher than the Nyquist Frequency), the total number of samples in an ECG cycle may be also very limited, so a piecewise cubic interpolation could be performed on each ECG cycle (Figure 3-6). The cubic interpolation method can preserve the monotony and the shape of the original curve.

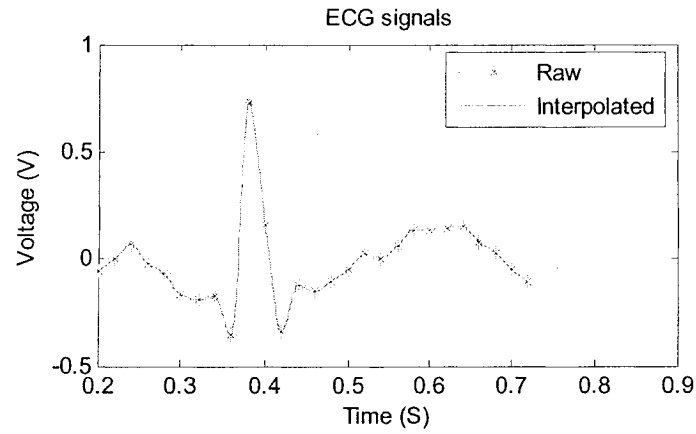


Figure 3-6 Interpolated ECG cycle

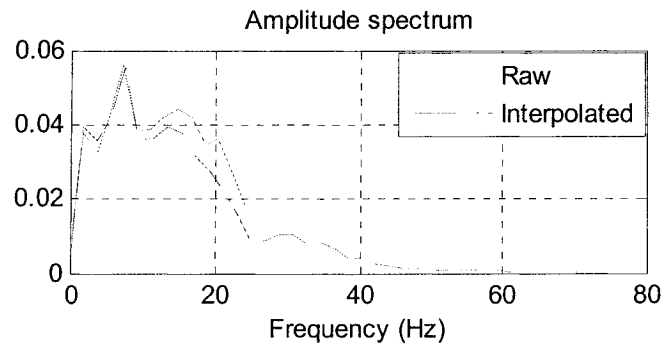


Figure 3-7 Amplitude spectrum of a segmented ECG signal

Figure 3-7 illustrates the amplitude spectrum of a raw ECG cycle shown in Figure 3-4, and the amplitude spectrum of its corresponding interpolated signal. Their amplitude spectrums are very similar, but the interpolated one shows more detail information of the high frequency components.

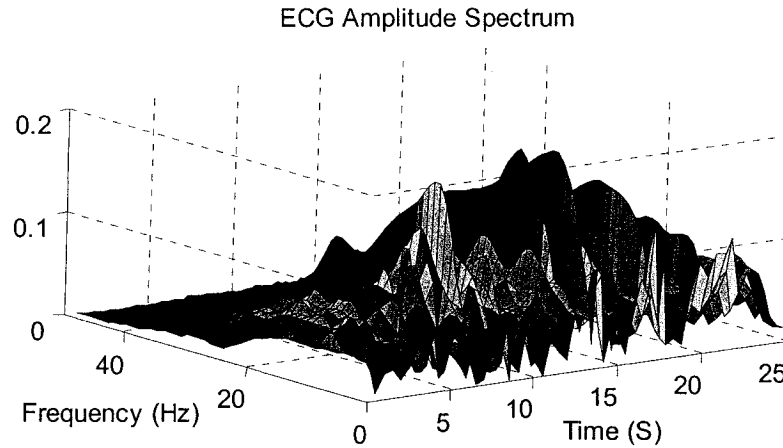


Figure 3-8 Amplitude spectrum of a continuous ECG signal

In Figure 3-8, the power spectrum of a continuous ECG signal is shown in sliced ECG cycles. In other words, the FFT analysis is performed on each segmented ECG cycle.

For each ECG cycle, the mean value and standard deviation of power spectrums are two important variables to represent its characteristics.

Figure 3-9 shows the mean value and the standard deviation of segmented ECG amplitude spectrums changing with time. The change of the mean value and standard deviation indicates the alternation of the heart activity, so it has potential to indicate the change of the mental stress. In fact, compared with the steering angle in the same figure 3-9, the abrupt alteration section of the mean value and the standard deviation is just the moment for the driver to steer the vehicle to make a lane change manoeuvre.

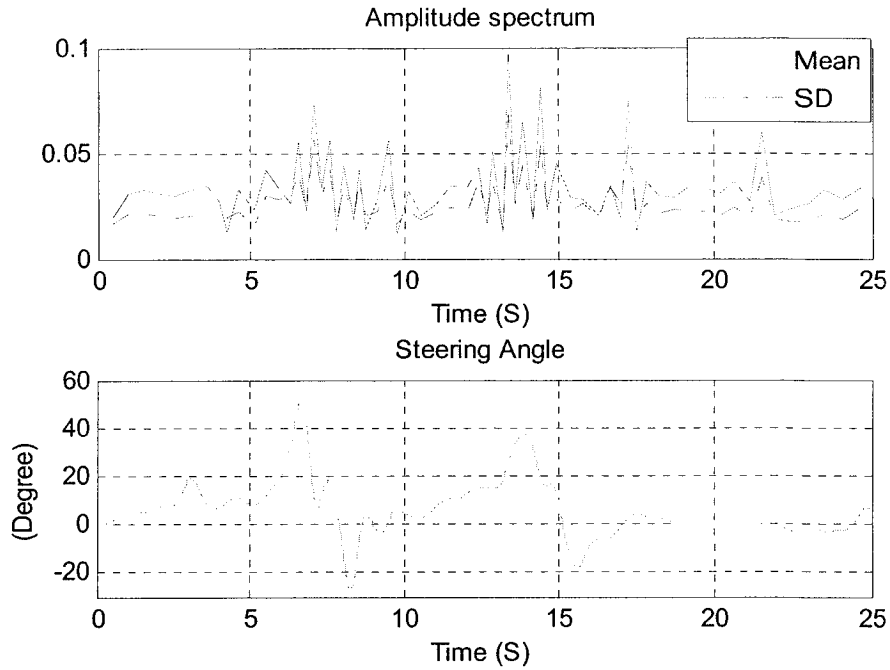


Figure 3-9 ECG amplitude spectrum vs steering angle

Obviously, there is a disadvantage for the segmented ECG FFT analysis. Although the distribution of the frequency and power spectrums of a long duration continuous ECG signal can be analyzed cycle by cycle, the time resolution of segmented ECG FFT analysis is decided by the length of ECG cycles, usually varying from 0.3 to 1 second. Moreover, to cut ECG signal to individual ECG cycles is another tedious manual work. In order to explore the detail information of frequency variance within 0.3 seconds, other methods have to be concerned. Short time FFT is just an improved FFT analysis method based on the automatic signal segmentation.

(3) Short Time FFT

In order to oversee the change of a signal's frequency components varied with time, the signal should be automatically cut into separate sections and then the corresponding

spectrum of each section can be calculated. This improved spectrum analysis method is called Short Time Fourier Transform (STFT). It is usually used to compute the windowed discrete-time Fourier transform of a signal using a sliding window (Young, 1985).

$$X(\omega, m) = \sum_{n=-\infty}^{\infty} x(n-m)\omega(n)e^{-j\omega n} \quad (3.1)$$

$$X(\omega, m) = \sum_{n=0}^{R-1} x(n-m)\omega(n)e^{-j\omega n} \quad (3.2)$$

Where $\omega(n)$ is the window function with a window length R . The window function cuts the raw signal to separate sections by sliding with time. One of the commonly used window functions is the Hamming window.

The STFT of a signal is a function of two variables: time and frequency. STFT can indicate the strength of particular frequency components at a given instant. To calculate STFT, the following parameters should be chosen: the length and the type of the sliding window, the amount of overlap between the adjacent signal sections. Generally, the STFT analysis can provide higher resolution on time than the classical FFT analysis.

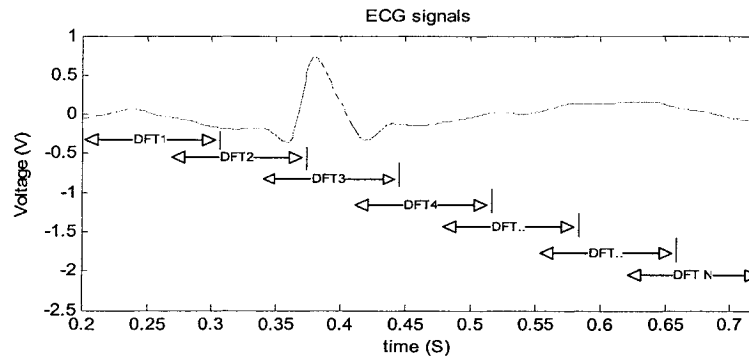


Figure 3-10 Sliding windows of STFT on an ECG cycle

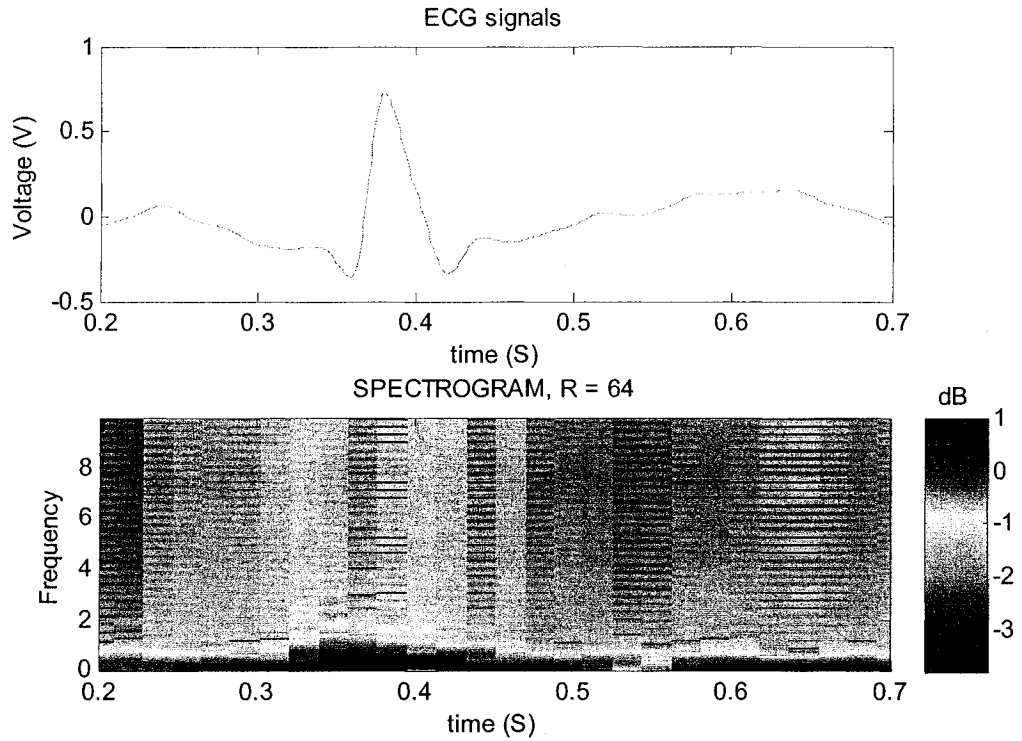


Figure 3-11 One ECG cycle and its corresponding STFT

In Figure 3-11, the frequency-amplitude characteristics of an ECG signal at each time point can be observed. The frequency spectrum of R wave that contains the ECG peak show richer components than those of other waves.

3.2.3 Wavelet analysis of ECG signals

3.2.3.1 Wavelet transforms

Similar to the Fourier transform, the wavelet transform is another well-known signal analysis tool. Fourier transforms and wavelet transforms represent the expansion of a continuous-time signal or a discrete-time signal on a serial of sine waves and wavelet bases, respectively. Unlike sine waves, extending from minus infinity to plus infinity, a

wavelet is a limited duration signal and has an average value of zero. The wavelet transform is a linear operation, which decomposes a signal into a serial of shifted and scaled wavelet base functions.

Generally, $\psi(t)$ is an oscillatory signal and the sum of area is zero [Sahambi et al., 1997]. Usually, a group of wavelet functions can be gotten from the base function $\psi(t)$ and they are $\frac{1}{\sqrt{a}}\psi(\frac{t-\tau}{a})$, Where a is a scale factor and τ is a position parameter. The wavelet transform of a function $f(t)$ is represented as [Sahambi et al., 1997]:

$$Wf(a, \tau) = \frac{1}{\sqrt{a}} \int_{-\infty}^{\infty} f(t) \psi^*\left(\frac{t-\tau}{a}\right) dt \quad (3.3)$$

Where $\psi^*\left(\frac{t-\tau}{a}\right)$ denotes the complex conjugation of $\psi\left(\frac{t-\tau}{a}\right)$.

Scale a and position τ are two key parameters of wavelet transforms. For a small values of scale a , the wavelet transform gives information of detail parts of signal $f(t)$, i.e. the high frequency components; For a large value of scale a , the wavelet transform gives information of global view of $f(t)$, i.e. the low frequency components.

Not all mother wavelets have explicit expressions, so filters are commonly used for the analysis of the approximations and the details. The approximations are the high-scale, low-frequency components of the signal, while the details are the low-scale, high-frequency components of the signal.

3.2.3.2 Wavelet transforms of ECG signals

In the wavelet transform analysis, there are two types of transform used frequently: continuous wavelet transforms and discrete wavelet transforms. For continuous wavelet transforms, the scale a usually changes in $1, 2, 3, 4, \dots, N$. N is a positive number, but for discrete wavelet transforms, the scale a usually changes in $1, 2, 4, 8, \dots, 2^N$.

In Figure 3-12, an ECG signal in one cycle and its continuous wavelet transform are shown. The mother wavelet function is the Daubechies wavelet. The coefficients of the wavelet transform represent the characteristics of the original signal.

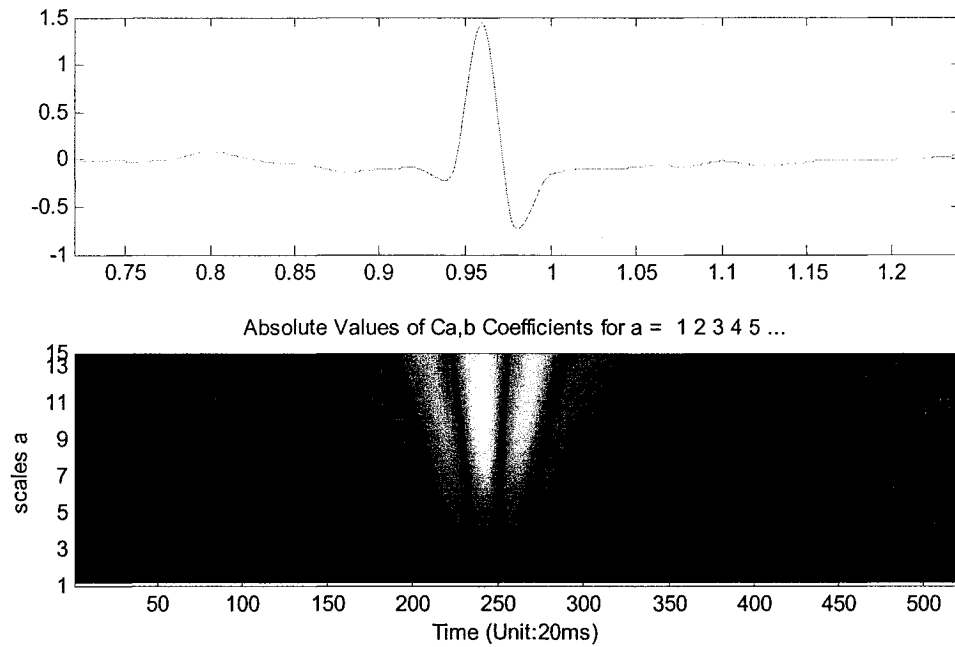


Figure 3-12 ECG signal and its continuous wavelet transform

3.2.3.3 ECG features extraction by wavelet transforms

(1) Features of power spectrum

Usually, R peaks can be located easily in the time-domain. Minami et al. (1999) pointed out that the normal length of the QRS window is 256 ms. When a more accurate QRS width is required, the algorithm including Q, R, and S wave peaks locating (Li et al., 1995) can be applied.

After the determination of the beginnings and the endings of QRS complexes, FFT is performed on each QRS complex to get the corresponding power spectrum. Five components of the power spectral with the central frequencies at 3.9, 7.8, 11.7, 15.6, and 19.5 Hz (Minami et al., 1999) are selected as the features expressed with P_{f1} , P_{f2} , P_{f3} , P_{f4} , and P_{f5} .

(2) LF and HF extraction

DWT coefficients of the discrete ECG signal $x(n)$ have relations with the frequency domain, shown as Table 3-1 (Murai et al., 2001). Therefore, the LF and HF components can be extracted easily.

Table 3-1 Relations between wavelet coefficients and frequency domain

Frequency components	Wavelet coefficients	Frequency domain (Hz)
HF	$W_{2^1}x(n)$	0.25 - 0.5
	$W_{2^2}x(n)$	0.125 - 0.25
LF	$W_{2^3}x(n)$	0.0625 - 0.125
	$W_{2^4}x(n)$	0.03125 - 0.0625

The LF corresponds to the sum of the DWT coefficients of the ECG signal $x(n)$ at scales 2^3 and 2^4 , while the HF corresponds to the sum of the DWT coefficients of the ECG signal $x(n)$ at scales 2^1 and 2^2 . After the calculation of LF and HF, it is very easy to calculate the LF/HF ratio, expressed as LHR.

3.3 Methodology of mental workload estimation

Normally, drivers' routine actions in driving can be roughly classified into the following three typical vehicle manoeuvre: single-lane change, double-lane change, and sine-lane motion. A driver's mental workload may vary with time and the motion type. Based on a common sense, it would be reasonable to grade the driver mental workload (MWL) in several levels, such as baseline, a little high, high, and very high. Accordingly, the variance tendency of mental workload can be observed by looking at the alteration of the driver's mental workload level.

However, the essential problem is how many levels of a driver's MWL should be divided into. Specifying N , the number of MWL levels, completely by subjectivity is the simplest way, and an effective way in some circumstances. But this method may be not a good one because it is too subjective. In contrast, it is a good way to specify the number N based on the cluster analysis of ECG features.

3.3.1 Clustering analysis of ECG features

Assume \mathbf{X} is a n -by- p data matrix of ECG features. Rows of \mathbf{X} , n corresponds to the time points, columns p corresponds to the variables which stands for the ECG features at the same time point. Currently, there are 8 types of ECG feature so $p = 8$.

In cluster analysis, the distance between different sub-sets is used to measure the similarity of categorical data. The commonly used dissimilarity measures contain Euclidean distance, City block distance, and Pearson correlation [Jambu, 1983].

$$\text{Euclidean distance } d_{ij} = \left(\sum_{k=1}^p (x_{ik} - x_{jk})^2 \right)^{1/2} \quad (3.4)$$

$$\text{City block distance } d_{ij} = \sum_{k=1}^p |x_{ik} - x_{jk}| \quad (3.5)$$

Pearson correlation $\delta_{ij} = (1 - \phi_{ij}) / 2$ with

$$\phi_{ij} = \sum_{k=1}^p (x_{ik} - \bar{x}_{i\bullet})(x_{jk} - \bar{x}_{j\bullet}) / \left(\sum_{k=1}^p (x_{ik} - \bar{x}_{i\bullet})^2 \sum_{k=1}^p (x_{jk} - \bar{x}_{j\bullet})^2 \right)^{1/2} \quad (3.6)$$

$$\text{Where } \bar{x}_{i\bullet} = \frac{1}{p} \sum_{k=1}^p x_{ik} \text{ and } \bar{x}_{j\bullet} = \frac{1}{p} \sum_{k=1}^p x_{jk}.$$

In this study, city block distance is used. For each sub sets, or called cluster, there is a centroid. The cluster analysis performs an iterative algorithm to minimize the sum of point-to-centroid distances over all clusters.

3.3.2 Determining the number of mental workload level

Denote Q as the set formed by the ECG features collected from three types of vehicle manoeuvre at different speeds. A clustering algorithm is employed to partition set Q into 2, 3, 4, 5, or more sub-sets. Because there is no much meaning to classify the mental workload into two levels only, we are certain that the number N should have to lie within the numbers of sub-sets c . Let $c \in [3, 4, 5, \dots]$ be the number of sub-sets, and $d(c)$ represent the average distance between c sub-sets. Because the larger the distance is, the greater dissimilarity between the categories is, the reasonable and optimal number of sub-sets is satisfied with

$$N = \arg \max_c \{d(c)\} \quad (3.7)$$

N means the driver mental workload in a specific situation can be roughly classified into N levels. When the number of total levels of driver mental workload is determined, the centroid of each sub-set is also determined.

3.3.3 Sorting the mental workload levels

The cluster analysis implies that the driver's mental workload is best to be divided into N levels corresponding to the determined centroids. However, it is unknown that which centroid corresponds to the specific MWL level. In other words, we really do not know which MWL level corresponds to the specific centroid exactly. In order to solve this problem, several representative sections of ECG signal are picked up from each sub-set firstly. Then let FFT to be performed on the corresponding ECG strips, so the power spectrum of each representative ECG strip can be derived. Finally the mean value of the

power spectrum $M_{p_i} (i = 1, 2, \dots, N)$ and the mean value of the frequency spectrum $M_{f_i} (i = 1, 2, \dots, N)$ can be calculated. Rearrange $M_{p_i} (i = 1, 2, \dots, N)$ and $M_{f_i} (i = 1, 2, \dots, N)$ in ascending order as the follows.

$$M_{p_1} < M_{p_2} < M_{p_3} < M_{p_4} \quad (3.8)$$

$$M_{f_1} < M_{f_2} < M_{f_3} < M_{f_4} \quad (3.9)$$

As a usual rule, the heavier the driver's MWL is, the richer the frequency is in the power spectrum, i.e., the bigger the mean value is. This tendency can be also observed from Figure 3-9. Thus M_{p_1} or M_{f_1} corresponds to the baseline, while M_{p_N} or M_{f_N} corresponds to the heaviest MWL. If the rank of $M_{p_i} (i = 1, 2, \dots, N)$ and $M_{f_i} (i = 1, 2, \dots, N)$ is not the same, it would be better to use the rank of $M_{f_i} (i = 1, 2, \dots, N)$ to sort the mental workload levels.

Table 3-2 Define the variance scope of each MWL level

MWL level	MWL	Meaning
<i>Level 1</i>	[0, 0.25)	Baseline
<i>Level 2</i>	[0.25, 0.5)	A little high
<i>Level 3</i>	[0.5, 0.75)	High
<i>Level 4</i>	[0.75, 1]	Very high

If the cluster analysis suggests the driver mental workload could be divided into four levels. Then, the variance scope of each mental workload level can be defined as Table 3-2.

Where, the value scope of each MWL level keeps roughly consistence with the RSME (Rating Scale Mental Effort) scale [Appendix A], but not exactly. Overall, the interval [0, 1] in Table 3-2 corresponds to the interval [0, 110] of RSME scale.

RSME is a subjective scale to rate the overall MWL in a specific task and it is not used for estimating the MWL variance in real time. In the RSME scale, the mental effort is scaled from 0 to 150. Where, 0 indicates absolutely no effort, 26 indicates a little effort, 57 indicates rather much effort, 85 indicates great effort, and 112 indicates extreme effort.

3.3.4 Mental workload estimated by competitive networks

The LVQ (learning vector quantization) competitive network is designed in two layers: the competitive layer and the linear combining output layer. The competitive layer classifies the input vectors into several different categories through competition, while the output layer calculates the driver's MWL in each category.

In this thesis, the five typical components of the QRS power spectrum, LF and HF, as well as the LF/HF ratio of HRV are constructed into the input vectors with eight variables. Because the driver's MWL is divided into N levels by using cluster analysis, the competitive neural network is designed to have N competitive neurons corresponding to N different levels. On each level, the driver's MWL is a function of the distance between the input vector and the centroid of the features in that level.

Denote the input vector of the LVQ competitive network as

$$\begin{aligned} p_j &= [P_{f1}, P_{f2}, P_{f3}, P_{f4}, P_{f5}, LF, HF, LHR]^T \\ &= [p_{j1} \quad p_{j2} \quad \cdots \quad p_{j8}]^T \end{aligned} \quad (3.10)$$

Where $j = 1, 2, \dots$ stands for the numbering of all ECG feature data. According to the LVQ algorithm, we can obtain the output vector \mathbf{a} of the competitive layer as

$$\mathbf{a} = [a_1 \quad a_2 \quad \dots \quad a_N]^T = \text{compet}(\mathbf{p}^1) \quad (3.11)$$

$$\mathbf{p}^1 = - \begin{bmatrix} p_1^1 \\ p_2^1 \\ \vdots \\ p_N^1 \end{bmatrix} = - \begin{bmatrix} \|\mathbf{w}_1 - \mathbf{p}_j\| \\ \|\mathbf{w}_2 - \mathbf{p}_j\| \\ \vdots \\ \|\mathbf{w}_N - \mathbf{p}_j\| \end{bmatrix} \quad (3.12)$$

where $\mathbf{W}_{N \times 8} = [\mathbf{w}_1 \quad \mathbf{w}_2 \quad \dots \quad \mathbf{w}_N]^T$ represents the weight matrix, \mathbf{w}_i ($i = 1, 2, \dots, N$) is called as weight vector, and $\text{compet}(\cdot)$ is a competitive function which sets '1' to the neuron corresponding to the input vector closest to the weight vector. This neuron is called the victorious one which means that the driver's MWL belongs to one of the N levels. For example, if the driver's MWL is on the i^{th} level, then $\mathbf{a} = [0 \quad 0 \quad \dots \quad a_i = 1 \quad 0 \quad 0]^T$.

Denote $\mathbf{c}_i = [c_{i1} \quad c_{i2} \quad \dots \quad c_{i8}]^T$ ($i = 1, 2, \dots, N$) as the centroid of the i^{th} level, and D_i as the sub-set formed by all input vectors belonged to the i^{th} level, then the driver's MWL y_i on the i^{th} level can be calculated as:

$$y_i = a_i \times \left[\frac{y_i^{\min} - y_i^{\max}}{d_i^{\max} - d_i^{\min}} \times d_i^k + \frac{y_i^{\max} d_i^{\max} - y_i^{\min} d_i^{\min}}{d_i^{\max} - d_i^{\min}} \right] \quad (3.13)$$

$$d_i^k = \|\mathbf{c} - \mathbf{p}_k\|, \mathbf{p}_k \in D_i, k = 1, 2, \dots, K \quad (3.14)$$

$$d_i^{\max} = \max \{d_i^k\} \quad (3.15)$$

$$d_i^{\min} = \min \{d_i^k\} \quad (3.16)$$

where K is the number of the elements in sub-set D_i , y_i^{\max} and y_i^{\min} are the maximum and minimum value of the driver's MWL in the i^{th} level respectively, and are determined by the rank of the level. Denote b_i , \mathbf{B} and \mathbf{Y} as

$$b_i = \frac{y_i^{\min} - y_i^{\max}}{d_i^{\max} - d_i^{\min}} \times d_i^k + \frac{y_i^{\max} d_i^{\max} - y_i^{\min} d_i^{\min}}{d_i^{\max} - d_i^{\min}} \quad (3.17)$$

$$\mathbf{B} = [b_1 \quad b_2 \quad \cdots \quad b_N]^T \quad (3.18)$$

$$\mathbf{Y} = [y_1 \quad y_2 \quad \cdots \quad y_N]^T \quad (3.19)$$

According to Eq.(3.33), the output vector \mathbf{Y} of the competitive neural network can be calculated as

$$\mathbf{Y} = \mathbf{a} \cdot \mathbf{B} \quad (3.20)$$

where “ \cdot ” represents dot product.

The overall structure of the LVQ competitive network is demonstrated in Fig.3-13.

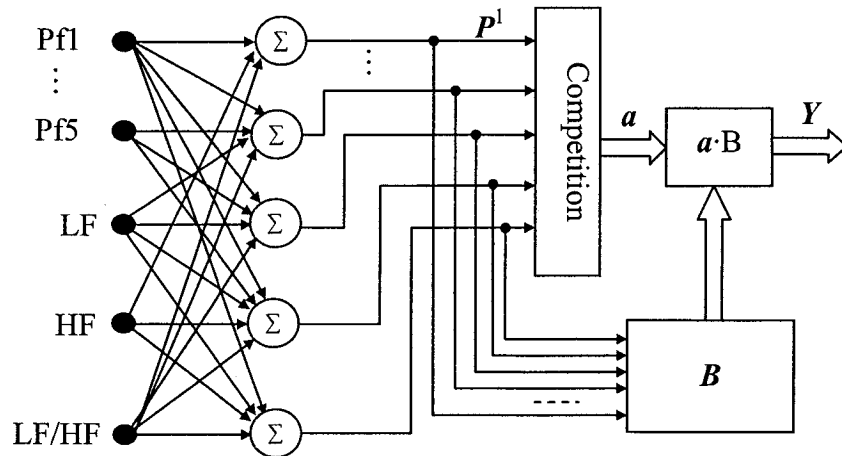


Figure 3-13 Overall structure of the LVQ competitive network

3.4 Experiment and simulation

3.4.1 ECG features in the typical vehicle manoeuvre

The data source has been introduced in section 2.5. For the collected ECG signals, the ECG features can be extracted according to the algorithm introduced in section 3.2.

Figure 3-14 shows the continuous ECG signal of driver ‘Y’ in the #1 single-lane change manoeuvre at 60 Km per hour.

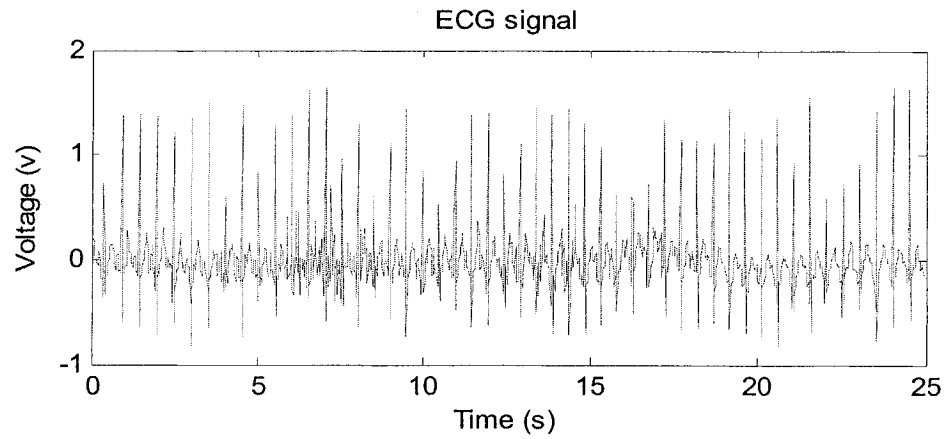


Figure 3-14 ECG signal of driver ‘Y’ (#1 single-lane, 60km/h)

Normally, based on the algorithm of local maximum judgment, the peaks of R waves can be recognized in the time domain when there is little noise in the raw ECG signals. However, when the raw ECG signal has been interfered by heavy noise, the wavelet analysis based R wave recognition algorithm, introduced in the section 3.2 has to be adopted.

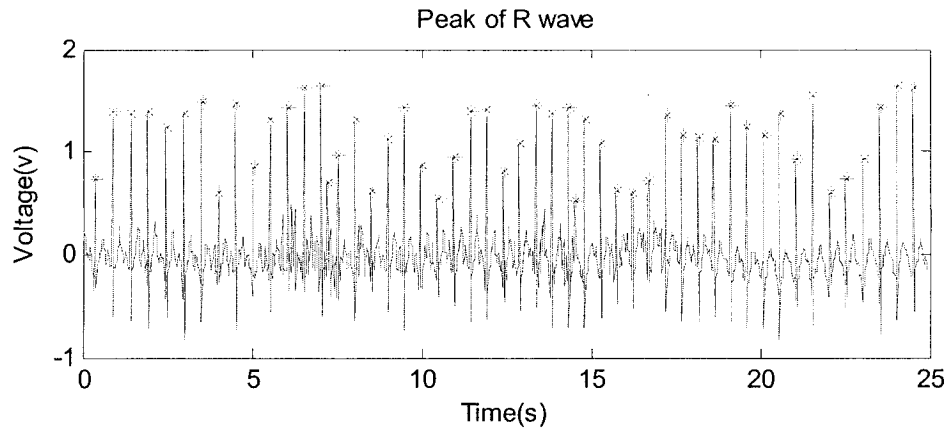


Figure 3-15 Peaks of R waves (driver 'Y', #1 single-lane, 60Km/h)

(1) QRS complex

After the peaks of R waves have been located (Figure 3-16), the QRS complex can be picked out according to the algorithm introduced in the section 3.2. Figure 3-18 shows an ECG QRS complex and its power spectrum. This QRS complex belongs to the ECG signal of driver 'Y' in the #1 single-lane change at 60 Km per hour.

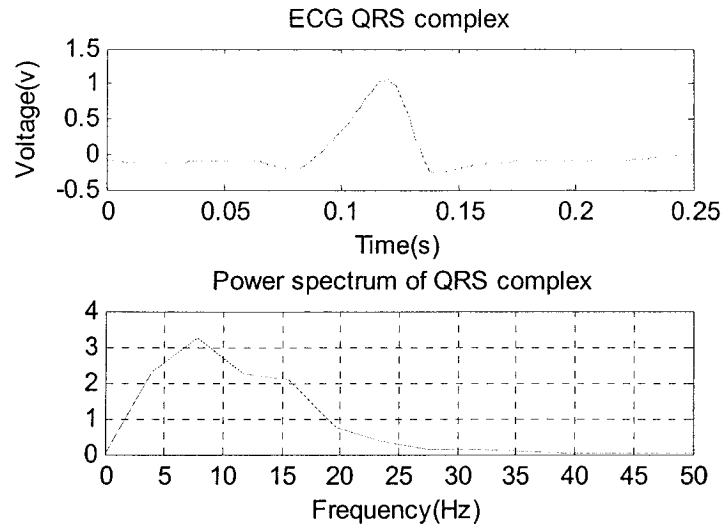


Figure 3-16 ECG QRS complex and its power spectrum

(Driver 'Y', #1 single-lane, 60Km/h)

Table 3-3 shows the representative frequencies and the corresponding power values of the QRS complex in Figure 3-18. Thus, the QRS complex is characterized by the five components of its power spectrum.

Table 3-3 Representative frequencies and the corresponding power value

i	1	2	3	4	5
f_i (Hz)	4	8	12	16	20
P_{fi}	2.31	3.24	2.23	2.09	0.73

Figure 3-17 shows the five power components of QRS complexes which belong to driver 'Y' in the #1 single-lane change manoeuvre at 60 Km per hour. This manoeuvre lasts 25 seconds.

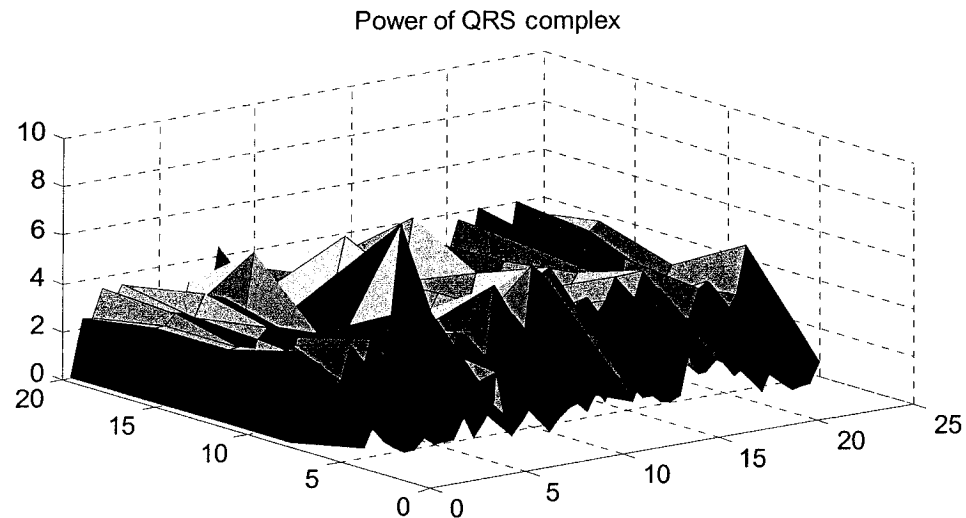


Figure 3-17 Power distribution of QRS complexes
(Driver 'Y', #1 single-lane, 60 Km/h)

(2) HRV

Figure 3-18 shows the heart rate variability of driver 'Y' in the #1 single-lane change manoeuvre at 60 Km/h. Although the value of HRV is usually very small, less than 0.5 beat/s per second, it does alter significantly at some points. The abrupt change implies the suddenly irregular activities of the driver's heart. In fact, it indicates the moment of driver's mental workload change.

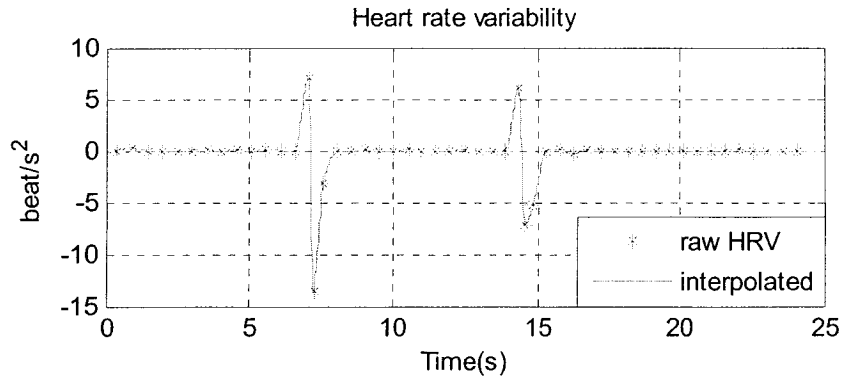


Figure 3-18 Heart rate variability of driver 'Y' (#1 single-lane, 60Km/h)

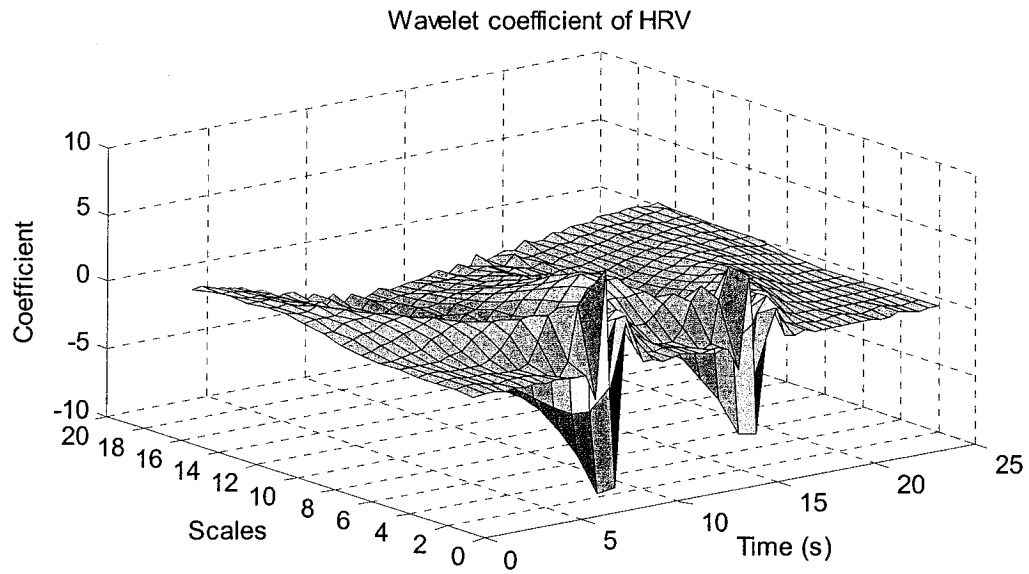


Figure 3-19 Wavelet coefficients of HRV (Driver 'Y', #1 single-lane, 60km/h)

Figure 3-19 shows the wavelet coefficients of HRV shown in Figure 3-18. The transform scales vary from 1 to 20. According to section 3.2, the low frequency components (LF) are characterized by the sum of coefficients at scales 2^3 and 2^4 . The

high frequency components (HF) are characterized by the sum of coefficients at scales 2^1 and 2^2 . The corresponding curves of LF, HF, LF/HF are shown in Figure 3-20.

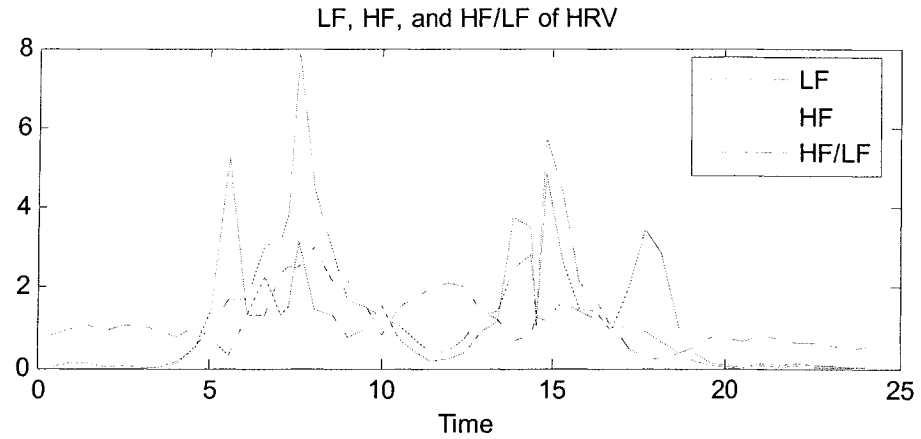


Figure 3-20 LF, HF, and HF/LF of the heart rate variability

Similar to the above process, the ECG features of the driver 'Y' in all other trials (Table 2-1) can also be abstracted.

3.4.2 Clustering results of ECG feature samples

When ECG features have been extracted, the feature data of selected motions can be put together to be set Q (Table 3-4) for clustering. The selected ECG features include those data in the single-lane change manoeuvre at 60 Km/h (Figure 3-21), the double-lane change manoeuvre at 80 Km/h (Figure 3-22), and the sine-lane motion manoeuvre at 60 Km/h (Figure 3-23).

Table 3-4 Set Q of ECG features

	t_1	t_2	t_3	t_4	t_5	t_6	t_n
P_{f1}	0.69269	1.6315	0.79241	0.47432	0.28112	0.25856	...
P_{f2}	0.065178	3.7548	3.3597	3.0604	1.7068	2.2705	...
P_{f3}	0.024617	2.9249	2.9164	1.842	3.1218	3.5589	...
P_{f4}	0.041918	2.92	2.9483	3.3697	3.2882	3.0988	...
P_{f5}	0.016136	2.4702	2.343	3.5245	2.6797	3.5749	...
LF	0.80406	0.98704	1.0439	0.9239	1.0526	1.0768	...
HF	0.034455	0.12019	0.11493	0.04162	0.056719	0.031626	...
HF / LF	0.042851	0.12177	0.1101	0.045048	0.053886	0.029371	...

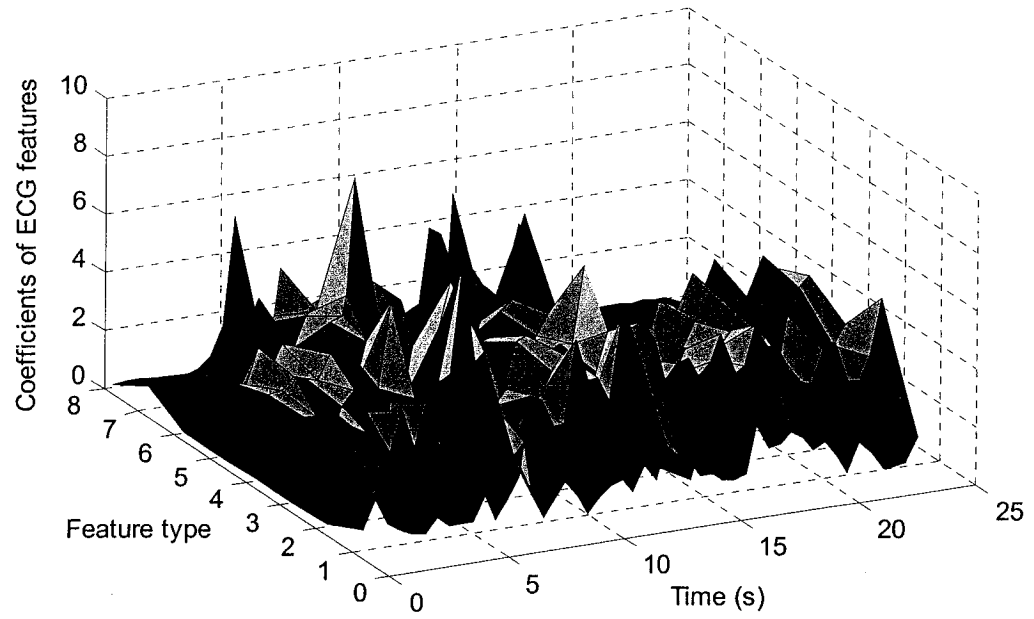


Figure 3-21 ECG features of the #1 single-lane change manoeuvre (60Km/h)

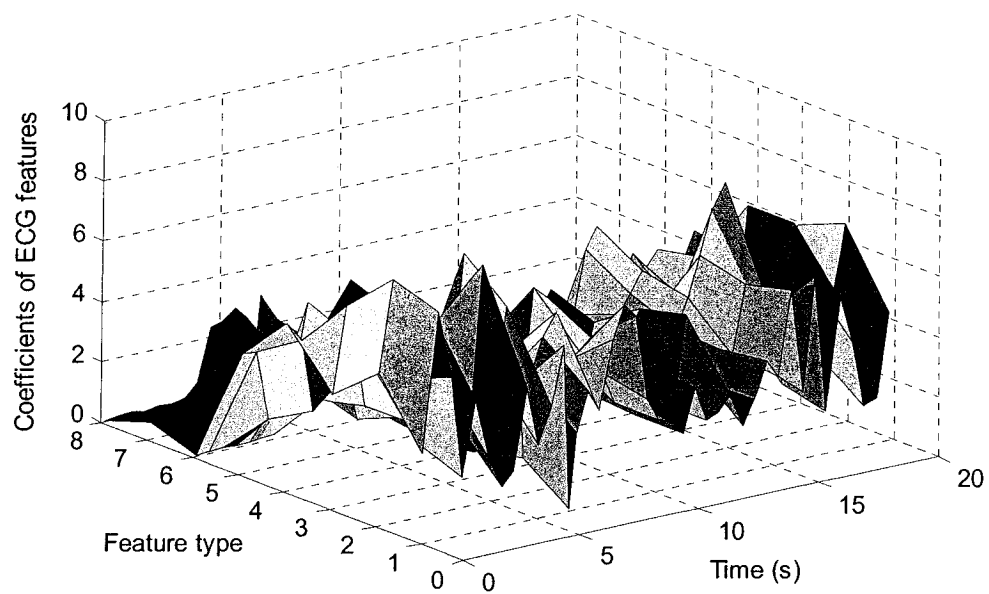


Figure 3-22 ECG features of the #1 double-lane change manoeuvre (80Km/h)

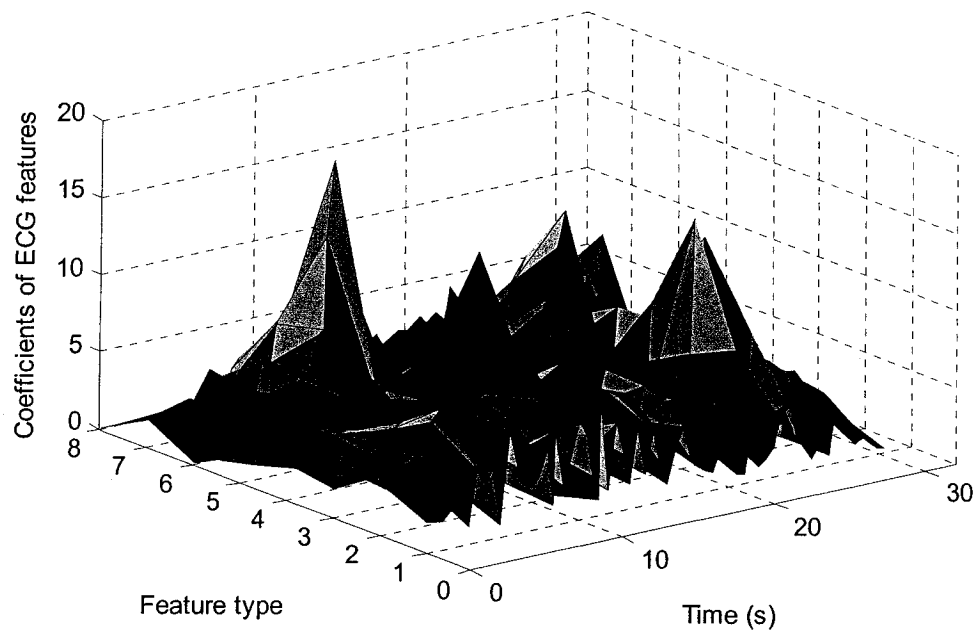


Figure 3-23 ECG features of the #1 sine-lane motion manoeuvre (60Km/h)

According to the method introduced in section 3.3, the ECG feature data can be divided into 3, ..., N clusters. The average distances of N clusters are shown in Table 3-5.

Table 3-5 Average distance $d(c)$ for different cluster numbers

	$c=2$	$c=3$	$c=4$	$c=5$	$c=6$...
$d(c)$	0.3420	0.1948	0.2456	0.1535	0.1704	...

Although $d(2)$ is the biggest one, implying that it is better to divide the driver's mental workload to two levels in such a short time trial, it is too coarse to analyze it in depth. Except $c=2$, the biggest average distance among Table 3-5 appears at $c=4$, so it is reasonable that the driver's mental workload in the experiments is divided into four levels. When $N=4$, the clustering results of the set Q are shown in Fig.3-26, 3-27, and 3-28.

Fig. 3-24 shows the result of ECG features clustering in the #1 single-lane change manoeuvre at 60 Km per hour. Fig. 3-25 shows the result of ECG features clustering in the #2 double-lane change manoeuvre at 80 Km per hour. Fig. 3-26 shows the result of ECG features clustering in the #1 sine-lane motion manoeuvre at 60 Km per hour. The horizontal axis represents time. The vertical axis indicates the category number of ECG features belonging to at that specific time.

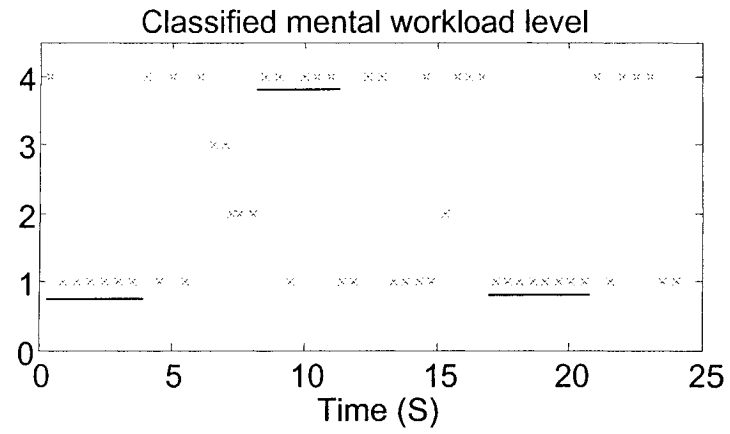


Figure 3-24 MWL Level of the #1 single-lane change manoeuvre (60Km/h)

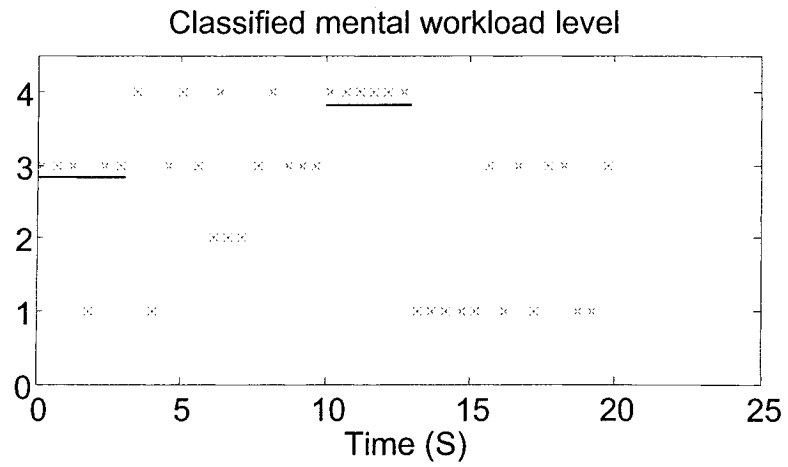


Figure 3-25 MWL Level of the #2 double-lane change manoeuvre (80Km/h)

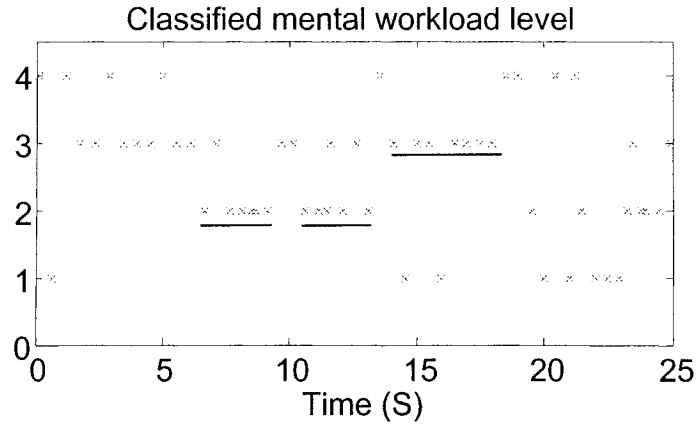


Figure 3-26 MWL Level of the #1 sine-lane motion manoeuvre (60Km/h)

Table 3-6 Cluster centroids of four MWL levels

	P_{f1}	P_{f2}	P_{f3}	P_{f4}	P_{f5}	LF	HF	HF / LF
<i>Level 1</i>	0.8451	2.277	1.8507	1.4791	1.0436	0.066322	0.69587	0.67681
<i>Level 2</i>	2.5161	3.4812	2.7255	1.6285	1.0093	4.7283	3.8794	1.588
<i>Level 3</i>	1.0349	3.0082	2.9783	3.0168	2.8515	0.044528	0.34835	0.64069
<i>Level 4</i>	4.009	5.2458	5.3055	3.6254	3.1474	0.30359	1.6338	0.22665

Unfortunately, up to now although we have already known the centroid of each level (shown in Table 3-6), we still cannot distinguish which level means a heavier mental workload compared with the other one. However, we do notice that the percentile distribution of the four mental workload levels seem to vary significantly between the different manoeuvre. It implies that the driver's mental workload in the different driving task differs from each other obviously.

3.4.3 Grading the mental workload levels

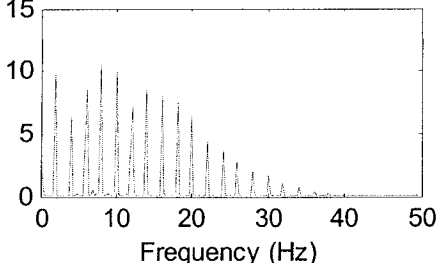
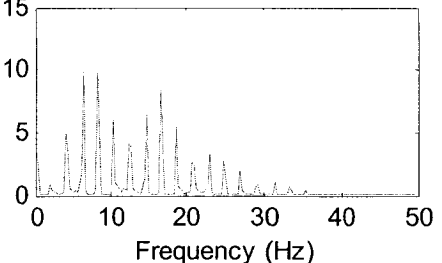
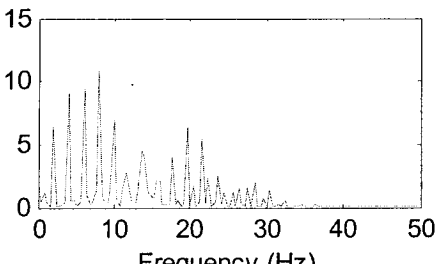
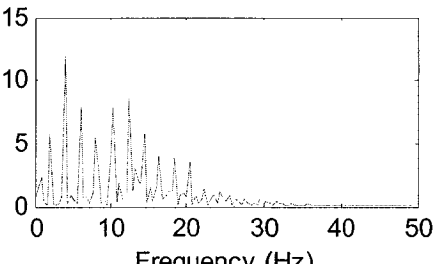
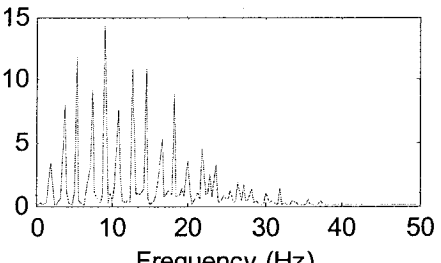
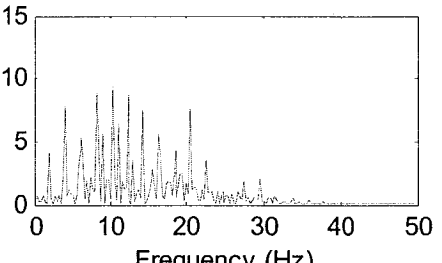
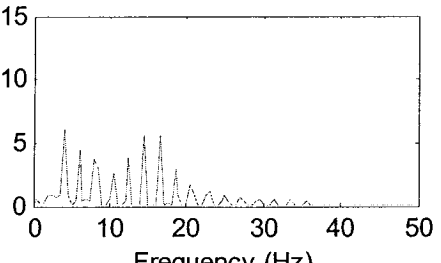
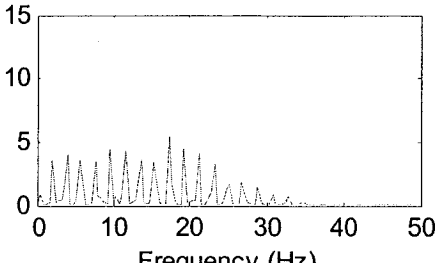
Based on the clustering results of the experimental data, the typical durations of each mental workload level can be recognized and picked out from the Figs 3-24, 3-25, and 3-26. For the candidates of the picked out time periods (Table 3-7), the mental workload should almost remain at the same level as long as possible.

Table 3-7 Typical durations of each MWL level in different manoeuvre

MWL Level	Single-lane change (Fig. 3-26)	Double-lane change (Fig. 3-27)	Sine-lane motion (Fig. 3-28)
Level 1	1.0s~3.5s, 17.5s~20.5s		
Level 2			6.5s-9s, 10.5s-13s
Level 3		0s~3s	14s-18s
Level 4	8.5s~10.5s	10s~13.5s	

According to the determined start time and the end time, the ECG strips can be picked out easily in the time domain. Table 3-8 shows the mean value of the power spectrum (M_p) and the mean value of the frequency spectrum (M_f) for the corresponding ECG strips.

Table 3-8 Mean value of the power and frequency for ECG strips

Level 1	 <p>$M_p = 0.63 \quad M_f = 9.25$</p>	 <p>$M_p = 0.69 \quad M_f = 8.97$</p>
Level 2	 <p>$M_p = 0.93 \quad M_f = 12.08$</p>	 <p>$M_p = 0.95 \quad \text{std} = 11.47$</p>
Level 3	 <p>$M_p = 1.1 \quad M_f = 15.22$</p>	 <p>$M_p = 1.01 \quad M_f = 13.63$</p>
Level 4	 <p>$M_p = 0.58 \quad M_f = 7.54$</p>	 <p>$M_p = 0.61 \quad M_f = 8.06$</p>

The averaged mean value and the averaged standard deviation value of are calculated and shown in Table 3-9.

Table 3-9 Sorting the mental workload levels

Mental workload level (<i>i</i>)	Mean value of power (M_{Pi})	Mean value of frequency (M_{fi})	Resorted by M_{Pi}	Resorted by M_{fi}
1	0.66	9.11	B	B
2	0.94	11.77	C	C
3	1.06	14.43	D	D
4	0.59	7.80	A	A

In table 3- 9, $M_{P4} < M_{P1} < M_{P2} < M_{P3}$. In addition, $M_{f4} < M_{f1} < M_{f2} < M_{f3}$.

Therefore, the resorted mental workload level is $MWL_4 < MWL_1 < MWL_2 < MWL_3$.

The new rank of mental workload level is A(4), B(1), C(2), D(3). The value scope of each mental workload level is shown in Table 3-10.

Table 3-10 The value scope of each mental workload level

MWL level	MWL value	Meaning
<i>Level A (4)</i>	[0, 0.25)	Baseline
<i>Level B (1)</i>	[0.25, 0.5)	A little high
<i>Level C (2)</i>	[0.5, 0.75)	High
<i>Level D (3)</i>	[0.75, 1]	Very high

3.4.4 Estimation of mental workload level and variance

Based on the determined centroid and the value scope of each mental workload level, the competitive neural network can be applied to the other ECG feature sets to estimate the driver's mental workload. The results are shown in Figs 3-27, 3-28, 3-29, and 3-30.

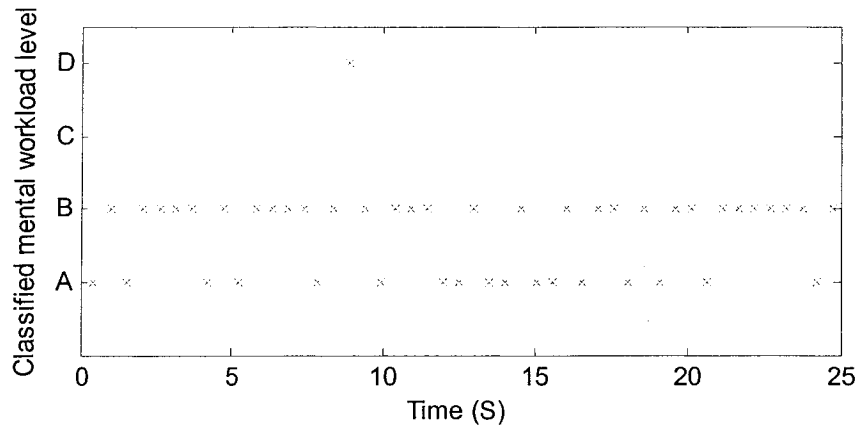


Figure 3-27 MWL Level in the #2 single-lane change manoeuvre (60 Km/h)

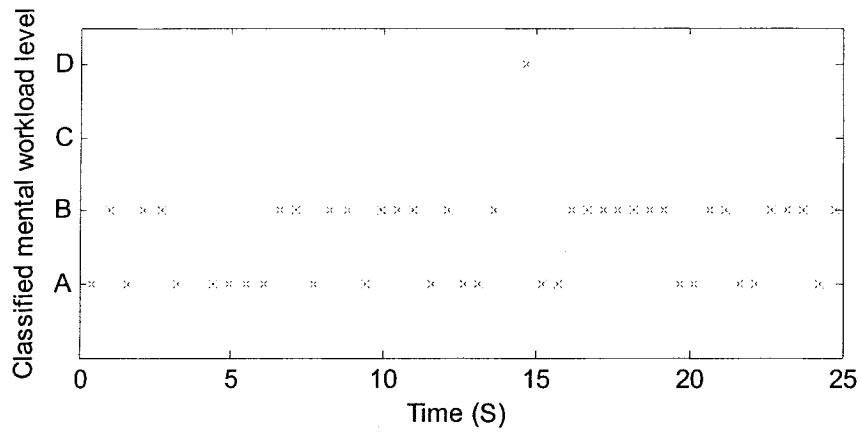


Figure 3-28 MWL level in the #1 single-lane change manoeuvre (80 Km/h)

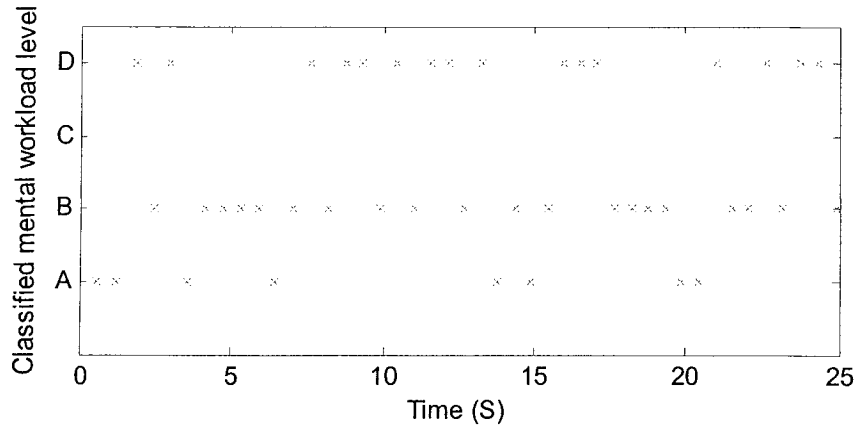


Figure 3-29 MWL level in the #1 double-lane change manoeuvre (60 Km/h)

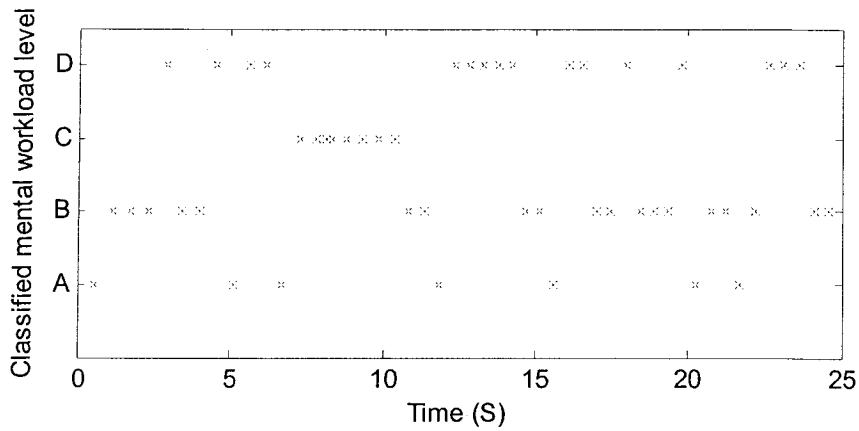


Figure 3-30 MWL level in the #1 sine-lane motion manoeuvre (50 Km/h)

When the driver's mental workload levels in all manoeuvre have been determined, the percentage of each mental workload level can be calculated by summing up the duration of each mental workload level maintaining. The results are shown in Tables 3-11. In Tables 3-11, as for the names of the manoeuvre, please refer to section 2.5.

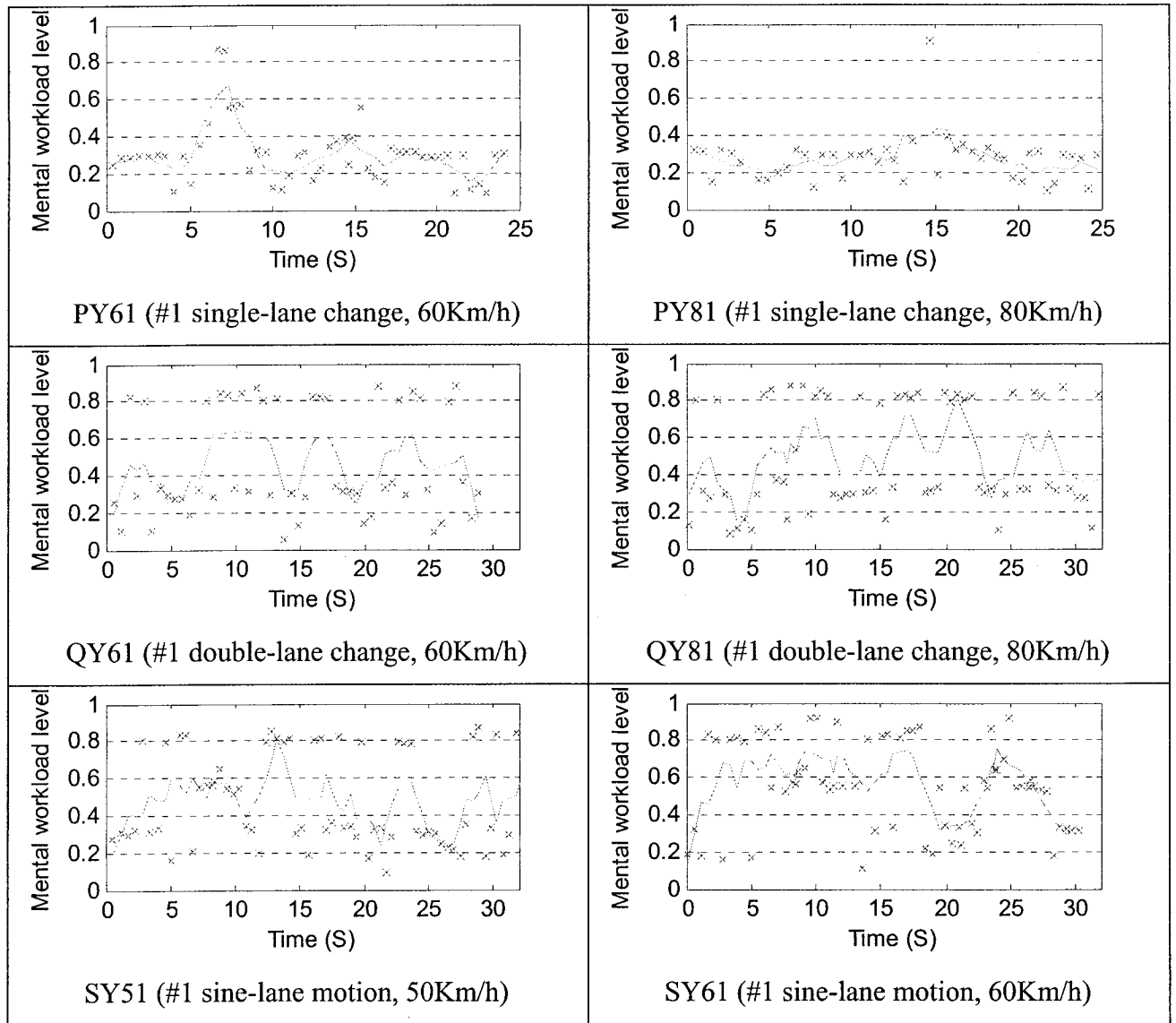
Table 3-11 Summary of percentile distribution for each mental workload level

Manoeuvre type	Level A (Baseline)	Level B (A little high)	Level C (High)	Level D (Very high)
PY61	37%	55%	6%	2%
PY62	46%	53%	0%	1%
PY81	37%	60%	0%	3%
PYA1	42%	33%	25%	0%
PYA2	44%	45%	11%	0%
QY61	21%	43%	0%	36%
QY81	21%	36%	5%	38%
QY82	37.5%	60%	0%	3.5%
SY51	18%	40%	5%	37%
SY5h1	6%	13%	50%	31%
SY61	12%	22%	43%	23%

In Figures 3-27 to 3-30, the value of mental workload is marked by a serial of discrete points, but they cannot clearly show the variance tendency of the driver's mental workload.

When the discrete MWL values are smoothed by moving averaged filters [Savitzky & Golay, 1964], the driver's mental workload variance can be observed. Table 3-12 shows the mental workload variance curve of driver 'Y' in typical vehicle manoeuvre. In those figures, 0 indicates absolutely no effort, 1 indicates extreme effort.

Table 3-12 Mental workload variance in typical vehicle manoeuvre



3.4.5 Results and discussion

The percentile analysis in Table 3-11 shows the impacts of motion speed, motion type, and the experience of manoeuvre on the driver's mental workload.

(1) The impacts of motion speed on the mental workload

Compared with the motion of PY62, in terms of the different mental workload levels, the driver spends less time on level A, level B, but more time on level C in the motion of PYA1. Thus PYA1 shows a clear tendency to have a higher mental workload than that of PY62 because of the significantly higher velocity. The similar relationship can also be observed between QY61 and QY81, SY51 and SY5h1.

(2) The impacts of motion type on the mental workload

Compared with the motion of PY61, the driver spends less time on level A, level B of the mental workload, but more time on level D in the motion of QY61, so QY61 shows a clear tendency of having a higher mental workload than that of PY61 because of the more complex operation. A similar relationship can be also observed between PY61 and SY61, QY61 and SY61.

(3) The impacts of manoeuvre experience on the mental workload

For some motion types, the driver was required to repeat the task at the same motion speed, so the impacts of manoeuvre experience can be observed.

Compared with the motion of PY61, so far as the level of driver mental workload is concerned, the driver spends a little bit more time on level A and B, and slightly less time on level C and D in the motion of PY62, so PY62 shows the tendency of having lower mental workload than that of PY61 because of the recently gained task experience. A similar relationship can be also observed between PYA1 and PYA2, QY81 and QY82.

Regarding the mental workload variance, previous research has shown that it is important to compare the operator's mental workload while working with its baseline value [De Waard, 1996]. The challenge is to determine when it is the baseline of the driver mental workload.

In Table 3-12, it can be found that at the beginning of most of the trials, the driver's mental workload increased quickly. Only in the low speed simple single-lane change manoeuvre, did the driver's mental workload seem to remain at a constant level for some time, such as 4 seconds for the 60 Km/h single-lane change.

This implies that the operator's mental workload does not definitely remain at the baseline level at the beginning period of performing tasks. The reason may be that the operator is aroused soon after the task is declared and he begins the warm-up process. Therefore, it is not always reasonable to choose the beginning period as the baseline level of the operator's mental workload.

According to the Rating Scale Mental Effort scale (see Appendix A), the mental effort in Table 3-12 can be perceived as follows:

(1) In the #1 60 Km/h single-lane change manoeuvre, the driver did not seem familiar with the task. His mental workload stayed at less than 0.3 for most of the time, but it reached 0.6 at the instant of the first turn. Therefore, although the task required him to exert only "a little effort" most of the time, it required him to take "rather much effort" to make the first lane-change manoeuvre.

(2) In the #2 60Km/h single-lane change manoeuvre, the driver's mental workload variance indicates that the task required the driver to take just "a little effort" to accomplish.

(3) In the #1 60Km/h and #1 80Km/h double-lane change manoeuvre, the driver's mental workload varied between 0.3 and 0.6, 0.3 and 0.7, respectively. This indicates that the driver had to take "some effort" or even "rather much effort" to accomplish the task.

(4) In the rather difficult task, #1 60Km/h single-lane manoeuvre, the driver's mental workload stayed at around 0.7 for most of the time. This suggests that the driver had to take "considerable effort" most of the time to complete the task.

Generally, the mental effort in each trial above is consistent with the feeling of the driver in the field.

In all the trials above, the task duration is very short and usually lasts only half a minute. In such a short period, it is not easy to distinguish so many different mental states of the driver because there are some limits to the real time response of human physiological reflection. Indeed, the cluster analysis of the experiment data suggested that the total levels of the driver mental workload should be divided into two levels. It means that there are mainly two different mental states in the short time trials above.

In a long duration task, the estimation method of driver mental workload may be more applicable.

In summary, the following conclusions can be concluded by using the mental workload percentile analysis and the mental workload variance analysis.

(1) At a similar driving speed, the driver's mental workload in a complex manoeuvre is higher than that in a simple manoeuvre.

(2) For a same type of manoeuvre, the driver's mental workload in a high-speed motion is higher than that in a low-speed motion.

(3) For a same type of manoeuvre and at a similar driving speed, the driver's mental workload in the second manoeuvre is more likely lower than that in the first manoeuvre. This means that the experience of performing a task can be beneficial in the reduction of the mental workload.

(4) The results of the driver mental workload estimation show consistency with the Rating Scale of Mental Effort (RSME).

3.5 Summary

In this chapter, a cluster analysis and a Learning Vector Quantization neural network-based measure are presented to estimate the driver mental workload level and to quantify its variance. The ECG feature data used for clustering and unsupervised neural network classifying are pre-processed by using short time FFT transforms and wavelet transforms.

The simulation results based on the experiment data are consistent with the common perception of the mental workload variance in typical vehicle manoeuvre, such

as single-lane changes, double-lane changes, and sine-lane motions. Furthermore, the simulation results show consistency with the evaluation of the RSME scale.

This estimation measure shows a capability of determining the total number of mental workload levels objectively, including locating the possible baseline of mental workload variance. Not all the mental workload at the beginning of experiments is suitable to use as the baseline because of possible early arousing.

The estimation method of evaluating the driver mental workload may be more applicable for tasks of long duration.

CHAPTER 4 DANGER ZONE BASED RISK LEVEL ESTIMATION

4.1 Introduction

Usually it can be imagined that there is a danger zone around a moving vehicle. In this zone, obstacles represent a potential threat to the vehicle's safety, and vice versa. Different drivers experience different perceptions of the same driving risk and usually have different mental feedbacks. Therefore, the variance of the drivers' mental workload may be partly caused by the change of the driver risk level.

The size of the danger zone has a close relation to the safe headway. For example, when the movement is in a forward direction, the closer together two moving vehicles are, the higher the possibility of collision is. Similarly, a sharp turn in a road and unfamiliar surroundings also cause drivers to feel nervous.

In this chapter, a fuzzy model is established to describe the danger zone for the driving risk level estimation. In addition, the membership functions of the danger zone are discussed. Although there are many factors affecting the driving risk level, at this stage, this study concerns only two major factors that alter the driving risk level: the obstacles in the danger zone and the road shape. Finally, examples of the driving risk level estimation are given. The relation between the driver mental workload variance and the driving risk level change is also briefly discussed.

4.2 Danger zone of moving vehicle

4.2.1 Definition of danger zone

Consistent to previous research, hazard is defined as “the way in which a thing or a situation can cause harm” [Greene, A.]. Danger zone (DZ) is defined as a space area with a potential hazard [Shahrokhi, 2004]. Risk is the quantified characteristic of hazard, namely hazard severity, for a likelihood target being exposed to a hazard [UK, 2001]. Many factors can lead to hazard, so risk has a great degree of uncertainty. In another word, risk is the probability of an unwanted top event and its consequences in terms of possible damage severity to property, environment, and people [Jo & Parkd, 2003] [Labodova, 2004].

As obstacles mean objects with possibility of creating hazard, in driving, the hazard usually means collisions, out of the track, and their consequences. Out of the track can be also perceived as a type of collision with roadside targets. Two types of harm exist in driving. One is the harm to the surrounding objects caused by the moving vehicle. Another is the harm cause by outside obstacles to the moving vehicle including the onboard passengers.

The danger zone of a moving vehicle is a space area where potential hazard can happen. Driving risk level means the quantified hazard severity in terms of possible collisions. Normally, the higher the driving risk level is, the more serious the potential hazard is, and the more nervous a driver usually feels.

Shahrokhi & Bernard [2004] presented a fuzzy space concept to define the dangerous zone of industrial systems in the virtual reality environment. This concept is also used in this research for the further discussion of the danger zone of a moving vehicle.

4.2.2 Fuzzy space denotation of danger zone

The danger zone of a moving vehicle can be denoted as a two-dimensional geometrical space in which there is a certain degree of risk at each location. A world reference coordinate system is set up here. Let

$$X \subset R^2. \ x, y \in X \quad (4.1)$$

Where x, y represents the longitudinal distance and the lateral distance from the original respectively. Denote A_x, A_y as the risk level fuzzy sets, $u_{A_x}(x)$, $u_{A_y}(y)$ as the membership function over A_x, A_y , respectively. A_x, A_y are described as [Chen,1996],:

$$A_x = \{(x, u_{A_x}(x)) \mid x \in X\} \quad (4.2)$$

$$A_y = \{(y, u_{A_y}(y)) \mid y \in X\} \quad (4.3)$$

$$u_{A_x}(x), u_{A_y}(y) \in [0,1] \quad (4.4)$$

Assume that it is a clear and free space on the vertical direction, and no hazard may happen on the vertical direction, thus the fuzzy set on the vertical direction can be omitted.

Fig.4-1 shows a π shape fuzzy membership function on the longitudinal direction. Fig.4-2 shows a bell shape fuzzy membership function on the lateral direction. In Figures

4-1 and 4-2, the further away from the moving vehicle is, the less risk of the potential hazard is.

For any driver, it is a critical cognitive task to maintain safe time headway from the next vehicle ahead. Similarly, it is also mandatory for a driver to make the vehicle keep proceeding in the target lane. Hence the membership functions on the longitudinal direction and the lateral direction can be roughly determined in the following ways.

Assume the vehicle position is (x_0, y_0) . In Figures 4-1 and 4-2, the distance $x_1 - x_0$ is determined by the minimum time headway T_m . The distance $x_2 - x_0$ is determined by the psychology safe time headway T_s . $y_1 - y_0$ is determined by the vehicle width W_v while $y_2 - y_0$ is determined by the lane width W_l .

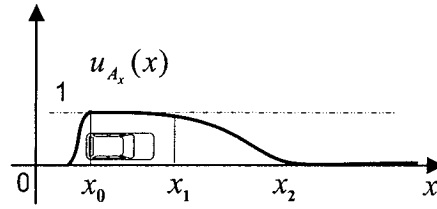


Figure 4-1 Longitudinal danger zone

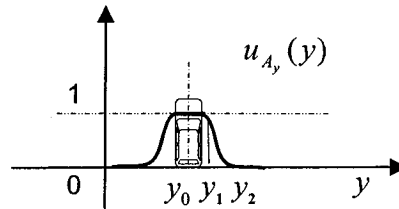


Figure 4-2 Lateral danger zone

In general, it is difficult to precisely define the membership function $u_{A_x}(x)$, $u_{A_y}(y)$. Although experiences and experiments are two valuable sources of approach, there are no universe theoretical methods. The following ways are preferred in this study.

In the vehicle reference coordinate system, the membership function of $A_{x'}$ (x' : the longitudinal direction) in terms of risk can be assumed as:

$$u'_{A_{x'}}(x') = \frac{1}{1 + e^{-a_1(x'-c_1)}} - \frac{1}{1 + e^{-a_2(x'-c_2)}} \quad (4.5)$$

Where $u'_{A_{x'}}(x')$ is constructed by the difference value of two sigmoid membership functions. The parameters in Eq. (4.5) are determined by the minimum time headway T_m (the corresponding risk is supposed to be 0.9) and the psychology safe time headway T_s (the corresponding risk is supposed to be 0.1) for the specific driver so that the final shape is similar to that shown in Figure 4-1.

Along the lateral direction, the membership function of $A_{y'}$ in terms of risk can be assumed as:

$$u'_{A_{y'}}(y') = \frac{1}{1 + \left| \frac{y'}{a} \right|^{2b}} \quad (4.6)$$

The parameters in Eq. (4.6) are determined by the vehicle width W_v (the corresponding risk is supposed to be 0.9) and the lane width W_l (the corresponding risk is supposed to be 0.5). The final shape of the membership function is similar to that shown in Figure 4-2.

Assume the vehicle position in the world coordination system is (x_0, y_0) and the deviation angle of the vehicle's proceeding direction from the road direction is θ . Then, the coordination transform can be done in Eq. (9).

$$\begin{bmatrix} u_{A_x}(x) \\ u_{A_y}(y) \end{bmatrix} = \begin{bmatrix} \cos(\theta) & -\sin(\theta) \\ \sin(\theta) & \cos(\theta) \end{bmatrix} \begin{bmatrix} u'_{A_x}(x') \\ u'_{A_y}(y') \end{bmatrix} + \begin{bmatrix} x_0 \\ y_0 \end{bmatrix} \quad (4.7)$$

After determining the risk degree distribution on the longitudinal and latitudinal directions, the fuzzy space can be constructed by multiplying the two one-dimensional membership functions.

$$B_{xy}(x, y) = \{((x, y), u_{A_x}(x)u_{A_y}(y)) \mid x, y \in X\} \quad (4.8)$$

Where B_{xy} represents the danger zone of a moving vehicle.

Generally, besides the way of constructing the membership function shown in Eq. (4.8), there are still three ways could be used to construct a membership function.

(1) Based on common sense, it is reasonable to choose the maximum risk level as the final risk level.

$$u_{B1}(x, y) = \max(u_{A_x}(x), u_{A_y}(y)) \quad (4.9)$$

(2) Based on the fuzzy logic operation rule, it is not unusual to choose the minimum value as the final risk level.

$$u_{B2}(x, y) = \min(u_{A_x}(x), u_{A_y}(y)) \quad (4.10)$$

(3) Based on the possibility theory, the final risk can be calculated as the following:

$$u_{B3}(x, y) = 1 - (1 - u_{A_x}(x))(1 - u_{A_y}(y)) \quad (4.11)$$

(4) Based on the concept of geometry space rotation, the final risk can also be calculated as algebra multiplication.

$$u_{B4}(x, y) = u_{A_x}(x)u_{A_y}(y) \quad (4.12)$$

Among the four risk level membership functions in Table 4-1, we would like to know which one is the best suitable to the driving risk level estimation?

Obviously, $u_{B1}(x, y)$, $u_{B3}(x, y)$ are not proper for being risk level membership functions. In current research, the membership function over B_{xy} is not denoted as the usually accepted fuzzy logic manipulation $\min(u_{A_x}(x), u_{A_y}(y))$, but the algebra multiplication $u_{A_x}(x)u_{A_y}(y)$. It is because those two one-dimensional membership functions are in π shape and bell shape, respectively, and the algebra multiply manipulation can be beneficial to avoid the insensitivity on the longitudinal direction x , and to reduce the false warning of roadside obstacles. The further analysis can be obtained from the comparison between their sensitivity over x and y direction (Table 4-2).

$$S_2(x, y) = \frac{\partial^2 u_{B2}(x, y)}{\partial x \partial y} \quad (4.13)$$

$$S_4(x, y) = \frac{\partial^2 u_{B4}(x, y)}{\partial x \partial y} \quad (4.14)$$

Although B_{xy} , the fuzzy space denotation of a danger zone can be extended to contain more fuzzy variables in the way of Eq. (4.8). In fact, the impacts of some other

factors have been reflected from the membership functions $u_{A_x}(x), u_{A_y}(y)$ partially, especially from the minimum time headway T_m (closely related to the road environment and the vehicle dynamic parameters) and the psychology safe time headway T_s (closely related to the driver's physiological and psychological factors).

For example, the weather impacts of fog or rain influence the size of danger zone by increasing the time headway T_m and T_s . The velocity and inertia of the vehicle will also alter the time headway T_m and T_s . In addition, the danger zone of a moving vehicle is driver-dependent because drivers have varied reaction time and safe headway. Hence, the impacts of drivers' factors have been contained partially in the model.

Above all, the time headway is critical to calculate the danger zone of a moving vehicle. Detail information of time headway can be found in the traffic engineering theory [Disbro & Frame, 1990].

Table 4-1 Membership functions of the fuzzy space

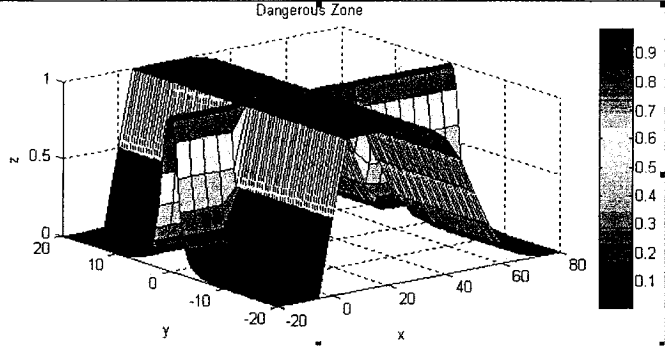
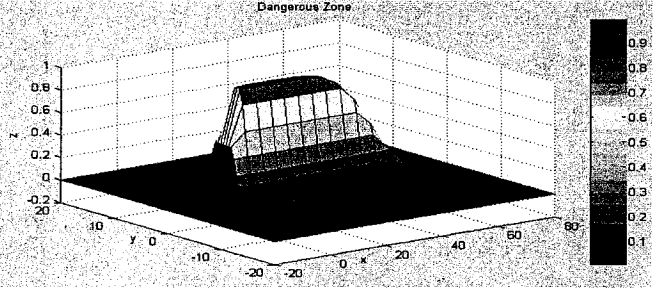
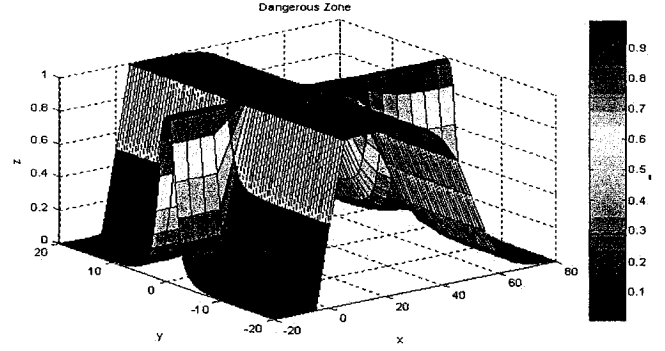
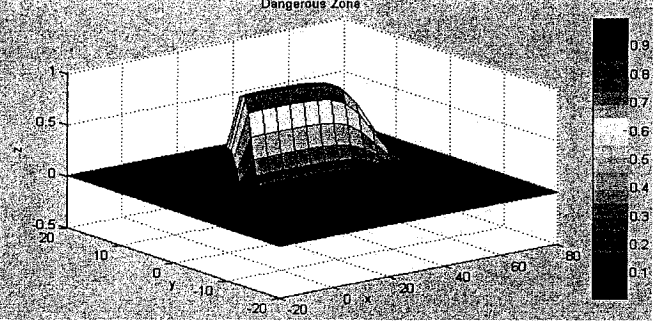
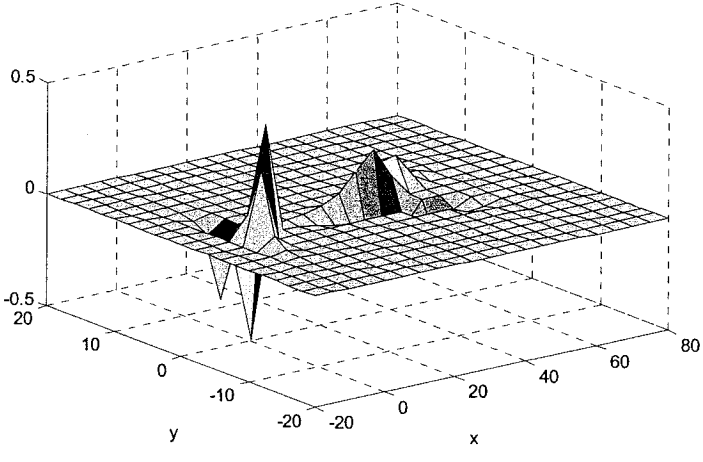
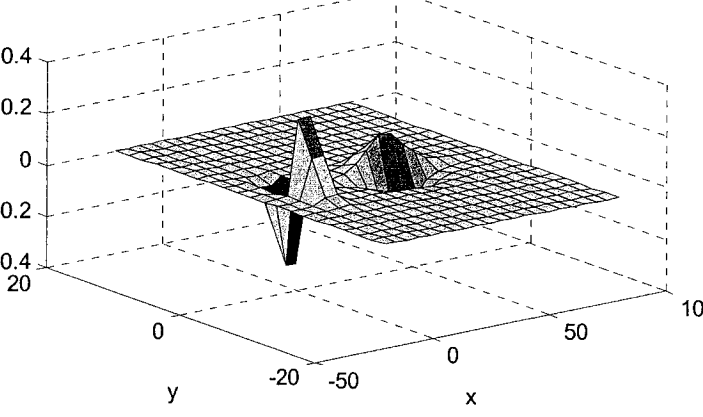
Membership functions	The shape of danger zone
$u_{B1}(x, y)$	 <p>A 3D surface plot titled "Dangerous Zone" showing the membership function $u_{B1}(x, y)$. The vertical axis is labeled z and ranges from 0 to 1. The horizontal axes are labeled x (ranging from -20 to 80) and y (ranging from -20 to 20). The surface is highly irregular with multiple peaks and valleys. A color bar on the right indicates values from 0.1 (dark) to 0.9 (light).</p>
$u_{B2}(x, y)$	 <p>A 3D surface plot titled "Dangerous Zone" showing the membership function $u_{B2}(x, y)$. The vertical axis is labeled z and ranges from 0 to 1. The horizontal axes are labeled x (ranging from -20 to 80) and y (ranging from -20 to 20). The surface is a single, smooth, bell-shaped peak centered around $x=20, y=0$. A color bar on the right indicates values from 0.1 (dark) to 0.9 (light).</p>
$u_{B3}(x, y)$	 <p>A 3D surface plot titled "Dangerous Zone" showing the membership function $u_{B3}(x, y)$. The vertical axis is labeled z and ranges from 0 to 1. The horizontal axes are labeled x (ranging from -20 to 80) and y (ranging from -20 to 20). The surface is highly irregular with multiple peaks and valleys, similar to u_{B1} but with different peak heights. A color bar on the right indicates values from 0.1 (dark) to 0.9 (light).</p>
$u_{B4}(x, y)$	 <p>A 3D surface plot titled "Dangerous Zone" showing the membership function $u_{B4}(x, y)$. The vertical axis is labeled z and ranges from 0 to 1. The horizontal axes are labeled x (ranging from -20 to 80) and y (ranging from -20 to 20). The surface is a single, smooth, bell-shaped peak centered around $x=20, y=0$, similar to u_{B2} but with a slightly different shape. A color bar on the right indicates values from 0.1 (dark) to 0.9 (light).</p>

Table 4-2 Sensitivity of the risk detection over the location variance

Membership functions	Sensitivity of the risk detection over the location variance
$u_{B2}(x, y)$	<p style="text-align: center;">Risk sensitivity over XY</p> 
$u_{B4}(x, y)$	<p style="text-align: center;">Risk sensitivity over X and Y</p> 

4.3 Methodology of driving risk level estimation

4.3.1 Background risk level estimation

The road environment creates the background driving risk level, or the baseline of the driving risk level, which is denoted as D_{BRL} . D_{BRL} can be roughly estimated by Eq.(4.15).

$$D_{BRL} = \frac{\iint_{\mathcal{X}} B_{xy}(x, y) U(x, y) dx dy}{\iint_{\mathcal{X}} B_{xy}(x, y) dx dy} \quad (4.15)$$

Where $U(x, y) \in [0, 1]$ is the possibility distribution of all obstacles around a vehicle. $U(x, y)$ is very difficult to determine in theory, but some simple ways can be applied for coarse evaluation. If the vehicle has immediate danger when it rush out of the track, it can be assumed that all the space outside of the track is full of obstacles; hence, $U(x, y)$ can be simplified to a step function with a factor $k \in [0, 1]$ referring to the possible hazard severity.

4.3.2 Overall risk level estimation

Any practical obstacle in the danger zone may lead to a potential risk. This type of risk may bring hazard not only to obstacles themselves, but also to the vehicle and the onboard driver. Therefore, it is necessary to concern the possible obstacle distribution in order to estimate the driving risk level. In present research, only those obstacles that are detected on the road zone are considered. Other obstacles can be classified to the roadside environment and they make contribution to the background risk level. The obstacles on road are simplified to discrete points as follows.

$$O_{x_i, y_i} = \{(x_i, y_i), i = 1 \dots m\} \quad (4.16)$$

Where m represents the number of obstacles. Concerning the membership function of the danger zone, the corresponding risk level D_{RL} is denoted as follows.

$$D_{RL} = \max_{O_{x_i y_i}}(B(x_i, y_i)) \quad (4.17)$$

The final driving risk level D_{FRL} is defined as the maximum of D_{BRL} and D_{RL} .

$$D_{FRL} = \max(D_{BRL}, D_{RL}) \quad (4.18)$$

When obstacles stay far away from the danger zone, they contribute little to the final D_{RL} . In this situation, the driver usually cannot feel the hazard coming from them and the driving risk level mainly comes from the influences of the background environment.

In practical, the vehicle position and the forwarding direction can be obtained in many ways, such as Differential Global Position System (DGPS), vision recognition systems, and magnet markers in future Advanced Vehicle Highway System (AVHS). The digit description of road shape can be obtained from the digit map of navigation systems. However, the real challenge is whether the precision of those data can meet the practical requirement of the roughly estimation of the driving risk level.

4.4 Experiment and simulation

In this section, the background driving risk levels in the typical vehicle manoeuvre scenarios are estimated. Its relationship to a driver's mental workload variance is briefly discussed.

4.4.1 Calculation of the minimum safe headway

According to the traffic engineering theory [Disbro & Frame, 1990], the minimum spacing between vehicles is calculated as Eq. (4.19). The minimum safe time headway is calculated as Eq. (4-20).

$$H = Vt_c + \frac{V^2}{2} \left(\frac{1}{a_e} - \frac{1}{a_f} \right) \quad (4.19)$$

$$T = \frac{L+H}{V} = \frac{L}{V} + t_c + \frac{V}{2} \left(\frac{1}{a_e} - \frac{1}{a_f} \right) \quad (4.20)$$

Where L is the reserved safe gap, V is the vehicle speed, t_c is a time constant, a_e is the emergency deceleration, and a_f is the failure deceleration.

For a common automobile with $L = 2.5m$, $t_c \leq 0.1$ s, $a_e = 0.6g$, $a_f = \infty$. The minimum safe headway is shown in Table 4-3.

Table 4-3 Minimum safe headway in different speeds

V (Km/h)	V (m/s)	T (s)	H (m)
60	16.7	1.6	25
80	22.2	2.1	44
90	25	2.3	55
105	29.2	2.6	75
120	33.3	3.0	98

In the driving process, the psychological safe time is composed of four parts: perception time, decision time (including reaction time), execution time, and mechanical

time. Perception time and decision time depend upon the activity of the driver's brain. The psychological safe time is also affected by the laws. For example, the New Zealand Road Code recommends that drivers remain at least two seconds behind any vehicle they are following [Thakur, 1997]. Road Code of Canada has a similar regulation too.

4.4.2 Estimation of DRL in the single-lane change

According to Table 4-2, for a moving automobile with a velocity of 60Km per hour (16.7 m/s), its minimum safe time headway is about 1.6 seconds. We choose the popular accepted 3 seconds as the psychological safe time headway. Then, the moving vehicle' dangerous space can be described as Eq. (4.21) and (4.22).

$$u'_{A_{x'}}(x') = \frac{1}{1 + e^{-x'}} - \frac{1}{1 + e^{-0.2(x'-40)}} \quad (4.21)$$

$$u'_{A_{y'}}(y') = \frac{1}{1 + \left| \frac{y'}{1.5} \right|^{3.5}} \quad (4.22)$$

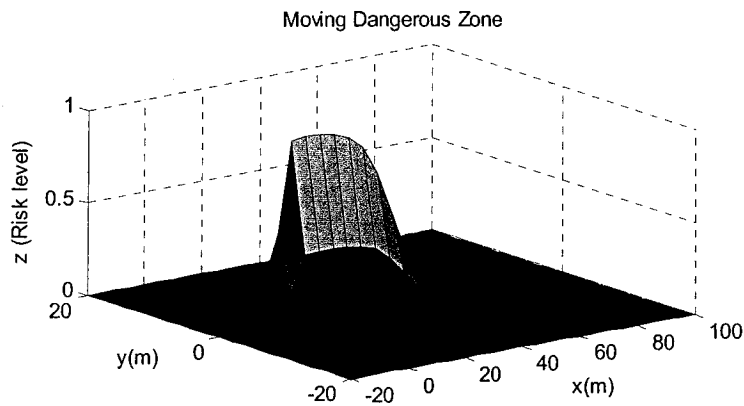


Figure 4-3 Danger zone of a moving automobile at 60 km per hour

In Figure 4-3, at the distance of minimum headway, the risk level may reach as high as 0.9 (The possibility of collision).

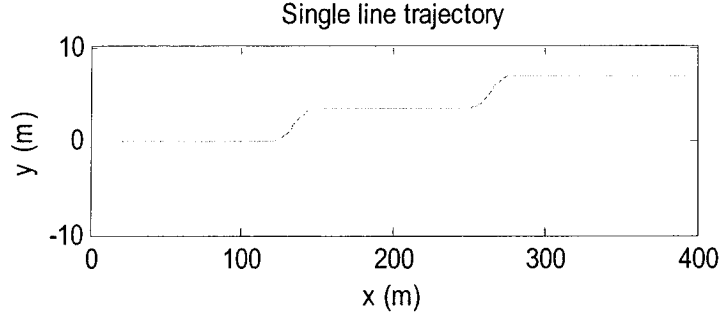


Figure 4-4 Track of the single-lane change manoeuvre

The track of the single-lane change manoeuvre (Fig.4-4) can be described by a segmented function $y_R = C(x)$ (Eq. (4.23)). In the experiments, the driver was instructed to drive along a given route marked by traffic cones. Therefore it can be assumed that obstacles are equally distributed outside of the track and it has high level of hazard severity. Then $U(x, y)$ can be simply expressed as Eq. (4.24).

$$C(x) = \begin{cases} 3.5 \times \frac{1}{1 + e^{-0.25(x-135)}} & x \in [0, 200] \\ 3.5 + 3.5 \times \frac{1}{1 + e^{-0.25(x-265)}} & x \in (200, 400] \end{cases} \quad (4.23)$$

$$U(x, y) = \frac{1}{1 + \left| \frac{y - C(x)}{1.75} \right|^{-20}} \quad (4.24)$$

Figure 4-5 shows the background driving risk level distribution in a single-lane change manoeuvre. Compared with Figure 4-4, the driving risk level begins to increase

from where the driver starts to execute the decision. The peaks of the driving risk level appear at the curve sections.

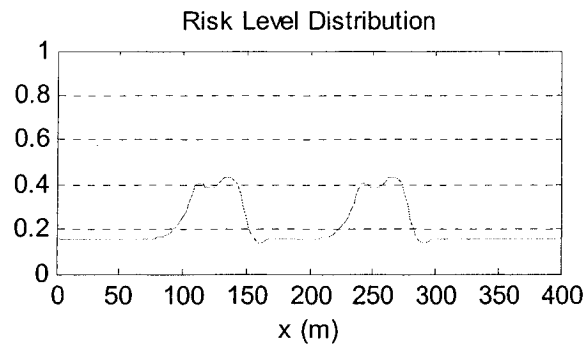


Figure 4-5 Driving risk level distribution in single-lane change manoeuvre (60km/h)

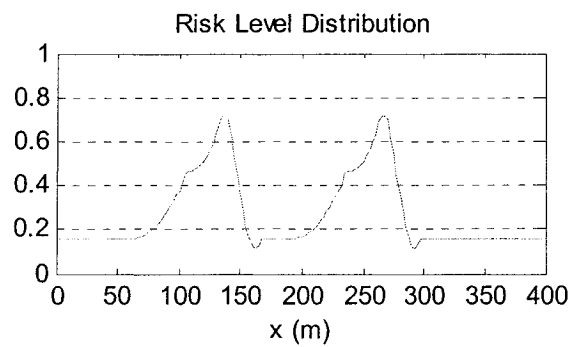


Figure 4-6 Driving risk level distribution in single-lane change manoeuvre (80km/h)

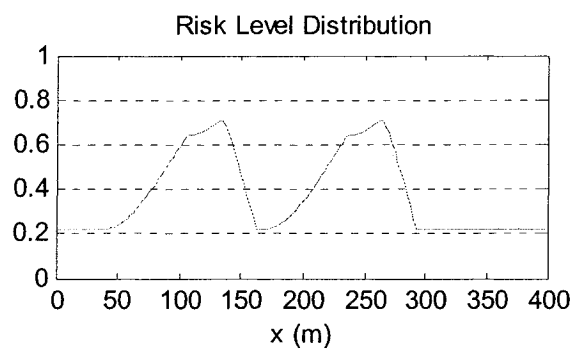


Figure 4-7 Driving risk level distribution in single-lane change manoeuvre (100km/h)

4.4.3 Relationship between MWL and DRL

Figure 4-8 shows the driver mental workload variance and the driving risk level variance in the same first single-lane change manoeuvre at 60 Km per hour. Although there is no comparability between their absolute value, the locations of the driver mental workload peak and the positions of driving risk level do appear at the similar place. This means that it is more likely that the driver mental workload is going to become higher when the driving risk level increases.

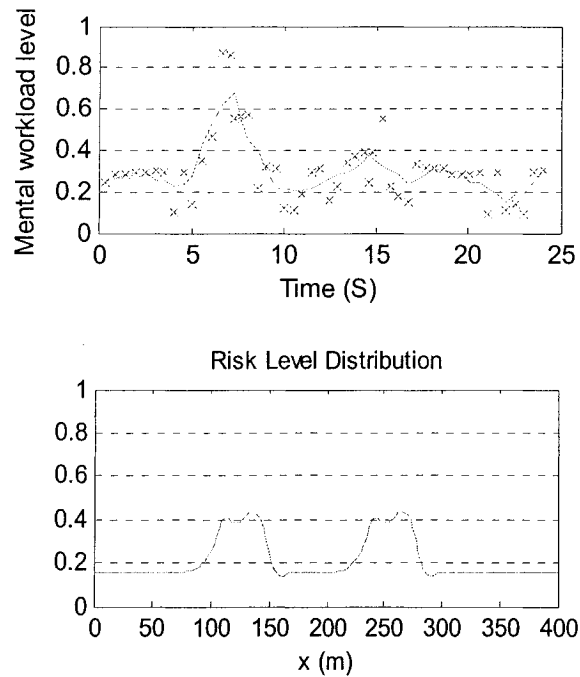


Figure 4-8 Comparison of MWL and DRL in the same single-lane change manoeuvre

In the other single-lane changes, such as 80 Km per hour and 100 Km per hour, when the driving risk level arises, the mental workload also shows a tendency to increase. Unfortunately, because the driver gradually adapts to the road environment in the test

experiments, the driver mental workload does not necessarily suddenly increase at all locations of the driving risk level peak.

4.5 Summary

In this chapter, the danger zone of a moving vehicle is characterized as a two-dimensional fuzzy space. Considering the obstacles in the danger zone and the impacts of the road environment, the method of driving risk level estimation is proposed. The driving risk level and the mental workload have been compared based on the experiment data of the single-lane change vehicle manoeuvre.

The simulation results indicate that the driver mental workload variance show close relationship to the change of the driving risk level. When the driving risk level rises, the driver mental workload more likely increases. However, when the driver becomes familiar with the road environment, in other words, when the driver gains more experience of task performance, the change in the driving risk level does not necessarily affect the alteration of the driver mental workload.

The simulation results obtained have only logical and qualitative support. An exact quantitative comparison is not yet immediately possible.

CHAPTER 5 NEURAL NETWORK BASED DRIVER MODELS

5.1 Introduction

Neural networks, especially Multilayer Perceptrons (MLP), have been used for simulating driver models. MLP networks are feed-forward networks, suitable for naturally performing static mapping between the input and the output. There is another type of neural network: recurrent networks. In recurrent networks, partial outputs are fed back to the same or preceding layers. This feature makes recurrent networks particularly suitable for application to dynamic systems.

Considering that the driving manoeuvre is behaviors having time series characteristics, the recurrent neural networks with specialized architectures for processing time series may have a better potential for simulating drivers' steering strategy than MLP networks do.

This chapter is organized as follows: in the next section, the background information of MLP neural networks and Elman recurrent networks is briefly reviewed. Then, the architectures of MLP and Elman networks for driver steering behavior models are discussed. The following section introduces the Two-Degree-of-Freedom vehicle model for vehicle dynamics simulation. Following that, the impacts of the driver mental workload on the driver's steering performance are discussed. The final section summarizes the conclusions briefly.

5.2 Background of Multi-Layer Perceptron (MLP) and Recurrent neural networks

5.2.1 Architecture of MLP networks and learning algorithms

The Multi-Layer Perceptron (MLP) is a supervised feedforward multi-layer neural network with continuous valued multi-input and multi-output. MLP networks usually utilize the back-propagation (BP) algorithm for training [Antognetti & Milutinovic, 1991] and that is why they are also called BP networks.

Figure 5-1 shows a typical layer in MLP networks [MATLAB 7.0, Handbook]. All of the nodes in each layer are fully connected to the nodes of the adjacent next layer.

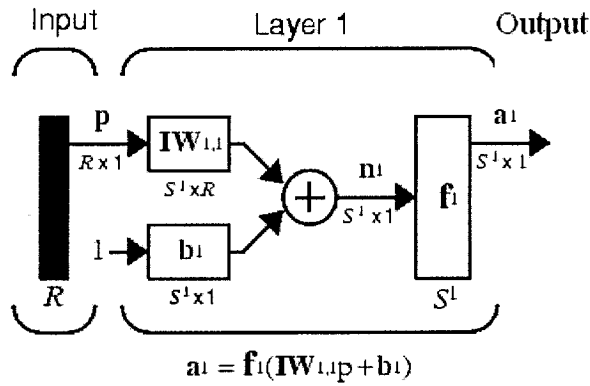


Figure 5-1 One layer MLP with R input elements and S^1 neurons

In Figure 5-1, input \mathbf{p} is a R -by-1 vector, weight $\mathbf{IW}^{1,1}$ is a $S^1 \times R$ matrix, bias \mathbf{b}^1 is a S^1 -by-1 vector, output \mathbf{a}^1 is a S^1 -by-1 vector, and f^1 is the transfer function.

$$\mathbf{a}^1 = f^1(\mathbf{IW}^{1,1}\mathbf{p} + \mathbf{b}^1) \quad (5.1)$$

For any supervised neural network, pairs of the input vectors and the corresponding output vectors are necessary for training until it can approximate a function, such as associating the input vectors with the specific output vectors, or classifying the input vectors in an appropriate way as defined.

When the neural network has been trained perfectly with the input / output pairs:

$$\{p_1, t_1\}, \{p_2, t_2\}, \{p_3, t_3\}, \dots, \{p_Q, t_Q\},$$

for a new input $p = p_q$, there is a new output $a = a_q$, where $p_q = p_Q + \delta$, $a = t_Q + \varepsilon$, and $\delta \rightarrow 0$, $\varepsilon \rightarrow 0$.

Mean square of error is usually used for the performance measurement.

$$F(x) = E[e^2] = E[(t - a)^2]. \quad (5.2)$$

The Widrow-Hoff learning rule, also called Least Mean Square (LMS) algorithm is [Hagan et al., 1996]:

$$\mathbf{W}(k+1) = \mathbf{W}(k) + 2\alpha e(k)\mathbf{p}^T(k) \quad (5.3)$$

$$\mathbf{b}(k+1) = \mathbf{b}(k) + 2\alpha e(k) \quad (5.4)$$

where α is the learning rate.

The commonly used BP algorithm is another general LMS algorithm, and the only difference is the computation of error derivative. It is consisted of two phases: a feed-forward process and a back-propagation process. Learning is achieved by adjusting the

weights associated with each neural node. First, an input vector is presented to the network and transferred to the output layer, known as the feed-forward process. Second, the output vector generated is then compared with the desired output vector and the error created by the comparison is propagated back through lower layers. The weight matrix of each layer is adjusted based on the back-propagation process.

However, the classical BP algorithm (the steepest descent back-propagation) is too slow for most practical applications. More advanced algorithms, such as variable learning rate back-propagation, conjugate gradient back-propagation, Quasi-Newton back-propagation algorithm, Levenberg-Marquardt algorithm, have been developed and can be used to improve the efficiency of training [Antognetti & Milutinovic, 1991].

Previous literature has indicated that MLP networks with biases, a sigmoid layer, and a linear output layer (Eq. (5.5)) are capable of approximating any function with a finite number of discontinuities [Hornik, 1989]. That is the reason why back-propagation networks have been widely used in many fields, also no exception in this research.

$$\mathbf{a}^1 = \text{tansig} (\mathbf{IW}^{1,1} \mathbf{p} + \mathbf{b}^1) , \mathbf{a}^2 = \text{purlin} (\mathbf{IW}^{2,1} \mathbf{a}^1 + \mathbf{b}^2) \quad (5.5)$$

5.2.2 Architecture of Elman recurrent networks

The Elman network is one of popular recurrent networks. In an Elman network, there is a recurrent layer comprised of context nodes which accept the feedback from the hidden output nodes, so the output of the network depends on an aggregate of previous states and the current input [Elman, 1990].

Compared with other types of multilayered network, such as MLP, the most important advantage of the Elman network is its robust feature extraction ability, which provides feedback connections from the hidden layer to the input layer. More over, feedback connections from the hidden layer to the input layer support the capability of reflecting dynamical characters of natural systems. A two-layer Elman network is shown in Figure 5-2 [MATLAB 7.0, Handbook].

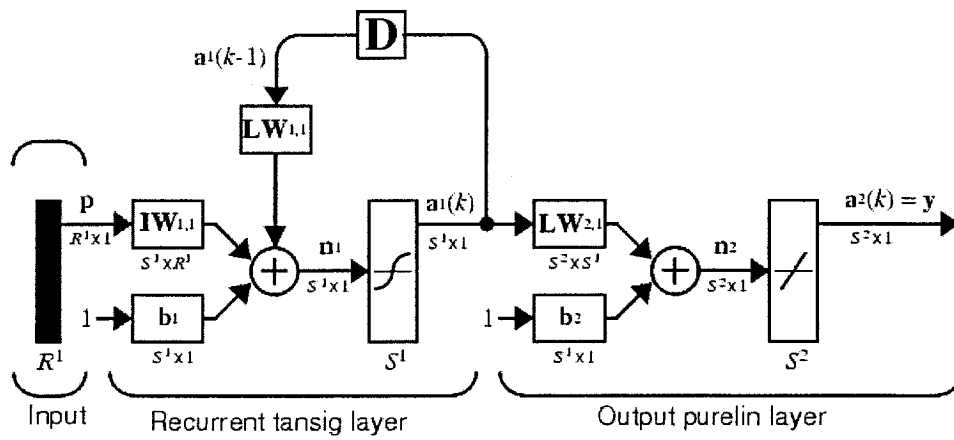


Figure 5-2 A two-layer Elman network.

In Figure 5-2, the Elman network has S^1 tansig neurons (with hyperbolic tangent sigmoid transfer functions) in its hidden (recurrent) layer, and S^2 purelin neurons (with linear transfer functions) in its output layer. This combination is special in that the two-layer networks with these transfer functions can approximate any function (with a finite number of discontinuities) with arbitrary accuracy. The only requirement is that there must be enough neurons in the hidden layer. In practical, more hidden neurons and layers are needed for more complex systems.

The input \mathbf{p} is a $R^1 \times 1$ vector, weight $\mathbf{IW}^{1,1}$ is a $S^1 \times R^1$ matrix, and bias \mathbf{b}^1 is a $S^1 \times 1$ vector. The $\mathbf{a}^1(k)$ is the output of the recurrent layer at time k [Matlab 7.0, Handbook].

$$\mathbf{a}^1(k) = \text{tansig}(\mathbf{IW}^{1,1}\mathbf{p} + \mathbf{LW}^{1,1}\mathbf{a}^1(k-1) + \mathbf{b}^1) \quad (5.6)$$

The weight $\mathbf{IW}^{2,1}$ is a $S^2 \times S^1$ matrix, and bias \mathbf{b}^2 is a $S^2 \times 1$ vector. The $\mathbf{a}^2(k)$ is the output of the second layer at time k [Matlab 7.0, Handbook].

$$\mathbf{a}^2(k) = \text{purelin}(\mathbf{LW}^{2,1}\mathbf{a}^1(k) + \mathbf{b}^2) \quad (5.7)$$

Except the hidden recurrent layer, Elman networks are similar to MLP networks, so the training algorithm of Elman recurrent networks is also back-propagation training based, such as quasi-Newton back-propagation, and Levenberg-Marquardt back-propagation (LM). However, LM algorithm tends to proceed so rapidly that it does not necessarily do well in Elman networks. The detail explanation of training algorithms can be found in much literature [Hagan M.T., Demuth H.B., Beale M.H., 1996].

5.3 Neural networks based driver steering behavior models

5.3.1 Interaction between driver model and vehicle model

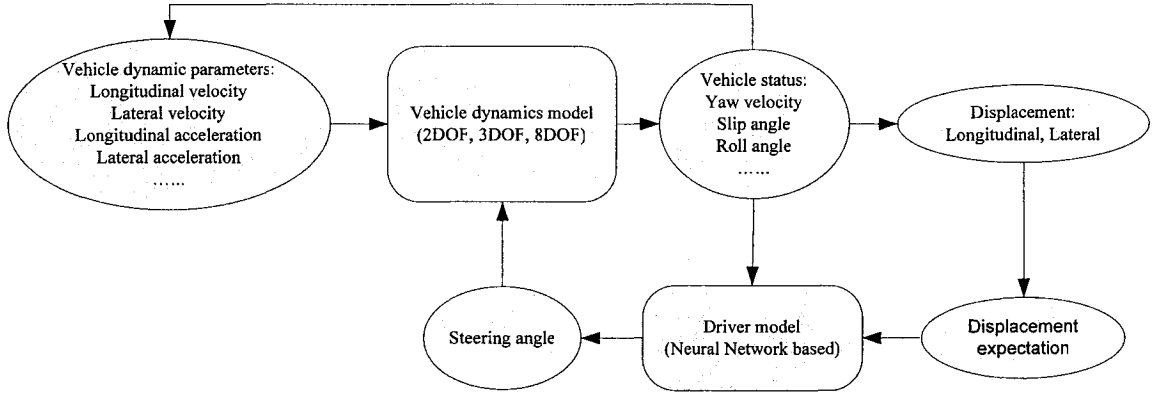


Figure 5-3 Interaction between vehicle model and driver model

Normally, driver models and vehicle models are used simultaneously in close-loop Driver-Vehicle-Environment simulation systems. One of the major functions of vehicle dynamics models is to calculate the next vehicle state according to the current vehicle state and the given steering angle. Driver models calculate the steering angle (including throttle control sometimes) based on the current vehicle state and the displacement expectation (or the displacement error).

In this study, in the artificial neural network based driver models, the input vector contains following parameters: (1) longitudinal velocity \dot{X} , (2) lateral velocity \dot{Y} , (3) longitudinal acceleration \ddot{X} , (4) lateral acceleration \ddot{Y} , (5) yaw velocity γ , (6) roll angle ρ , (7) lateral displacement expectation ΔY , and (8) driver's mental workload level.

The desired output vector contains only one parameter: (i) steering angle δ .

In order to investigate the impacts of driver's mental workload variance, the quantified driver's mental workload should be contained in the input vector of driver models. In this study, a constant mental workload and a continuous varied mental workload are added to two driver models for the comparison, respectively. The constant mental workload is set as the average (mean) value of the driver's mental workload in each manoeuvre.

When steering angle δ has been calculated out by ANN based driver models, it can be input to a 2-DOF vehicle model to investigate the variance of yaw rate and slip angle, and even to estimate the longitudinal displacement and the lateral displacement. Thus, the impacts of driver's mental workload on the driver's steering performance can be observed.

5.3.2 Back-propagation network based driver model

Figure 5-4 shows a MLP network based driver model. The MLP neural network has two layers. The hidden layer is comprised of a sigmoid transfer function, and the output layer is comprised of a linear transfer function. Levenberg-Marquardt back-propagation algorithm is used for neural network training. The training goal is to make the least mean square error of the expected output meet a designated small value.

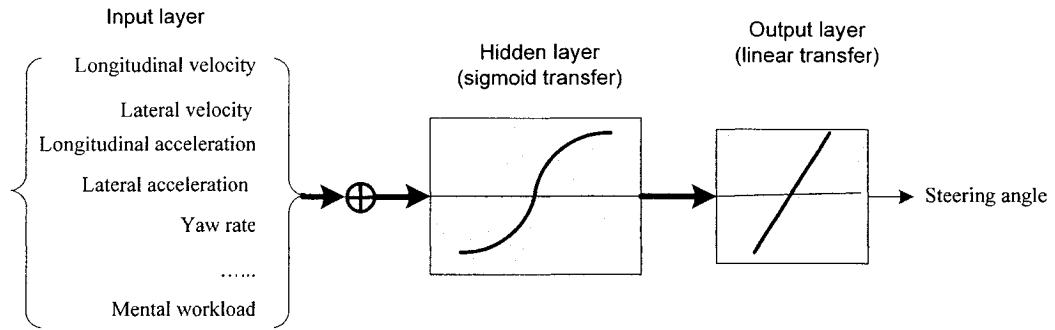


Figure 5-4 MLP network based driver model

In order to simulate a driver's steering behavior, the MLP neural network based driver model should be trained thoroughly. It means that the training pairs should contain enough experimental data coming from multiple single-lane change manoeuvre, double-lane change manoeuvre, and sine-lane motion manoeuvre at many different speeds.

5.3.3 Elman network based driver model

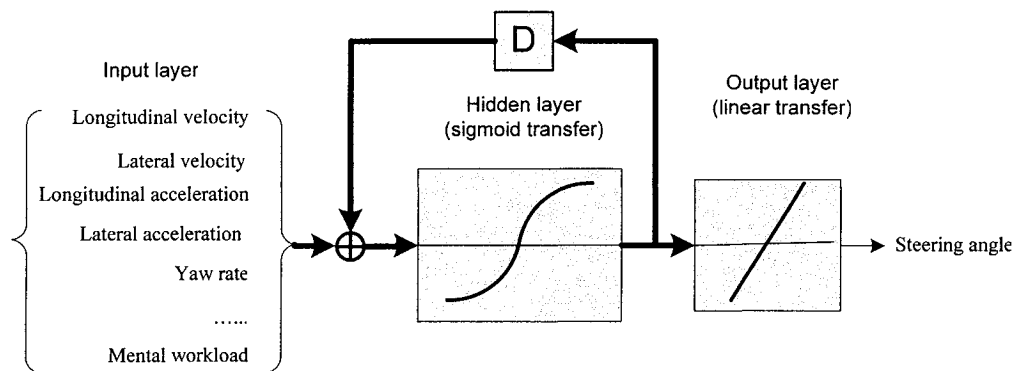


Figure 5-5 Elman network based driver model

Figure 5-5 shows an Elman network based driver model. The Elman neural network based driver model has two layers plus a recurrent layer. The hidden layer is comprised

of a sigmoid transfer function, and the output layer is a linear transfer function. In Figure 5-5, **D** represents one order delay. Quasi-Newton back-propagation algorithm is used for the neural network training. The training goal is to make the least mean square error of the expected output meet a designated small value.

Similar to MLP networks, Elman neural networks should also be trained thoroughly before simulating a driver's steering behaviors. In order to compare the performance of MLP network based and Elman network based driver models, the training pairs and simulation targets should be the same as those of the former discussed MLP networks.

5.4 Two-DOF linear vehicle model

5.4.1 State equations of 2-DOF vehicle model

There are numerous degrees of freedom associated with vehicle dynamics. One of simplified vehicle dynamic models is the two-degree-of-freedom bicycle model (2-DOF), representing the lateral and the yaw motions. The idea behind this model is that sometimes it is not necessary or desirable to include the longitudinal direction because it does not affect the lateral or the yaw stability of the vehicle.

The 2-DOF model is especially suitable for the application in which the longitudinal velocity remains almost constant. In fact, previous literature have pointed out that the 2-DOF model is applicable when the lateral acceleration is less than 0.2g [Hernandez J.I. & Kuo C.Y., 2004]. Therefore, because the drivers in the experiments of this study were required to maintain their vehicle's velocity at a constant speed roughly and without sharp turning, the 2-DOF model should be able to simulate the vehicle movement including single-lane change, double-lane change, and sine-lane motion.

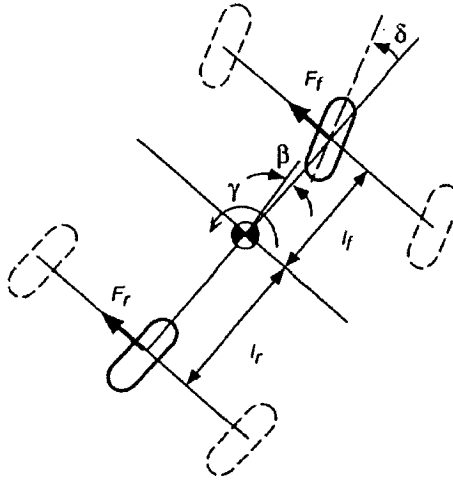


Figure 5-6 Two-degree-of-freedom vehicle model [Wong , 1978]

Figure 5-6 shows a two-degree-of-freedom vehicle steering model (SAE vehicle axis system). The state equations of the motion of this system are described as follows [Wong , 1978]:

$$\dot{\chi} = A\chi + B\mu \quad (5.8)$$

where

$$\chi = \begin{bmatrix} \beta \\ \gamma \end{bmatrix}, \mu = \begin{bmatrix} \delta \\ 0 \end{bmatrix} \quad (5.9)$$

$$A = \begin{bmatrix} -\frac{c_f + c_r}{MV} & -1 - \frac{l_f c_f - l_r c_r}{MV^2} \\ -\frac{l_f c_f - l_r c_r}{I_z} & -\frac{l_f^2 c_f - l_r^2 c_r}{I_z V} \end{bmatrix} \quad (5.10)$$

$$B = \begin{bmatrix} \frac{c_f}{MV} & \frac{c_r}{MV} \\ \frac{l_f c_f}{I_z} & -\frac{l_r c_r}{I_z} \end{bmatrix} \quad (5.11)$$

Here, β, γ indicate the slip angle and the yaw rate of the vehicle, respectively. M, V, I_z indicate the vehicle mass, the velocity, and the vehicle yaw moment of inertia, respectively. $l_f(l_r)$ shows the distance from the center of gravity to the front (rear) tires. $c_f(c_r)$ shows the cornering stiffness at the front (rear) tires. δ shows the front steering angle.

The trajectory of the center of gravity can be derived by Eqs. (5.12) (5.13) (5.14) follows [Wong , 1978]:

$$\theta = \theta_0 + \int_0^t \gamma dt \quad (5.12)$$

$$X = X_0 + V \int_0^t \cos(\beta + \gamma) dt \quad (5.13)$$

$$Y = Y_0 + V \int_0^t \sin(\beta + \gamma) dt \quad (5.14)$$

where X_0, Y_0, θ_0 mean the initial position and the yaw angle at time $t = 0$.

5.4.2 Validation of the 2-DOF vehicle model

In order to validate the 2-DOF model whether it is accurate enough for the current research, the yaw rate and the slip angle are simulated based on the acquired experimental data. The mean square error (MSE) of the steering angle between the simulation value and the experimental data are calculated for the vehicle model's performance comparison.

Table 5-1 Vehicle parameters used for 2-DOF simulation [Lin, 1997]

Property	Value
Vehicle mass (M)	1570 Kg
Yaw moment of inertia (I_z)	2873 Kg.m ²
Front axle to the center of gravity (l_f)	1.1 m
Rear axle to the center of gravity (l_r)	1.58 m
Cornering stiffness at front , rear tires (c_f, c_r)	20417 N/rad, 58653 N/rad

Figure 5-7 shows the 2-DOF model based yaw rate simulation of the #2 single-lane change manoeuvre at 60 Km per hour. Figure 5-8 shows the yaw rate simulation of the #1 sine-lane motion manoeuvre at 50 Km/h. The mean square error of the yaw rate between the experiment data and the simulation result for the #2 single-lane change manoeuvre and the #1 sine-lane motion manoeuvre are 0.1077 and 1.3523, respectively. The two mean square errors are very small compared with the absolute value of the yaw rate. In fact, the longitudinal acceleration and the lateral acceleration in the experiments are far less than 0.2g and meet the requirements of the 2-DOF model; therefore, the 2-DOF model can provide acceptable simulation results for this research.

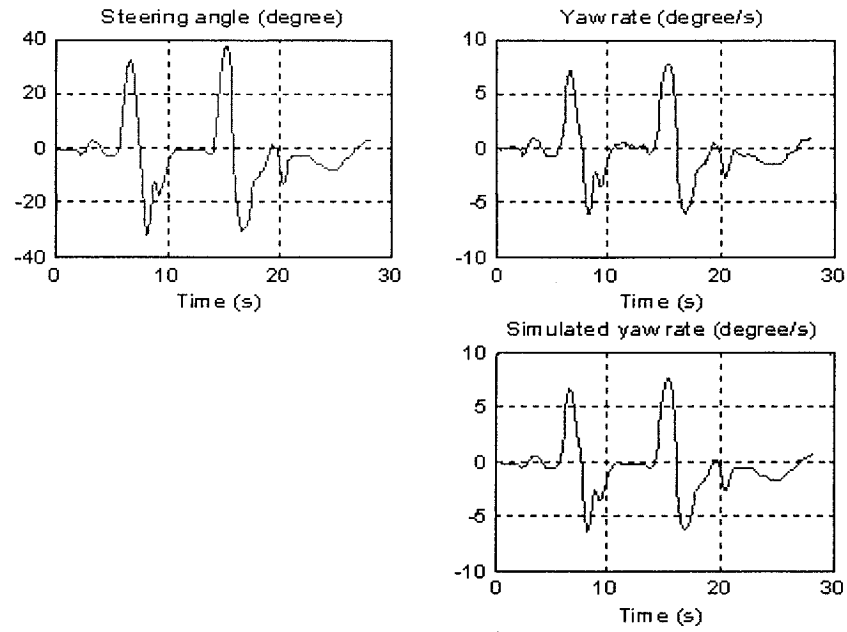


Figure 5-7 2-DOF model based simulation of the #2 single-lane change
(60 Km/h, MSE=0.1077)

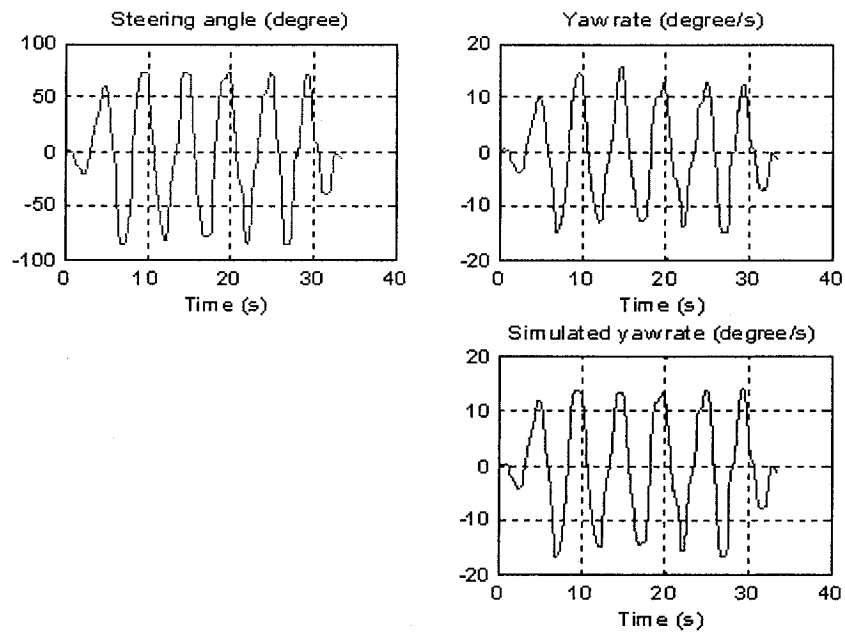


Figure 5-8 2-DOF model based simulation of the #1 sine-lane change
(50 Km/h, MSE=1.3523)

5.5 Experiment and simulation

5.5.1 Simulation results of MLP networks

Based on the grouping of the experiment data, this research uses one part of the experiment data for the neural network training, and another part of the experiment data for the test.

The training pairs of MLP neural network come from the following motions:

- (1) PY62: #2 single-lane change manoeuvre at 60 Km per hour;
- (2) PYA1: #1 single-lane change manoeuvre at 100 Km per hour;
- (3) QY61: #1 double-lane change manoeuvre at 60 Km per hour;
- (4) QY82: #2 double-lane change manoeuvre at 80 Km per hour;
- (5) SY61: #1 sine-lane motion manoeuvre at 60 Km per hour.

The simulation target is the steering angle in the following motions:

- (1) PY61: #1 single-lane change manoeuvre at 60 Km per hour;
- (2) PY81: #1 single-lane change manoeuvre at 80 Km per hour;
- (3) PYA2: #2 single-lane change manoeuvre at 100 Km per hour;
- (4) QY81: #1 double-lane change manoeuvre at 80 Km per hour;
- (5) SY51: #1 sine-lane motion manoeuvre at 50 Km per hour.

In the MLP network based driver models (Figure 5-4), the lateral displacement expectation is not included into the input vector because of its unavailability. The driver's

mental workload is considered in the following two ways to construct driver models. The first driver model contains an overall mental workload level (a constant mental workload level) (Const. MWL) in the input and the second model contains a continuous varied mental workload level (Cont. MWL) in the input. Other inputs of the two models are totally identical. Hence, the impacts of driver's mental workload variance on the steering performance can be compared between the two models.

In this research, the overall mental workload level (Const. MWL) in the input is assumed as the average MWL in each manoeuvre. They are shown in Table 5-2.

Table 5-2 Average mental workload in each trial

Manoeuvre type	Mean value	Standard deviation value
1 st Single-lane change at 60Km/h	0.2996	0.1066
2 nd Single-lane change at 60Km/h	0.2438	0.0591
1 st Single-lane change at 80Km/h	0.2701	0.0584
1 st Single-lane change at 100Km/h	0.2709	0.1170
2 nd Single-lane change at 100Km/h	0.2820	0.0874
1 st Double-lane change at 60Km/h	0.4412	0.1396
1 st Double-lane change at 80Km/h	0.4700	0.1401
2 nd Double-lane change at 80Km/h	0.5184	0.1496
1 st Sine-lane motion at 50Km/h	0.4843	0.1261
1 st Sine-lane motion at 60Km/h	0.5572	0.1480

The value in Table 5-2 is calculated out according to Table 3-15. The mental workload variance is derived by smoothing the discrete value of the mental workload

level. Because for the same manoeuvre with similar motion velocity, the difference of the average mental workload level between #1 trial and #2 trial is very small, it means that the neural network can obtained a nearly full training. In another word, the little difference of constant mental workload in the neural network input will not bring significant impact to the output when compared with a same fixed value. That is why it is used for the reference to compare with the influence of continuous mental workload variance.

The hidden layer of the MLP network is comprised of a sigmoid transfer function with 40 neurons, and the output layer is a linear transfer function with 1 output neuron. The training goal (the least mean square error) is set to 2×10^{-4} and 300 epochs maximum.

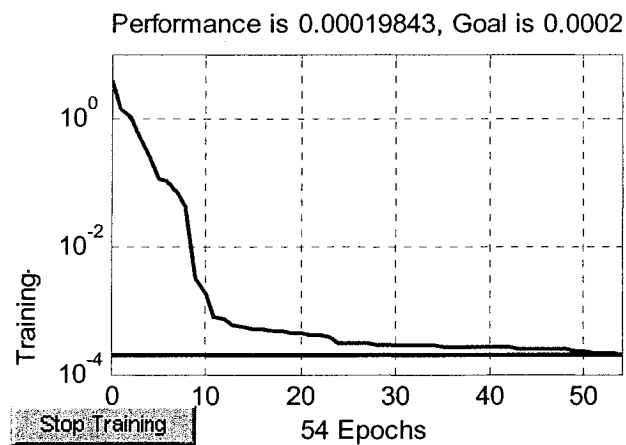
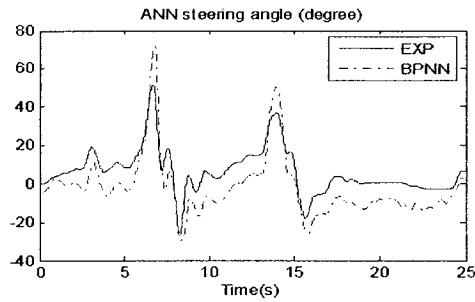


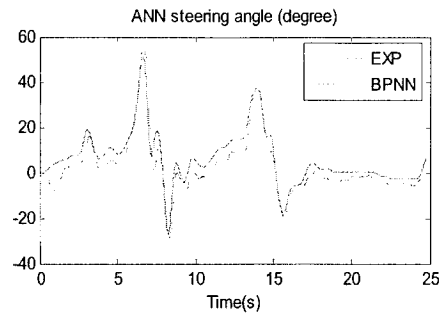
Figure 5-9 Training procedure of the MLP network

According to Figure 5-9, the LM back-propagation algorithm is very efficient. It reaches the goal in only 55 steps.

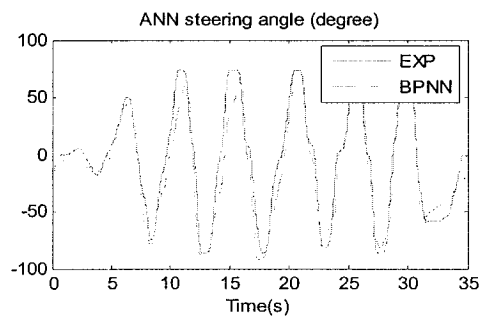
In Figure 5-10, EXP means the experiment data while BPNN means the simulation results by the MLP based driver model.



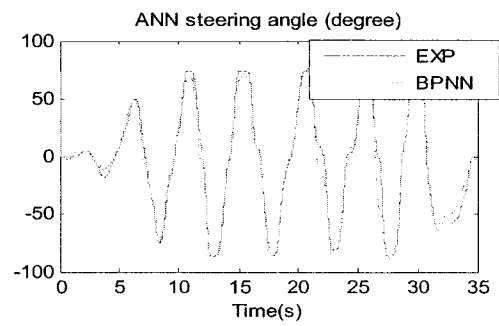
Single-lane (60 Km/h)
(MLP model with Const. MWL)



Single-lane (60 Km/h)
(MLP model with Cont. MWL)



Sine-lane (50 Km/h)
(MLP model with Const. MWL)



Sine-lane (50 Km/h)
(MLP model with Cont. MWL)

Figure 5-10 Simulation results of steering angle based on two MLP driver models

Table 5-3 MSE of the steering angle between the simulation and the experiments

Motion type	Single-lane (60 Km/h)	Single-lane (80 Km/h)	Single-lane (100 Km/h)	Double-lane (80Km/h)	Sine-lane (50 Km/h)
MSE (Const. MWL)	107.4	106.0	39.6	360.1	147.5
MSE (Cont. MWL)	23.4	13.5	57.1	238.5	79.3
Comparison of the simulation results	Better	Better	Slightly poorer	Better	Better

According to Table 5-3, the majority of MLP driver models with the input of continuous MWL variance provide better simulation results of steering angle than those MLP driver models with the input of constant MWL. It implies that the mental workload variance can make good contributions in the driver steering behavior models.

5.5.2 Simulation results of Elman networks

The training pairs of the Elman neural networks are the same as those of the MLP networks. There are also two Elman network based driver models. One contains a constant mental workload level as input and another contains a continuous mental workload variance as input. Hence, the simulation results of the steering angle between the two models can be compared.

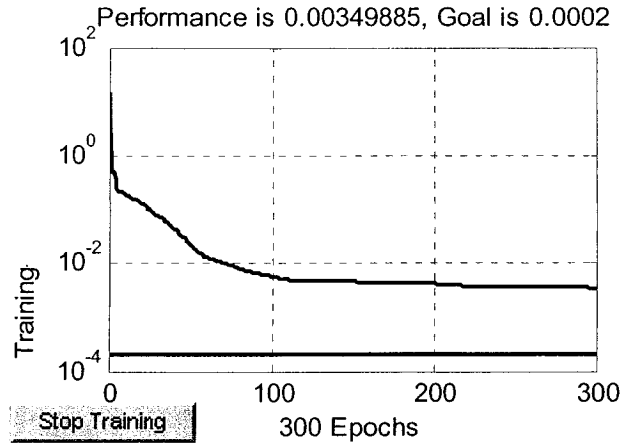


Figure 5-11 Training procedure of the Elman network

According to Figure 5-11, compared with LM algorithm, the quasi-Newton back-propagation algorithm is not very fast. Furthermore, the goal is difficult to meet. The final MSE is only 3.5×10^{-3} after the training of 300 epochs.

In Figure 5-12, EXP means the experiment data and RC-NN means the simulation results by the recurrent network based driver model.

According to Table 5-4, the majority of Elman network based driver models with the input of MWL variance provide better simulation results of steering angle than those Elman driver models with the input of constant MWL. It also shows the benefits of considering mental workload variance in the driver steering behavior models.

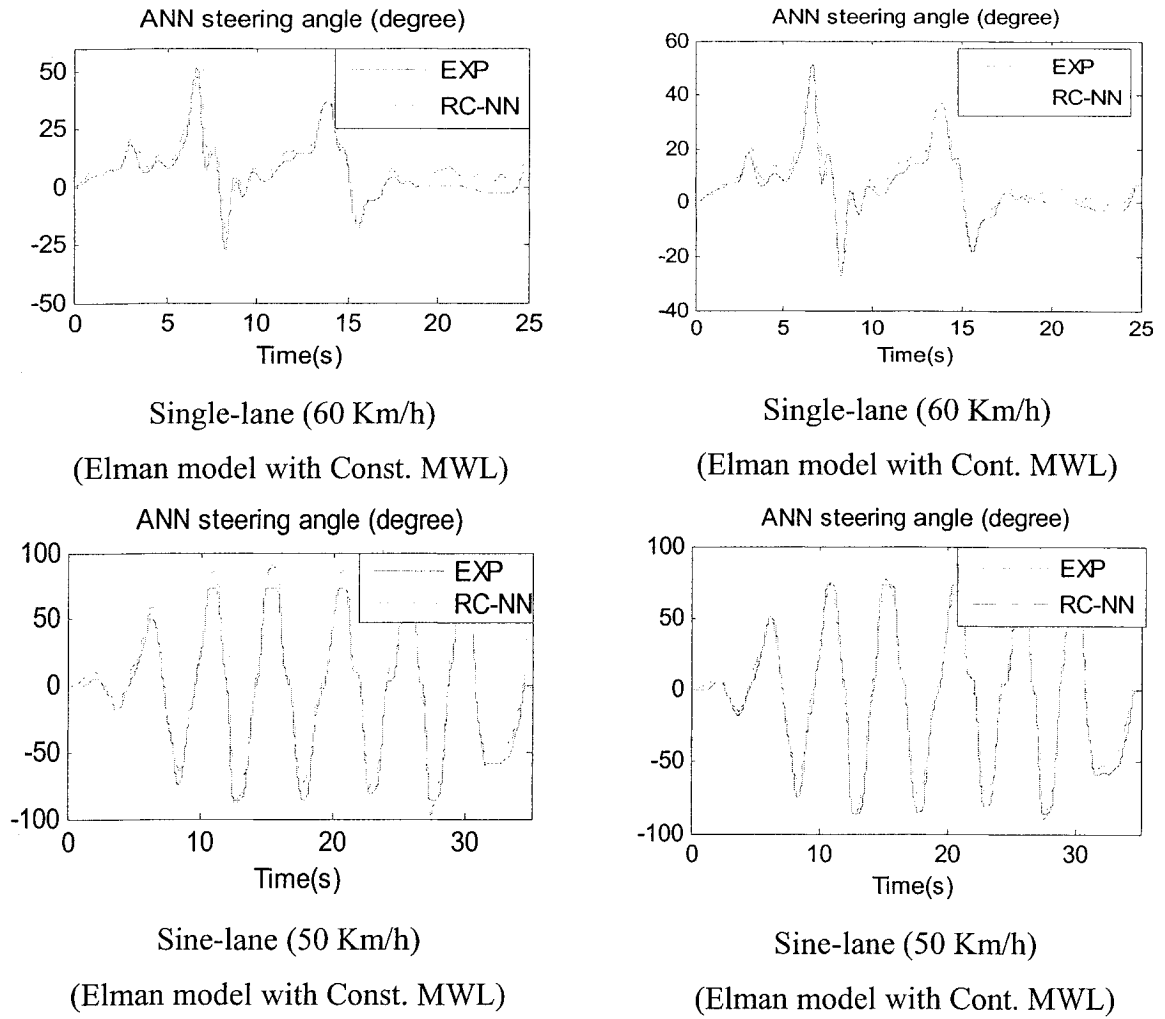


Figure 5-12 Simulation results of steering angle based on two Elman driver models

To compare Table 5-3 and 5-4, it can be found that the simulation results of Elman networks are closer to the experiment data than those of MLP networks. It indicates that Elman recurrent networks are more likely suitable to simulate drivers' steering behavior than Multi-Layer Perceptron networks. The better performance of Elman networks than that of MLP networks is just because of its recurrent capabilities as discussed in section 5.2.2.

Table 5-4 MSE of the steering angle between the simulation and the experiments

Motion type	Single-lane (60 Km/h)	Single-lane (80 Km/h)	Single-lane (100 Km/h)	Double-lane (80Km/h)	Sine-lane (50 Km/h)
MSE (Const. MWL)	17.6	21.2	34.8	327.3	67.8
MSE (Cont. MWL)	9.8	27.7	13.8	150.2	39.9
Comparison of the simulation results	Better	Slightly poorer	Better	Better	Better

To compare Table 5-3 and 5-4, it can be found that the simulation results of Elman networks are closer to the experiment data than those of MLP networks. It indicates that Elman recurrent networks are more likely suitable to simulate drivers' steering behavior than Multi-Layer Perceptron networks. The better performance of Elman networks than that of MLP networks is just because of its recurrent capabilities as discussed in section 5.2.2.

5.5.3 2-DOF model based vehicle state simulation

Although the vehicle's longitudinal displacement and the lateral displacement can be calculated out according to Eqs. (5.15, 5.16), they cannot be used as criteria to measure the results of 2-DOF simulation in this study because the practical trajectory was not recorded during the former experiments.

According to Wong [1978], the yaw rate of the vehicle in response to a steering input is a good index for a handling and steering response, so in this research, the yaw rate of the vehicle in experiments is used to evaluate the simulation results of neural networks by using the 2-DOF vehicle model-based simulation.

According to Tables 5-3 and 5-4, the simulation results of the steering angle based on Elman recurrent networks are closer to the experiment data than those by MLP networks, so the yaw rate simulation by 2-DOF vehicle models is based only on the output of the Elman networks in this research.

Besides the performance measurement of mean square error (MSE), correlation coefficients (C.C.) can also be used to estimate the proximity between the simulation value and the experiment value of vehicle yaw rate. The correlation coefficients are calculated in Eq. (3.25).

In terms of mean square error, according to Table 5-5, most of the Elman network-based driver models with the input of MWL variance provide better simulation results of the yaw rate than those Elman network models with the input of constant MWL.

In terms of the correlation coefficient, according to Table 5-6, all Elman network-based driver models with the input of MWL variance provide better simulation results of yaw rate than those Elman network models with the input of constant MWL.

Although it is commonly known that there is uncertainty in the training procedure of neural networks, Tables 5-5 and 5-6 do suggest that mental workload variance is more likely to provide positive implications on Elman networks based driver steering behavior simulation.

It can also be noticed that, in Tables 5-3, 5-4, 5-5, 5-6, and Figure 5-11, compared with the simulation results of single-lane changes and sine-lane motions, the simulation results of the double-lane change at 80 Km/h seem extraordinarily inferior. The fact is that this trial is not an acceptable double-lane manoeuvre because of the driver's abnormal operation. Both the MLP networks and the Elman networks do not obtain a complete training regarding this abnormal behavior.

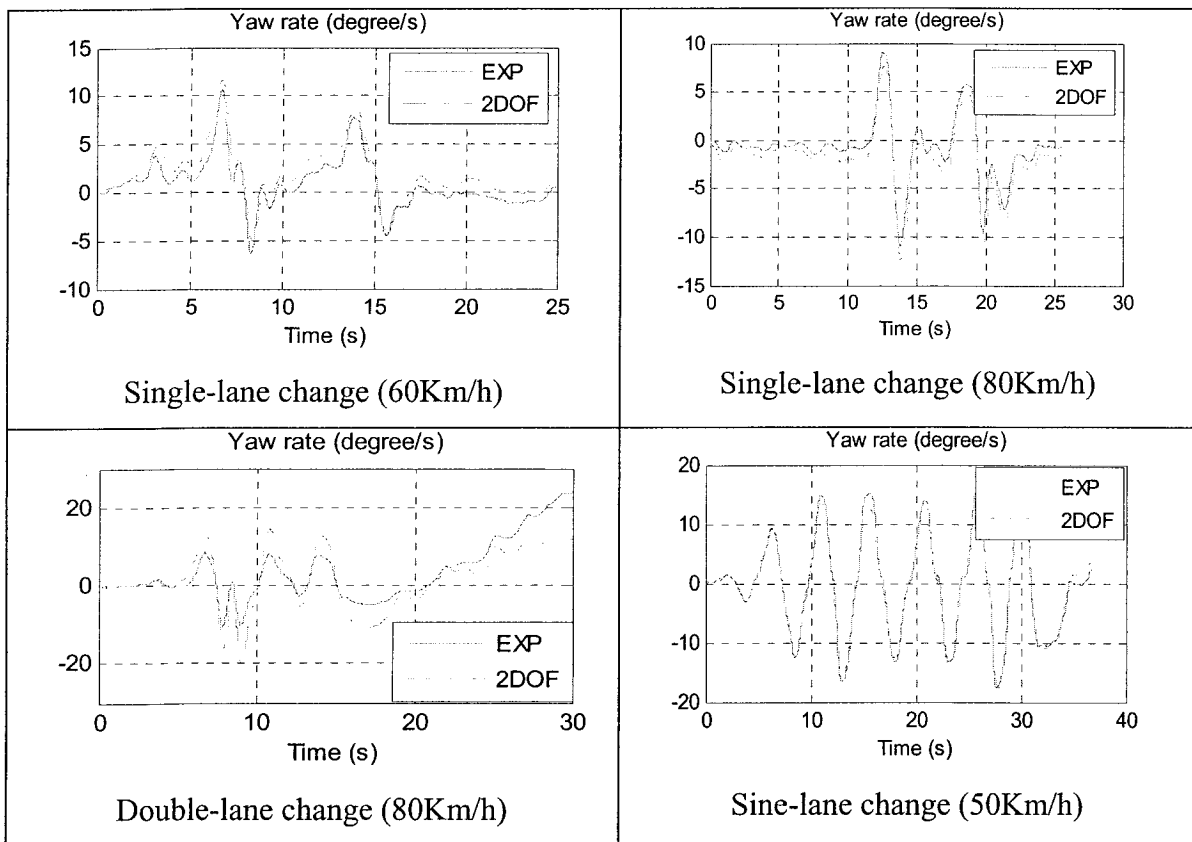


Figure 5-13 Yaw rate simulation on results of Elman network based driver models
(with Cont. MWL)

Table 5-5 MSE of the yaw rate between the simulation and the experiments

Motion type	Single-lane (60 Km/h)	Single-lane (80 Km/h)	Single-lane (100 Km/h)	Double-lane (80Km/h)	Sine-lane (50 Km/h)
MSE (Const. MWL)	2.6579	1.3474	2.5964	35.5389	3.7942
MSE (Cont. MWL)	1.5585	1.4415	0.7665	19.4	0.9242
Comparison of the simulation results	Better	Similar	Better	Better	Better

Table 5-6 C.C. of the yaw rate between the simulation and the experiments

Motion type	Single-lane (60 Km/h)	Single-lane (80 Km/h)	Single-lane (100 Km/h)	Double-lane (80Km/h)	Sine-lane (50 Km/h)
C.C. (Const. MWL)	0.9646	0.9602	0.9250	0.7041	0.9820
C.C. (Cont. MWL)	0.9768	0.9893	0.9766	0.8583	0.9946
Comparison of the simulation results	Better	Better	Better	Better	Better

5.6 Summary

In this chapter, the architectures of two artificial neural networks (Multilayer Perceptrons and Elman recurrent networks) used to build drivers' handling behavior models were first discussed. The average driver mental workload (a constant value) and

the continuous driver mental workload variance (a variable) were contained in the two neural network-based driver models, respectively. The performance of handling behavior in terms of the steering angle was verified by the two degrees of freedom vehicle model. The movement of the vehicle, in terms of the yaw rate, was evaluated using the mean square error and the correlation coefficient.

The simulation results indicate that Elman recurrent network-based driver models are superior to Multilayer perceptrons-based driver models in the simulation of the drivers' steering behaviors due to the characteristics of time-series. Moreover, both the MLP-based driver model and the Elman network-based driver model show simulation results closer to the experiment data when the driver mental workload variance is taken into account. This indicates that the driver mental workload variance has positive implications for the neural network-based driver models.

CHAPTER 6 CONCLUSIONS AND FUTURE WORK

6.1 General conclusions

Driver mental workload is an important factor in driving safety. Researchers have pointed out that mental workload has close correlations with drivers' performance, but so far few researchers have reported the method of mental workload quantification and the corresponding driver models with the influence of mental workload.

The main contributions of this thesis work are the following:

(1) An ECG features-based driver mental workload quantification method was proposed. It is based on clustering analysis and Learning Vector Quantization.

The estimation results of the mental workload in typical vehicle manoeuvre are consistent with both common sense and the RSME scale. The measure also demonstrates the possibility of reducing subjectivity.

(2) A preliminary model of driving risk level was established. Driving risk level can be estimated by using a fuzzy space model of the danger zone of a moving vehicle.

Driver mental workload variance shows a close relationship to the alteration of the driving risk level. The driving risk level is likely to indicate the driver's mental workload over-reduction.

(3) Neural network-based driver models with the input of the driver mental workload were proposed. They show good performance in typical vehicle manoeuvre simulations.

Elman recurrent networks are superior to Multilayer perceptrons (MLP) to simulate a driver's steering behaviors due to the driver's behaviors' time series characteristics.

Moreover, both neural network-based driver models show better driver performance simulation when the driver mental workload variance is taken into account.

6.2 Recommendations for future work

This present study is limited to the data source. The following future work is recommended:

(1) Only ECG features are studied in this present research. In the further research, other physiological signals possibly indicating the mental workload change, such as EEG, eye movement, could also be included. The estimation results would thus be more reliable.

(2) Time headway is one of the major parameters to build the fuzzy space in the danger-zone model of the present research. Other factors, e.g., the kinetic energy indicating the risk severity, could also be utilized in the modeling.

(3) In the recurrent network-based driver models, the input vector could contain more parameters, e.g., the lateral displacement error, the previewed lateral displacement. Furthermore, the instant driving risk level, combined with the reduced driver mental workload, could be added to the driver models to provide the opportunity to speculate on whether the driver model's steering performance can be improved. If so, the driving risk level may be valuable in the establishment of the compensation for the driver mental workload over-reduction.

(4) The simulation results obtained in this stage have only logical and qualitative support. Experiments and simulations should be extended to cover more subjects to conduct a further statistical data analysis.

REFERENCE

- Al-Fahoum, A.S. and Howitt, I. (1999). Combined wavelet transformation and radial basis neural networks for classifying life threatening cardiac arrhythmias. *Medical & Biological Engineering & Computing*, 37(5), pp. 566-573.
- An, P.E.; Harris, C.J. (1996). An intelligent driver warning system for vehicle collision avoidance. *Systems, Man and Cybernetics. Part A, IEEE Transactions*, Volume 26, Issue 2, pp.254 -261
- Anagnostopoulos, C., Anagnostopoulos, J., Vergados, D.D., Kayafas, E., Loumos, V., and Theodoropoulos, G. (2001). Training a learning vector quantization network for biomedical classification. *International Joint Conference on Neural Networks*, vol.4, pp. 2506 – 2511.
- Antognetti P., Milutinovic. (1991). *Neural Networks Concepts, Applications, and Implementations. Volume III.* ISBN 0-13-612516-6. Prentice-Hall, Inc.
- Backs, R. W., Seljos, K. A. (1994). Metabolic and cardiorespiratory measures of mental efforts of level of difficulty in a working memory task. *International Journal of Psychophysiology*, 16, pp.57-68.
- Bahoura, M., Hassani M., and Hubin M. (1997). DSP Implementation of Wavelet Transform for real time ECG Wave detection and Heart Rate Analysis. *Computer Methods and Programs in Biomedicine*, pp. 35-44.
- Bianchi, A.M., Mainardi, L., Petrucci, E., Signorini, M.G., Mainardi, M., Cerutti, S. (1993). Time-variant power spectrum analysis for the detection of transient episodes in HRV signal. *IEEE Transactions on Biomedical Engineering*, 40(2), pp. 136 – 144.

- Cai, H., Lin, Y. (2005), A Preliminary Study on a Fuzzy Driving Risk Model. IEEE International Conference on Systems, Man and Cybernetics (SMC) 2005, Hawaii, USA.
- Cai, H.; Lin, Y. (2005), Incorporating Quantized Mental Workload in Modeling of Driver's Handling Behavior. New England Chapter Human Factors and Ergonomics Conference, November 4, 2005, U.S.A.
- Chen, C.H., Fuzzy logic and neural network handbook. New York: McGraw-Hill, c1996.
- Cnossen, F. (1994). Mental effort from energetical and computational perspectives. Unpublished paper for the BCN course Cognitive Neuroscience. Haren, The Netherlands: Traffic Research Centre, University of Groningen.
- Collet, C., Petit, C., Champely, S., Dittmar, A. (2003). Assessing Workload through Physiological Measurements in Bus Drivers Using an Automated System during Docking. Human Factors, v 45, p 539-548
- De Waard, D. (1996). The measurement of driver's mental workload. Ph.D thesis, University of Groningen, The Netherlands, ISBN 90-6807-308-7.
- Disbro, J. E. and Frame, M. (1990). Traffic Flow Theory and Chaotic Behaviour. Transp. Res. Record, 1225, 109-115.
- Eggemeier, F.T., Wilson, G.F. (1991). Performance-based and subjective assessment of workload in multi-task environments. In D.L. Damos (Ed.), Multiple-task performance. (pp. 217-278). London: Taylor & Francis.
- Elman, J.L. (1990). Finding structure in time. Cognitive Science, 14:179-211.
- Ervin, B. and Guy, Y. (1986). The influence of weights and dimensions on the stability and control of heavy-duty trucks in Canada. UMTRI report, No. 86-35

- Fukuda, O., Nagata, Y., Homma, K., and Tsuji, T. (2001). Evaluation of heart rate variability by using wavelet transform and a recurrent neural network. IEEE Proceedings of the 23rd Annual International Conference on Engineering in Medicine and Biology Society, Vol. 2, pp. 1769 – 1772.
- Gamero, L.G.; Risk, M.; Sobh, J.F.; Ramirez, A.J.; Saul, J.P. (1996). Heart rate variability analysis using wavelet transform. Computers in Cardiology, pp.177 – 180.
- Gamo, C., Gaydecki, P., Zaidi, A., and Fitzpatrick, A. (2000). An implementation of the wavelet transform for ECG analysis. IEE First International Conference on Advances in Medical Signal and Information Processing, pp. 32 – 40.
- Gohara, T., Mizuta, H., Takeuchi, I., Tsuda, O., Yana, K. (1996). Heart rate variability change induced by the kllmental stress: The effect of accumulated fatigue. Southern Biomedical Engineering Conference - Proceedings, p 367-369
- Gorjestani A., Donath M., Alexander L., (1999). Radar based longitudinal virtual bumper collision avoidance system implemented on a truck. Technical report. Published by office of research administration, Minnesota department of transportation. March 1999.
- Greene, K. A., Bauer, K. W., Wilson, G. F., Russell, C. A., Rogers, S. K. and Kabrinsky, M. (2000). Selection of psychophysiological features for classifying air traffic controller workload in neural networks. Smart Eng. Syst. Design, vol. 2, pp. 315–330.
- Greene, A., A process approach to project risk management. Loughborough University.
- Gurusinghe, G. S., Nakatsuji, T. and Azuta, Y., et. al. (2003). Multiple Car Following Data Using Real Time Kinematic Global Positioning System. Transp. Res. Record, 1802, 166-180

- Hanskins, T.C., and Wilson, G.F. (1998). A comparison of heart rate, eye activity, EEG and subjective measures of pilot mental workload during flight. *Aviation, Space, Environ. Med.*, 69(4), pp. 360-367.
- Hart, S. G., and Staveland, L. E. (1988). Development of NASA-TLX (task load index): Results of empirical and theoretical research. In P. A. Hancock & N. Meshkati (Eds), *Human mental workload* (pp. 185-217), Amsterdam: Elsevier.
- Heino, A., Molen, Hugo, H., Wilde, G.J.S. (1996). Risk perception, risk taking, accident involvement and the need for stimulation. *Safety Science*, v 22, n 1-3, Feb-Apr, p 35-48.
- Hagan M.T., Demuth H.B., Beale M.H. (1996). *Neural network design*, ISBN7-111-07585-4.
- Hernandez J.I.& Kuo C.Y. (2004). Lateral Control of Higher Order Nonlinear Vehicle Model in Emergency Manoeuvre Using Absolute Positioning GPS and Magnetic Markers. *IEEE transactions on vehicular technology*, vol. 53, No. 2.
- Hogan, R.M. (1997). Impact of physical disengagement on driver alertness: implications for precursors of a fully automated highway system. *IEEE Conference on ITS*, 9-12 Nov. 1997, Pages: 613 – 618.
- Hornik K.M., Hornik K.M., Stinchcombe M. and White H. (1989). Multilayer feedforward networks are universal approximators, *Neural Networks*, Vol. 2, No.5, pp.359-366.
- ISO 3888-1:1999. Passenger cars -- Test track for a severe lane-change manoeuvre -- Part 1: Double lane-change.

- ISO 3888-2:2002. Passenger cars -- Test track for a severe lane-change manoeuvre -- Part 2: Obstacle avoidance.
- Ito, Y., Omatu, S. (1999). Extended LVQ Neural Network Approach to Land Cover Mapping. *IEEE Transactions on Geoscience and Remote Sensing*, 37(1), pp. 313 – 317.
- ITS Japan, 2002. ITS Handbook.
- Provaznik I. (2002). Wavelet Analysis for Signal Detection-Applications to Experimental Cardiology Research. Habilitation thesis, Brno University of Technology.
- Jambu, M. (1983). Cluster analysis and data analysis. New York: North-Holland Pub. Co., ISBN 0444866345.
- Ji, Q., Zhu, Z., and Lan, P. (2004). Real-time nonintrusive monitoring and prediction of driver fatigue. *IEEE Transactions on Vehicular Technology*, 53(4), pp. 1052-1068.
- Jo, Y.D., Parkd, K.S. (2003). Dynamic management of human error to reduce total risk. *Journal of Loss Prevention in the Process Industries*, No.16, pp.313-321.
- Jorna, P. G. A. M. (1992). Spectral analysis of heart rate and psychological state: A review of its validity as a workload index. *Biological Psychology*, 34, pp.237-257.
- Juang, C. F., and Lin, C. T. (1998). An on-line self-constructing neural fuzzy inference network and its applications. *IEEE Transactions on Fuzzy Systems*, 6(1), pp. 12-32.
- Koike, Y., Doya, K. (1999). Multiple state estimation reinforcement learning for driving model: driver model of automobile. *Systems, Man, and Cybernetics*, IEEE SMC '99 Conference Proceedings
- Kohler, B.U., Hennig, C., and Orglmeister, R. (2002). The principles of software QRS detection. *IEEE Engineering in Medicine and Biology Magazine*, 21(1), pp. 42 – 57.

- Kohonen, T. (1995). Self-organizing maps. New York: Springer-Verlag.
- Kohonen, T. (1990). The self-organizing map. *Proceedings of the IEEE*, 78(9), pp. 1464 – 1480.
- Koike Y., Doya, K. (2003). Driver model based on reinforced learning with multiple-step state estimation. *Electronics and Communications in Japan (Part III: Fundamental Electronic Science)*, Volume 86, Issue 10, Pages 85 – 95.
- Kramer, A.F. (1991). Physiological metrics of mental workload: a review of recent progress. In D.L. Damos (Ed.), *Multiple-task performance*. pp. 279-328.
- Kuriyagawa, Y.; Kageyama, I. (1999). A modeling of heart rate variability to estimate mental work load. 1999 IEEE International Conference on Systems, Man, and Cybernetics, vol.2, pp. 294 – 299.
- Kweon, Y.J., Kockelman, K.M. (2003). Overall injury risk to different drivers: Combining exposure, frequency, and severity models. *Accident Analysis and Prevention*, v 35, n 4, p 441-450.
- Laberge-Nadeau, C., Maag, U., Bellavance, F., Lapierre, S. D., Desjardins, D., Messier, S., Saidi, A. (2003). Wireless telephones and the risk of road crashes. *Accident Analysis and Prevention*, v 35, n 5, p 649-660
- Labodova, A. (2004). Implementing integrated management systems using a risk analysis based approach. *Journal of Cleaner Production*, No.12, pp.571-580.
- Laine, T.I., Bauer, K.W., Lanning, J.W., Russell, C.A., and Wilson, G.F. (2002). Selection of input features across subjects for classifying crewmember workload using artificial neural networks. *IEEE Transactions on Systems, Man and Cybernetics, Part A*, 32(6), pp. 691 – 704.

- Lanzilotta, E. J. (1995). Analysis of driver safety performance using safety state model. Source: Transportation Research Record, n 1485, Jul, 1995, p 140-147. ISSN: 0361-1981.
- Law, N.F., and Siu K. C. (2001). Fast Algorithm for Quadratic and Cubic Spline Wavelets. Proceedings of 2001 International Symposium on Intelligent Multimedia, video and Speech Processing, pp.247-250.
- LeBlanc, D., Ervin, R. (1996). CPAC: An implementation of a road-departure warning system. IEEE Contr. Syst. Mag., Vol. 16, 61-71
- Li, C.W., Zheng, C.X., Tai, C. (1995). Detection of ECG characteristic points using wavelet transforms. IEEE Transactions on Biomedical Engineering, 42(1), pp. 21-28.
- Lin Y. (1997). Study on Handling Stability of Driver-Vehicle-Environment Closed Loop System Based on Neural Networks and Fuzzy Theory. Doctor Dissertation, Department of Vehicle Engineering, China Agricultural University, Beijing.
- Lin, Y., Tang, P., Zhang, W.J., and Yu, Q. (2005). Artificial Neural Network Modeling of Driver Handling Behavior in a Driver-Vehicle-Environment System. Int. Journal of Vehicle Design, 37(1), pp. 24-45.
- MacAdam, C.C. and Johnson, G.E. (1996). Application of Elementary neural networks and preview sensors for representing driver steering control behavior. Vehicle system Dynamics, Vol. 25, 3-30
- Mallat, S. (1992). Characterization of signals from multiscale edges. IEEE Trans. Pattern Anal. Machine Intell., vol. 14, pp. 710-732.
- Mallat, S. (1991). Zero-crossings of a wavelet transform. IEEE Trans. Inform Theory, vol. 37, pp. 1019-1033.

- Martínez, J. P., Almeida, R., Olmos, S., Rocha, A. P., and Laguna, P. (2004). A Wavelet-Based ECG Delineator: Evaluation on Standard Databases. *IEEE transactions on biomedical engineering*, 51(4), pp.570-581.
- MATLAB 7.0 User Guides.
- Mazaeva, N., Ntuen, C., and Lebby, G. (2001). Self-Organizing Map (SOM) model for mental workload classification. *IFSA World Congress and 20th NAFIPS International Conference*, vol.3 pp.1822 – 1825.
- McCraty R., Atkinson M., Tiller W.A., Rein G., & Watkins A.D. (1995). The Effects of Emotions on Short-Term Power Spectrum Analysis of Heart Rate Variability. *The American Journal of Cardiology*, 76, 1089-1093.
- Michael, G., Grant, L. I., Edward, J. R., Ronald, R., Peter, M., and Wolfgang, L. (2004). Self-Organizing Neural Network Analyses of Cardiac Data in Depression. *Neuropsychobiology*, 49(1), pp.30-37.
- Michon, J.A. (Ed.) (1993). *Generic Intelligent Driver Support System*. London: Taylor & Francis.
- Mills, K.C., Spruill, S.E., Kanne, R.W., Parkman, K.M., Zhang, Y. (2001). The influence of stimulants, sedatives, and fatigue on tunnel vision: Risk factors for driving and piloting. *Human Factors*, v 43, n 2, 2001, pp.310-327.
- Minami, Kei-ichiro, Nakajima, H., and Toyoshima, T. (1999). Real-time discrimination of ventricular tachyarrhythmia with Fourier-Transform neural network. *IEEE Transaction on Biomedical Engineering*, 46(2), pp.179-185.
- Moray, N. (1988). Mental workload since 1979. *International Review of Ergonomics*, 2, pp. 123-150.

- Murai, K., Okazaki, T., and Hayashi, Y. (2004). Measurement for mental workload of bridge team on leaving/entering port. IEEE 2004 Position Location and Navigation Symposium (PLANS), pp. 746 – 751.
- Murai, K., Hayashi, Y., Wakabayashi, N. (2003). A basic study on navigator's mental workload by wavelet transform. IEEE Pacific Rim Conference on Communications, Computers and signal Processing, vol.2, pp. 1016 – 1019.
- Murai, K., Hayashi, Y., and Wakabayashi, N. (2001). Analysis of heart rate variability of navigator at in/from ports by wavelet transform. 2001 IEEE Pacific Rim Conference on Communications, Computers and signal Processing, vol.2, pp. 681 – 685.
- Neusser, S. (1993). Neural control for lateral vehicle guidance. IEEE Micro, pp.57-66.
- Newandee, A. D., and Reisman, S. S. (2003). Wavelet representation comparision for heart rate variability analysis. 2003 IEEE 29th Annual Bioengineering Conference, pp. 112 – 113.
- Newandee, D.A.; Reisman, S.S. (2002). Application of the wavelet transform to heart rate variability (HRV). Proceedings of the IEEE 28th Annual Northeast Bioengineering Conference, pp.35-36.
- Ni, D. (2003). 2DSIM: A prototype of nanoscopic traffic simulation, Intelligent Vehicles Symposium. Proceedings. IEEE 9-11 June 2003 Page(s):47 - 52
- Nickel, Peter Nachreiner, Friedhelm von Ossietzky, Carl. (2003). Sensitivity and diagnosticity of the 0.1-Hz component of heart rate variability as an indicator of mental workload. Human Factors. December 22, 2003.

- O'Donnell, R.D., and Eggemeier, F.T. (1986). Workload assessment methodology. Handbook of perception and human performance. Volume II, cognitive processes and performance. (pp 42/1-42/49). New York: Wiley.
- Okada M. (1979). A digital filter for the QRS complex detection. IEEE Trans Biomed Eng. 1979 Dec; 26(12):700-3.
- Ohno, H. (2000). Analysis and modeling of human driving behaviors using adaptive cruise control. Industrial Electronics Society, 2000. 26th Annual Conference of the IEEE Volume 4. Page(s):2803 – 2808 vol.4.
- Reid, G. B., and Nygren, T. E. (1988). Subjective workload assessment technique: A scaling procedure for measuring mental workload. In P. A. Hancock & N. Meshkati (Eds), Human mental workload (pp. 185-217), Amsterdam: Elsevier.
- Roscoe, A. H. (1992). Assessing pilot workload. Why measure heart rate, HRV and respiration? Biological Psychology, 34, pp.259-287.
- Rouse, W.B., Edwards, S.L. and Hammer, J.M. (1993). Modelling the dynamics of mental workload and human performance in complex systems. IEEE transactions on systems, man, and cybernetics, 23, 1662-1671.
- Sahambi, J.S., Tandon, S.N., Bhatt, R.K.P. (1997). Using wavelet transforms for ECG characterization. An on-line digital signal processing system. IEEE Engineering in Medicine and Biology Magazine, 16(1), pp.77-83.
- Savitzky A., and Golay, M.J.E. (1964). Analytical Chemistry. vol. 36, pp. 1627–1639.
- Schilling RJ, Peters NS, Davies DW. (1998). Simultaneous endocardial mapping in the human left ventricle using a non-contact catheter: comparison of contact and reconstructed electrograms during sinus rhythm. Circulation; 98:887–898

- Seong, H.M.; Lee, J.S.; Shin, T.M.; Kim, W.S.; Yoon, Y.R. (2004). The analysis of mental stress using time-frequency distribution of heart rate variability signal. 26th Annual International Conference of the Engineering in Medicine and Biology Society, Vol.1, pp.283 – 285.
- Shahrokhi, M., Bernard, A. (2004). A fuzzy approach for definition of dangerous zone in industrial systems. IEEE International Conference on Systems, Man and Cybernetics, Volume: 7, Pages:6318 - 6324.
- Simon, P., Rousseau, F., and Angue, J.-C. (1993). Quantitative analysis of mental workload influence on eye scanning movements. International Conference on Systems, Man and Cybernetics, vol.4, pp. 707 – 712.
- Sirevaag, E. J., Kramer, A. F., Wickens, C.D., Reisweber, M., Strayer, D. L. and Grenell, J. (1993). Assessment of pilot performance and mental workload in rotary wing aircraft. *Ergonomics*, 36(9), pp. 1121–1140.
- Sohambi, J.S., Tandon, S.N., and Bhatt, R.K.P. (1997). Using wavelet transforms for ECG characterization. *IEEE Engineering in Medical and Biology*, 16(1), pp. 77-83.
- Stutts J., Feaganes J. (2003). In *Everydaydriving*, University of North Carolina, Highway Safety Research Center, AAA Foundation for Traffic Safety, June, 2003.
- Stutts, J.C., Wilkins, J.W., Osberg, J.S., Vaughn, B.V. (2003). Driver risk factors for sleep-related crashes, *Accident Analysis and Prevention*, v 35, n 3, May 2003, pp.321-331.
- Tanaka, J., Ishida, S., Kawagoe, H., Kondo, S. (2000). Workload of using a driver assistance system, *Intelligent Transportation Systems. Proceedings. IEEE*, 1-3 Oct. 2000, Pages:382 – 386.

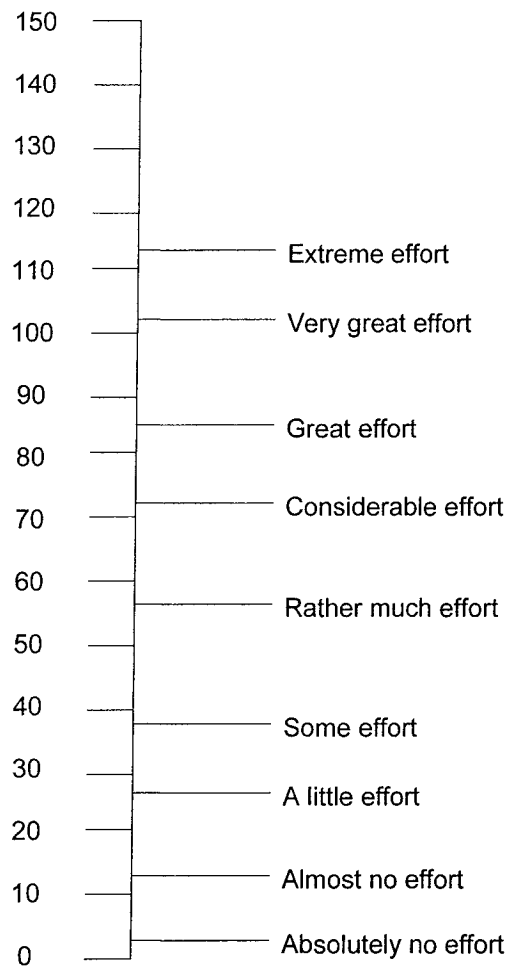
- Tascillo, A.L., DiMeo, D.M., Macneille, P.R., Miller, R.H. (2002). Predicting a vehicle or pedestrian's next move with neural networks, Neural Networks. IJCNN '02. Proceedings of the 2002 International Joint Conference.
- Thakur, K.P., White, D.M. (1997). Development of driver-vehicle model on 'risk time' basis. Source: Heavy Vehicle Systems, v 4, n 2-4, 1997, p 204-221. ISSN: 1351-7848.
- UK (2001). MoD Health & Safety Handbook, The ministry of Defence (UK), JSP 375 Vol2.
- Unema, P. (1995). Eye movements and mental effort. PhD Thesis, TU Berlin. Aachen, Germany: Verlag Schalter.
- Vuckovic, A., Radivojevic, V., Chen A. C. N., and Popovic, D. (2002). Automatic recognition of alertness and drowsiness from EEG by an artificial neural network. Medical Engineering & Physics, 24, pp. 349-360.
- Vysoký, P. (2004). Changes in car driver dynamics caused by fatigue. Neural Network World, 14(1), pp. 109-117.
- Vysoký, P. (2001). Central fatigue identification of human operator. Neural Network World, 11(5), pp. 525-535.
- Ward, N.J., Beusmans, J. (1998). Simulation of accident risk displays in motorway driving with traffic. Ergonomics, v 41, pp.1478-1499.
- Wickens, C.D. (1984). Processing resources in attention. In R.Parasuraman and D.R. Davies (Eds.). Varieties of attention. (pp.63-102). London: Academic Press.
- Wierwille, W.W., and Eggemeier, F.T. (1993). Recommendation for mental workload measurement in a test and evaluation environment. Human Factors, 35, 263-281.

- Wilson, G. F., and Fisher, F. (1995a). Cognitive task classification based upon topographic EEG data. *Biolog. Psychol.*, vol. 40, pp. 239–250.
- Wilson, G.F., Swain, C. R., and Brookings, J. B. (1995b). Workload related changes in eye, cardiac, respiratory and brain activity during simulated air traffic control. Air Force, Tech. Rep. AL/CF-TR-1995-0156.
- Wilson, G.F., and Russell, C.A. (2003). Real-time assessment of mental workload using psychophysiological measures and artificial neural networks. *Human Factors*, 45(4), pp.635-643.
- Wong J.Y. (1978). *The theory of ground vehicles*, John Wiley & sons, Inc.
- Xie, B., and Salvendy, G. (2001). Prediction of mental workload in single and multiple tasks environments. *International Journal of Cognitive Ergonomics*, 4(3), pp. 213-242.
- Yang, X., Stiharu, I., Rakheja, S. (1998). Study of driver factors affecting the directional response of an articulated vehicle using neural networks, *Transactions of CSME*, 22(3), 291-306.
- Young, T. (1985). *Linear systems and digital signal processing*, ISBN 0135373662. Publisher: Englewood Cliffs, NJ : Prentice-Hall, c1985.

APPENDIX A

Rating Scale Mental Effort

Please indicate, by marking the vertical axis below, how much effort it took for you to complete the task you've just finished



Rating Scale Mental Effort (Zijlstra, 1993)

Score is indicated by the digits on the left, the official scale is sized such that 150 equals 150 cm from origin to top